

6160

CALCULATION OF LAMINAR SEPARATION WITH FREE INTERACTION BY THE METHOD OF INTEGRAL RELATIONS
PART I—TWO-DIMENSIONAL SUPERSONIC ADIABATIC FLOW

JACK N. NIELSEN, LARRY L. LYNES, and
FREDERICK K. GOODWIN

VIDYA DIVISION, ITEK CORPORATION

CLEARINGHOUSE TECHNICAL REPORT AFFDL-TR-65-107
FOR FEDERAL GOVERNMENT
Hardcopy
\$4.00 + 0.75 12/1/65
ADVISORY
index

OCTOBER 1965

Distribution of this Document is Unlimited

AIR FORCE FLIGHT DYNAMICS LABORATORY
RESEARCH AND TECHNOLOGY DIVISION
AIR FORCE SYSTEMS COMMAND
WRIGHT-PATTERSON AIR FORCE BASE, OHIO

NOTICES

When Government drawings, specifications, or other data are used for any purpose other than in connection with a definitely related Government procurement operation, the United States Government thereby incurs no responsibility nor any obligation whatsoever; and the fact that the Government may have formulated, furnished, or in any way supplied the said drawings, specifications, or other data, is not to be regarded by implication or otherwise as in any manner licensing the holder or any other person or corporation, or conveying any rights or permission to manufacture, use, or sell any patented invention that may in any way be related thereto.

Copies of this report should not be returned to the Research and Technology Division unless return is required by security considerations, contractual obligations, or notice on a specific document.

CALCULATION OF LAMINAR SEPARATION WITH FREE INTERACTION BY THE METHOD OF INTEGRAL RELATIONS

PART I—TWO-DIMENSIONAL SUPERSONIC ADIABATIC FLOW

*JACK N. NIELSEN, LARRY L. LYNES, and
FREDERICK K. GOODWIN*

VIDYA DIVISION, ITEK CORPORATION

Distribution of this Document is Unlimited

FOREWORD

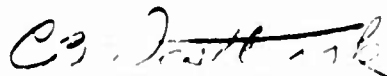
This report, "Calculation of Laminar Separation with Free Interaction by the Method of Integral Relations,"¹ represents the second technical report in an investigation of flow separation phenomena at hypersonic speeds carried out by the Vidya Division of the Itek Corporation, Palo Alto, California. It has been prepared under Contract No. AF 33(615)-1591, Project No. 8219, Task No. 821902. It is an expanded and extended version of a paper of the same title presented at the AIAA 2nd Aerospace Science Meeting in New York, January 25-27, 1965. The first report, numbered ASD-TDR-62-963, was performed under Contract No. AF 33(657)-7084 and was issued in November 1962.

Vidya is indebted to Dr. Douglas E. Abbott for his contributions during the initial stages of the work. Professor Maurice Holt's substantial contributions to the results are gratefully acknowledged. The authors are indebted to Mr. Morris W. Rubesin of Vidya for many helpful discussions.

The authors wish to thank Mr. Eugene Fleeman for his help, particularly for technical assistance in machine computations at Wright-Patterson Air Force Base.

This manuscript was released by the authors in June 1965, as an AFFDL Technical Report.

This technical report has been reviewed and is approved.



C. B. WESTBROOK, Chief
Control Criteria Branch
Flight Control Division

¹
This is Vidya Report No. 185.

ABSTRACT

Methods are presented for calculating the laminar boundary-layer flow through separation to reattachment under the influence of a prescribed pressure gradient or, in the case of a supersonic main stream, under the influence of "free interaction" between the boundary layer and the main flow. In contrast to the earlier work of the authors using the Tani method and quartic profiles, the present method is based on the Dorodnitsyn method of integral relations and uses a rational velocity profile which accounts properly for the separation singularity. As a result, the possibility of higher approximations is inherent in the method. The calculated solution for free interaction goes smoothly through the separation point and is in good agreement with certain features of the Navier-Stokes solution in the neighborhood of separation. Good agreement is exhibited between experimental and calculated pressure distributions up to reattachment for the several cases for which the comparisons were made. A computer program based on the work has been prepared for two-dimensional flow. It is planned to continue the work to cover nonadiabatic boundary layers and axisymmetric bodies.

TABLE OF CONTENTS

<u>Section</u>	<u>Page</u>
1. INTRODUCTION	1
2. GENERAL CONSIDERATIONS	3
2.1 Description of Problem	3
2.2 Assumptions	4
2.3 Partial Differential Equations and Boundary Conditions	4
2.3.1 Physical plane	4
2.3.2 Stewartson plane	6
2.3.3 Dorodnitsyn plane	7
3. REDUCTION OF INTEGRO-DIFFERENTIAL EQUATIONS TO ORDINARY DIFFERENTIAL EQUATIONS	9
3.1 Derivation of Integro-Differential Equations	9
3.2 Velocity Profiles	12
3.3 Integral Relations for Outer Flow	13
3.4 Integral Relation for the Inner Flow	16
3.5 Free-Interaction Equation	17
4. PRE-SEPARATION ANALYSIS, PRESCRIBED PRESSURE DISTRI- BUTION	19
4.1 Initial Conditions for Velocity Profile	19
4.2 Calculative Example	22
4.3 Comparison with Results of Leigh	23
4.4 Velocity Profiles at Separation	24
5. CALCULATIVE EXAMPLE FOR FREE INTERACTION	25
5.1 Initial Conditions	25
5.2 Other Parameters of Calculative Example	28
5.3 Behavior of the Solution in the Neighborhood of Separation	29
5.4 Adequacy of Boundary-Layer Theory in Neighborhood of Separation Point	32
5.5 Continuation of Solution Downstream of Separation	34
5.6 Asymptotic Behavior of Case C	37
5.7 Continuation of Solution to Reattachment Point	39
6. CALCULATIVE PROGRAM	41
6.1 General Aspects of Calculative Program	41
6.2 Assumptions of Calculative Program	43
6.3 Initial Conditions	43
6.4 Calculative Accuracy	46

TABLE OF CONTENTS (CONCLUDED)

<u>Section</u>	<u>Page</u>
7. SOME CALCULATIVE EXAMPLES	51
7.1 Systematic Calculations	51
7.2 Comparison Between Theory and Experiment	52
8. FLOW IN NEIGHBORHOOD OF REATTACHMENT POINT	53
9. CONCLUSIONS	56
10. RECOMMENDATIONS FOR FUTURE WORK	58
REFERENCES	60
TABLES I THROUGH V	61
FIGURES 1 THROUGH 24	68
APPENDIX I - CALCULATION OF g_n FUNCTIONS	98
APPENDIX II - DERIVATION OF FREE-INTERACTION RELATIONSHIP	99
DD FORM 1473	

TABLES

<u>Table</u>		<u>Page</u>
I.	CALCULATIVE VALUES TO ESTABLISH c_0, c_1, c_2, c_3 , FOR BLASIUS PROFILE.	61
II.	COMPARISON OF BLASIUS PROFILE WITH DORODNITSYN APPROXIMATION.	62
III.	VALUES OF c_0, c_1, c_2 , AND c_3 FOR CALCULATIVE EXAMPLE CORRESPONDING TO LEIGH CASE.	63
IV.	COMPARISON OF LEIGH PROFILE WITH PRESENT SOLUTION. (a) $X_s/l - X/l = 0.000142$.	64
IV.	CONCLUDED. (b) $X_s/l - X/l = 0.002542$.	65
V.	(a) COMPARISON OF DORODNITSYN, QUARTIC, AND SIMILARITY VELOCITY PROFILES AT SEPARATION.	66
V.	(b) COMPARISON OF DORODNITSYN AND QUARTIC VELOCITY PROFILE DERIVATIVES THROUGH THE BOUNDARY LAYER AT SEPARATION.	67

ILLUSTRATIONS

<u>Figure</u>	<u>Page</u>
1. Separated laminar supersonic flow over a flat plate with a ramp.	68
2. Domain of boundary value problem.	69
3. Variations of parameters in velocity profile for prescribed pressure distribution; pre-separation region.	70
4. Dimensions of example configuration.	71
5. Pre-separation pressure distributions for initial pressure disturbances of various magnitudes.	72
6. Variation of c_0 , c_1 , c_2 , and c_3 with axial distance.	73
7. Example velocity profiles given by Equation (36).	74
8. Behavior of c_0 , c_1 , c_2 , c_3 , going through separation point.	75
9. Sketches.	76
10. Comparison of various schemes for calculating post-separation pressure distributions.	77
11. Velocity parameters far downstream of separation on basis of various assumptions. (a) Velocity profiles.	78
11. Concluded. (b) Velocity gradients.	79
12. Downstream flow conditions developed asymptotically by solution for Case C.	80
13. Nondimensional velocity profiles developed asymptotically by solution for Case C.	81
14. Calculated flow pattern and pressure distribution in reattachment region.	82
15. Velocity distribution through the boundary layer in the region of the compression corner for Case C.	83
16. Flat plate with wedge with circular arc fairings of various radii.	84
17. Effect of fairing radius on calculated pressure distributions.	85

ILLUSTRATIONS (CONCLUDED)

<u>Figure</u>	<u>Page</u>
18. Effect of inner velocity profile approximation on calculated pressure distribution.	86
19. Effect of initial parameters on laminar separation with free interaction. (a) Reynolds number.	87
19. Continued. (b) Mach number.	88
19. Concluded. (c) Ratio of specific heats.	89
20. Comparison between measured and calculated pressure distributions for flat plate with 10° wedge. (a) $\alpha = 6^\circ$.	90
20. Continued. (b) $\alpha = 15^\circ$.	91
20. Concluded. (c) $\alpha = 16.7^\circ$.	92
21. Effect on calculated pressure distribution of systematic variations in beginning of interaction.	93
22. Variation with downstream distance of Oswatitsch reattachment angle and dividing streamline slope (relative to wedge).	94
23. Variation of Oswatitsch reattachment angle for different positions of beginning of interaction.	95
24. Variation of quantities along dividing streamline approaching reattachment. (a) Total pressure on dividing streamline.	96
24. Concluded. (b) Mach number on dividing streamline.	97

LIST OF SYMBOLS

a	local speed of sound
a_0	speed of sound at outer edge of boundary layer at x_0
a_1	speed of sound at outer edge of boundary layer for any value of x
B	illustrative function used in Equations (99) to (103)
c_0, c_1, c_2, c_3	coefficients specifying the velocity profile of the outer flow, Equation (36)
$\dot{c}_0, \dot{c}_1, \dot{c}_2, \dot{c}_3$	derivatives of velocity profile coefficients with respect to ξ
C	numerical constant in viscosity relationship, $\mu/\mu_0 = CT/T_0$
C_f	skin-friction coefficient
$f_n(\bar{u})$	family of smoothing functions, $(1 - \bar{u})^n$
f_s	value of f on $u = 0$ line
f'_s	$df/d\bar{u}$ at $\eta = \eta_s$
f_w	value of f at wall
f'_w	$df/d\bar{u}$ at $\eta = 0$
f'	$df/d\bar{u}$
f''	$d^2f/d\bar{u}^2$
$g_n(c_3)$	family of definite integrals given by Equation (43)
\dot{g}_n	dg_n/dc_3
j_k	series coefficients defined by Equation (I-6)
k	summation index
k_0, k_1, k_2, k_3	Dorodnitsyn coefficients for a Blasius velocity profile defined by Equation (57)
k_4, k_5	constants defined by Equation (75)
l	reference length, taken equal to x_0 , herein

l_1	axial length of compression corner, see Figure 4
L_b	distance from leading edge to end of wedge
L_c	length of flat plate prior to compression corner, see Figure 4
L_w	distance from leading edge to the beginning of wedge
m_0	$\left(\frac{\gamma - 1}{2}\right) \frac{u_0^2}{a_0^2}$
m_1	$\left(\frac{\gamma - 1}{2}\right) \frac{u_1^2}{a_1^2}$
M	local Mach number
M_D	Mach number along the dividing streamline
M_e	Mach number parallel to δ^* at edge of boundary layer
M_0	Mach number parallel to x-axis at edge of boundary layer at x_0
M_1	Mach number parallel to x-axis at edge of boundary layer for any value of x
M_∞	notation used in Reference 10 for the Mach number at the edge of the boundary layer, $M_\infty = M_1$
n	index
p	local static pressure
p_0	static pressure at x_0
p_t	local stagnation pressure
p_1	static pressure at edge of boundary layer for any value of x
$P_n(c_0, c_1, c_2, c_3)$	family of definite integrals given by Equation (44)
R	radius of compression corner
R_0	Reynolds number, $U_0 l / \nu_0$

$s(x)$	y-coordinate of $u = 0$ line between separation and reattachment
T	local absolute temperature
T_0	temperature at edge of boundary layer at $x = x_0$
T_t	local stagnation temperature
T_{t_0}	stagnation temperature at edge of boundary layer at x_0
T_1	temperature at edge of boundary layer at any value of x
T_∞	notation used in Reference 10 for the temperature at the edge of the boundary layer, $T_\infty = T_1$
u	axial velocity in x,y plane
$u_i(y)$	initial velocity profile at x_0
u_0	value of u at edge of boundary layer at x_0
$u_1(x)$	value of u at edge of boundary layer for any value of x
u_∞	notation used in Reference 10 for the velocity at the edge of the boundary layer, $u_\infty = u_1$
\bar{u}	U/U_1
$\bar{u}_i(\eta)$	value of \bar{u} at ξ_0
\bar{u}_s	symbol used to represent u component of velocity at the boundary between the inner and outer flow regions; it is always zero but the symbol is used for clarity
U	axial velocity in X,Y plane, ua_0/a_1
$U_i(Y)$	value of U at X_0 plane
U_0	value of U at edge of boundary layer for X_0
U_1	value of U at edge of boundary layer for any X
\dot{U}_1	$dU_1/d\xi$
v	normal velocity in x,y plane
v_s	value of v at $s(x)$

\bar{v}	normal velocity in ξ, η plane, $\frac{v}{U_1} \sqrt{\frac{U_0 l}{v_0}}$
\bar{v}_s	value of \bar{v} at η_s
V	normal velocity in X, Y plane
V_s	value of V at Y_s
$w(x)$	y-coordinate of solid surface
\bar{w}	$\bar{v} + \bar{u} \eta \frac{\dot{U}_1}{U_1}$
\bar{w}_s	value of \bar{w} at η_s
x_c	value of x where compression ramp begins
x_o	value of x where interaction begins
x_r	value of x downstream of reattachment point
x, y	coordinate of physical flow under consideration
x_R	value of x at the reattachment point
x_s	value of x at the separation point
x^*	axial distance used in Reference 10 and shown in Equation (90)
X_o	value of X corresponding to x_o
X_s	value of X at the separation point
X, Y	coordinates after Stewartson transformation, $X = \int_0^x \frac{\rho_1 a_1}{\rho_0 a_0} dx ; \quad Y = \int_{w(x)}^y \frac{\rho_1 a_1}{\rho_0 a_0} \frac{\rho}{\rho_1} dy$
Y_L	coordinate normal to wall used in Reference 6, and related to coordinates used herein by Equation (63)
Y_s	value of Y corresponding to $s(x)$
α_s	value of $\partial \bar{u} / \partial \eta$ at η_s
α_w	value of $\partial \bar{u} / \partial \eta$ at wall
$\dot{\alpha}_w$	value of $\partial^2 \bar{u} / \partial \eta \partial \xi$ at the wall

β_D	slope of the dividing streamline at separation, see Figure 9
β_u	slope of $u = 0$ line at the separation point, see Figure 9
γ	ratio of specific heats
δ^*	displacement thickness in physical plane, $\int_0^{\infty} \left(1 - \frac{\rho u}{\rho_1 u_1}\right) dy$
δ^{**}	momentum thickness in physical plane
δ_O^*	displacement thickness of outer flow
δ_I^*	displacement thickness of inner flow
δ_S^*	displacement thickness in the Stewartson plane, $\int_0^{\infty} \left(1 - \frac{U}{U_1}\right) dY$
δ_S^{**}	momentum thickness in the Stewartson plane, $\int_0^{\infty} \frac{U}{U_1} \left(1 - \frac{U}{U_1}\right) dY$
ϵ	a small value of ξ
ζ	defined by Equation (90)
$\eta_S(\xi)$	η -coordinate of the $u = 0$ line between separation and reattachment
λ_1, λ_2	constants defined by Equation (69)
μ	absolute viscosity
μ_O	absolute viscosity corresponding to x_O
ν	kinematic viscosity, μ/ρ
ν_O	kinematic viscosity at outer edge of boundary layer at x_O , $C\mu_O/\rho_O$
ν_1	value of ν at edge of boundary layer for any x
ν_{∞}	notation used in Reference 10 for the kinematic viscosity at edge of boundary layer, $\nu_{\infty} = \nu_1$

ξ_0	value of ξ corresponding to x_0
ξ_s	value of ξ at the separation point
ξ, η	coordinates of Dorodnitsyn plane, $\xi = \int_0^x \frac{U_1}{U_0} \frac{dx}{l}, \quad \eta = \frac{U_1}{U_0 l} \sqrt{\frac{U_0 l}{\nu_0}} y$
ρ	local mass density
ρ_0	value of ρ at edge of boundary layer at x_0
ρ_1	value of ρ at edge of boundary layer for any x
ρ_∞	notation used in Reference 10 for the value of ρ at edge of boundary layer, $\rho_\infty = \rho_1$
τ	shear stress at the wall
ϕ	slope of streamline outside of boundary layer
ϕ_0	value of ϕ at $x = x_0$
ϕ_1	value of ϕ at edge of boundary layer for any x
ψ	stream function, $\frac{\partial \psi}{\partial Y} = U$; $\frac{\partial \psi}{\partial X} = -v$ $\frac{\partial \psi}{\partial y} = \frac{\rho}{\rho_0} u; \quad \frac{\partial \psi}{\partial x} = -\frac{\rho}{\rho_0} v$
$\bar{\psi}$	mass flow in the boundary layer in the Dorodnitsyn plane, $\int_0^\eta \bar{u} d\eta$
ψ^*	stream function used in Reference 10 and shown in Equation (90)

CALCULATION OF LAMINAR SEPARATION WITH
FREE INTERACTION BY THE METHOD OF
INTEGRAL RELATIONS

PART I - TWO-DIMENSIONAL SUPERSONIC ADIABATIC FLOW

1. INTRODUCTION

This report deals with automatic computation studies which have been directed toward the calculation of laminar separated boundary-layer flows at subsonic and supersonic speeds. The objective of the present study is the development of a computer program for determining the viscous field including the separation and reattachment zones over flat plates with compression surfaces. In Reference 1, Abbott, Holt, and Nielsen developed a method for calculating such a flow field using the method of Tani and utilizing quartic velocity profiles. While the method predicted the experimental pressure distribution accurately up to separation and slightly beyond, it had definite limitations with regard to the region downstream of separation and with regard to cooled boundary layers. In Reference 2, Lees and Reeves used the method of Tani, together with similarity velocity profiles. In this report the authors abandon entirely the method of Tani and adopt the Dorodnitsyn method of integral relations of Reference 4.

The general approach of the foregoing methods is to make some plausible assumption regarding velocity profiles which is sufficient to reduce the integro-differential equations of the boundary layer to ordinary differential equations which can be readily solved numerically. For instance, in Reference 1, a one-parameter family of quartic profiles was used while in Reference 2, a one-parameter family of Stewartson reverse flow profiles was used. It seems that the critical factor determining the degree of success enjoyed by any one-parameter method for any particular case is the degree to which the assumed velocity profiles will fit the nonsimilar family of profiles which actually occurs.

However, a shortcoming of a one-parameter family of profiles in the existing methods is that they do not permit higher

approximations to the solution and thus do not permit assessment of how closely the assumed velocity profiles approximate the actual nonsimilar family of profiles. Another shortcoming is that one cannot expect a one-parameter family of velocity profiles to represent accurately all possible velocity profiles that can be developed in separated and attached flows.

In accordance with these critical remarks concerning one-parameter families of profiles, the method of the previous investigation (Ref. 1) has been completely abandoned and the Dorodnitsyn method of integral relations (Ref. 4) has been adopted. This method contains within its mathematical framework the possibility of carrying out higher approximations, and with the proper treatment of the singularities appears to contain the possibility of approximating exact solutions as closely as possible. In the present work a fourth approximation is used so that the velocity profile used in a four-parameter profile.

Among the questions to be discussed is the interesting one of whether the boundary-layer equations give an adequate representation of the flow in the neighborhood of the separation point, or whether the Navier-Stokes equations are required. Also, some light is shed on the question whether the concept of free interaction can be expected to apply with any degree of precision in the neighborhood of the separation and reattachment points. "Free interaction" implies that the body contour is increased by the boundary-layer displacement thickness when using inviscid supersonic flow theory to calculate the pressure distribution acting on the boundary layer.

2. GENERAL CONSIDERATIONS

2.1 Description of Problem

The problem under consideration is that of calculating accurately by automatic means laminar separated flows under the action of prescribed pressure gradients or under the influence of free interaction between the boundary layer and the supersonic outer flow. By "free interaction" we consider that the pressure distribution of the outer flow is the result of a mutual interaction between the boundary layer and the outer flow. The boundary layer, on the one hand, through its displacement thickness turns the outer flow; and the outer flow, on the other hand, through its pressure rise tends to thicken and separate the boundary layer.

Usually the boundary-layer equations are solved in a step-by-step integration as a straightforward parabolic boundary-value problem, despite the fact that pressure waves in the subsonic part of the boundary layer always make the boundary-value problem elliptic. In a sense it is a corollary of the free-interaction concept that the separated flow is independent of the direct influence of the downstream configuration. By this we mean that the downstream configuration cannot influence steady separated flow by means of upstream pressure waves, although it is thought that the downstream configuration actually fixes the position of separation in accordance with some reattachment criterion. The correct position of the separation point must be found by iteration in accordance with a reattachment criterion, and in this sense the boundary-value problem is elliptic. However, once the separation point has been specified, then solution of the boundary-layer equations including free-interaction is independent of the direct influence of the downstream configuration until the calculational marching procedure reaches the configuration.

The particular configuration which we will consider is shown in Figure 1. Herein a ramp induces separation on a flat plate and reattachment occurs on the ramp. This paper will present results for the pre-separation, post-separation, and reattachment

regions. The flow beneath the $u = 0$ line will be called the inner flow, and that above the $u = 0$ line, the outer flow.

With regard to the slopes of the compression surface, the assumption has been made that these are small so that the boundary-layer equations in a coordinate system parallel and perpendicular to the flat plate can be retained all the way to reattachment (see Fig. 1). The additional terms introduced into the boundary-layer equations in the reattachment region by not taking the vertical axis normal to the ramp are proportional to the slope of the ramp and are therefore negligible for small enough slopes.

2.2 Assumptions

A number of assumptions are made for the purpose of this paper.

(1) The governing equations are those for a compressible laminar boundary layer.

(2) The Prandtl number is unity.

(3) The air behaves as an ideal gas.

(4) The wall is adiabatic and at stagnation temperature.

(5) Within the range of interest the viscosity varies linearly with temperature.

(6) The pressure at the outer edge of the boundary layer is governed by the Prandtl-Meyer relationship.

(7) There is no upstream influence due to pressure waves in the boundary layer.

(8) A compression ramp with small slopes but otherwise of arbitrary shape induces separation of the boundary layer.

2.3 Partial Differential Equations and Boundary Conditions

2.3.1 Physical plane

The laminar boundary-layer equations being used are the usual ones.

$$\rho u \frac{\partial u}{\partial x} + \rho v \frac{\partial u}{\partial y} = - \frac{\partial p}{\partial x} + \frac{\partial}{\partial y} \left(\mu \frac{\partial u}{\partial y} \right) \quad (1)$$

$$\frac{\partial(\rho u)}{\partial x} + \frac{\partial(\rho v)}{\partial y} = 0 \quad (2)$$

The domain within which a solution to the boundary-layer equations is being sought is shown in Figure 2.

$$\text{Boundary A: } w(x) = 0; \quad x_0 \leq x \leq x_c \quad (3)$$

$$w(x) = \text{given function}; \quad x_c \leq x \leq x_r$$

$$\text{Boundary B: } x = x_0 \quad 0 \leq y \leq \infty$$

$$\text{Boundary C: } y = \infty \quad x_0 \leq x \leq x_r$$

The velocity boundary conditions are:

$$\text{Boundary A: } u = 0 \quad v = 0 \quad (4)$$

$$\text{Boundary B: } u = u_i(y)$$

$$u = u_0 \quad \text{at } y = \infty \quad (5)$$

$$\frac{\partial u}{\partial y} = 0 \quad \text{at } y = \infty$$

Boundary C: (a) Prescribed pressure distribution:

$$u = u_1(x) \quad (6)$$

$$u_1 = u_0 \quad \text{at } x = x_0$$

(b) Free interaction:

$$u_1 = u_0 \quad \text{at } x = x_0 \quad (7)$$

The pressure boundary conditions include the usual boundary-layer assumption that p depends only on x .

For prescribed pressure distribution:

$$p = p_1(x), \text{ a given function} \quad (8)$$

For free interaction:

$$p = p_0 \quad \text{at} \quad x = x_0 \quad (9)$$

The total temperature T_t is constant throughout the flow

$$T_t = T \left(1 + \frac{\gamma - 1}{2} M^2 \right) = T_{t_0} \quad (10)$$

2.3.2 Stewartson plane

In introducing the Stewartson transformation, Reference 3, we first make a nonlinear stretching in x and y to X and Y as follows:

$$X = \int_0^x \frac{\rho_1 a_1}{\rho_0 a_0} dx \quad Y = \int_{w(x)}^y \frac{\rho_1 a_1}{\rho_0 a_0} \cdot \frac{\rho}{\rho_1} dy \quad (11)$$

Under this transformation, it can be shown that Equations (1) and (2) transform to

$$U \frac{\partial U}{\partial X} + V \frac{\partial U}{\partial Y} = U_1 \frac{\partial U_1}{\partial X} + v_0 \frac{\partial^2 U}{\partial Y^2} \quad (12)$$

$$\frac{\partial U}{\partial X} + \frac{\partial V}{\partial Y} = 0 \quad (13)$$

where

$$U = u \frac{a_0}{a_1} \quad (14a)$$

$$V = \frac{p_0}{p_1} \left(\frac{a_0}{a_1} \right)^2 u \frac{\partial}{\partial x} \int_{w(x)}^y \frac{\rho_1 a_1}{\rho_0 a_0} \frac{\rho}{\rho_1} dy + \frac{p_0 a_0}{p_1 a_1} \frac{\rho}{\rho_0} v \quad (14b)$$

It is noted that the U profile is simply a uniform stretching or shortening of the u profile for a fixed value of x . The V profile is a nonlinear stretching or shortening of the v profile for fixed x .

Notice that the entire Boundary A goes into $Y = 0$ and Boundary C goes into $Y = \infty$. Boundary B goes into $X = X_0$. We thus have the velocity boundary conditions:

$$\text{Boundary A: } Y = 0 \quad U = 0 \quad V = 0 \quad (15)$$

$$\text{Boundary B: } X = X_0 \quad U = U_1(Y) \quad (16)$$

$$\text{Boundary C: } Y = \infty \quad U = U_1 = u_1 \frac{a_0}{a_1} \quad \frac{\partial U}{\partial Y} = 0 \quad (17)$$

2.3.3 Dorodnitsyn plane

Following Dorodnitsyn the physical coordinates ξ and η are introduced as follows:

$$\xi = \int_0^X \frac{U_1}{U_0} \frac{dX}{l}, \quad \eta = \frac{U_1}{U_0 l} \sqrt{\frac{U_0 l}{v_0}} Y \quad (18)$$

New velocity variables are introduced as follows:

$$\bar{u} = \frac{U}{U_1}, \quad \bar{v} = \frac{V}{U_1} \sqrt{\frac{U_0 l}{v_0}} \quad (19)$$

The partial differential equations then become

$$\left. \begin{aligned} \frac{\partial \bar{u}}{\partial \xi} + \frac{\partial}{\partial \eta} \left(\bar{v} + \bar{u} \eta \frac{\dot{U}_1}{U_1} \right) &= 0 \\ \bar{u} \frac{\partial \bar{u}}{\partial \xi} + \left(\bar{v} + \bar{u} \eta \frac{\dot{U}_1}{U_1} \right) \frac{\partial \bar{u}}{\partial \eta} &= \frac{\dot{U}_1}{U_1} (1 - \bar{u}^2) + \frac{\partial^2 \bar{u}}{\partial \eta^2} \end{aligned} \right\} (20)$$

Introducing the new variable

$$\bar{w} = \bar{v} + \bar{u} \eta \frac{\dot{U}_1}{U_1} \quad (21)$$

we have

$$\frac{\partial \bar{u}}{\partial \xi} + \frac{\partial \bar{w}}{\partial \eta} = 0 \quad (22a)$$

$$\bar{u} \frac{\partial \bar{u}}{\partial \xi} + \bar{w} \frac{\partial \bar{u}}{\partial \eta} = \frac{\dot{U}_1}{U_1} (1 - \bar{u}^2) + \frac{\partial^2 \bar{u}}{\partial \eta^2} \quad (22b)$$

The dot denotes differentiation with respect to ξ .

Under the Dorodnitsyn transformation, the velocity boundary conditions are transformed as follows:

$$\left. \begin{array}{l} \text{Boundary A: } \eta = 0; \quad \bar{u} = \bar{v} = \bar{w} = 0 \\ \text{Boundary B: } \xi = \xi_0; \quad \bar{u} = \bar{u}_i(\eta) \\ \text{Boundary C: } \eta = \infty; \quad \bar{u} = 1; \quad \frac{\partial \bar{u}}{\partial \eta} = 0 \end{array} \right\} \quad (23)$$

3. REDUCTION OF INTEGRO-DIFFERENTIAL EQUATIONS TO ORDINARY DIFFERENTIAL EQUATIONS

3.1 Derivation of Integro-Differential Equations

The scheme used to obtain solutions to the foregoing boundary-value problem is to derive from the system of partial differential equations given by Equation (22) a set of ordinary differential equations, the solution of which will be a close approximation to the exact solution. The possibility of increasing the accuracy of the approximation is also a feature specially being sought. The method of integral relations of Dorodnitsyn, Reference 4, seems to be one containing these features. For this purpose we derive the integro-differential equations for the inner and outer layer from which the ordinary differential equations are derived.

Let us first introduce a boundary $s(x)$ in the physical plane, Figure 1, which connects the separation point and reattachment point. Let u be zero along this line so that the direct flow and the reverse flow are separated into two regions called the outer and inner regions, respectively. Consider first the outer region in the Dorodnitsyn plane in which the boundary $s(x)$ transforms into $\eta_s(\xi)$. Introduce a family of smoothing functions $f_n(\bar{u})$ given as follows:

$$f_n(\bar{u}) = (1 - \bar{u})^n \quad (24)$$

Multiply the continuity equation (Eq. (22a)) by $f(\bar{u})$ and the momentum equation (Eq. (22b)) by $f'(\bar{u})$, add and integrate between η_s and ∞ to obtain

$$\int_{\eta_s}^{\infty} \frac{\partial}{\partial \xi} (f\bar{u}) d\eta + \int_{\eta_s}^{\infty} \frac{\partial}{\partial \eta} (f\bar{w}) d\eta = \int_{\eta_s}^{\infty} f' \frac{\dot{U}_1}{U_1} (1 - \bar{u}^2) d\eta + \int_{\eta_s}^{\infty} f' \frac{\partial^2 \bar{u}}{\partial \eta^2} d\eta \quad (25)$$

Let us now consider the velocity boundary conditions on the line $s(x)$ as it transforms into $Y_s(X)$ in the Stewartson plane and $\eta_s(\xi)$ in the Dorodnitsyn plane

$$\begin{aligned}
 s(x): \quad u &= 0 \\
 v_s &= -\frac{1}{\rho} \int_{w(x)}^s \frac{\partial(\rho u)}{\partial x} dy
 \end{aligned}
 \quad \left. \vphantom{\begin{aligned} s(x): \\ v_s \end{aligned}} \right\} \quad (26)$$

$$\begin{aligned}
 Y_s(x): \quad U &= 0 \\
 v_s &= \frac{p_0 a_0}{p_1 a_1} \frac{\rho(x, s)}{\rho_0} v_s \\
 Y_s &= \int_{w(x)}^{s(x)} \frac{\rho_1 a_1}{\rho_0 a_0} \frac{\rho}{\rho_1} dy
 \end{aligned}
 \quad \left. \vphantom{\begin{aligned} Y_s(x): \\ v_s \\ Y_s \end{aligned}} \right\} \quad (27)$$

$$\begin{aligned}
 \eta_s(\xi): \quad \bar{u} &= 0 \\
 \bar{v}_s &= \frac{v_s}{U_1} \sqrt{\frac{U_0 l}{\nu_0}} \\
 \bar{w}_s &= \bar{v}_s \\
 \eta_s &= \frac{U_1}{U_0 l} \sqrt{\frac{U_0 l}{\nu_0}} Y_s
 \end{aligned}
 \quad \left. \vphantom{\begin{aligned} \eta_s(\xi): \\ \bar{v}_s \\ \bar{w}_s \\ \eta_s \end{aligned}} \right\} \quad (28)$$

We can now show easily that

$$\begin{aligned}
 \int_{\eta_s}^{\infty} \frac{\partial}{\partial \xi} (f\bar{u}) d\eta &= \frac{d}{d\xi} \int_{\eta_s}^{\infty} f\bar{u} d\eta \\
 \int_{\eta_s}^{\infty} \frac{\partial}{\partial \eta} (f\bar{w}) d\eta &= -f_s \bar{v}_s \quad \text{since } f(\infty) = 0 \\
 \int_{\eta_s}^{\infty} f' \frac{\partial^2 \bar{u}}{\partial \eta^2} d\eta &= -f'_s \frac{\partial \bar{u}}{\partial \eta} \Big|_{\eta_s} - \int_{\eta_s}^{\infty} f'' \left(\frac{\partial \bar{u}}{\partial \eta} \right)^2 d\eta
 \end{aligned}
 \quad \left. \vphantom{\begin{aligned} \int_{\eta_s}^{\infty} \frac{\partial}{\partial \xi} (f\bar{u}) d\eta \\ \int_{\eta_s}^{\infty} \frac{\partial}{\partial \eta} (f\bar{w}) d\eta \\ \int_{\eta_s}^{\infty} f' \frac{\partial^2 \bar{u}}{\partial \eta^2} d\eta \end{aligned}} \right\} \quad (29)$$

Equation (25) thus becomes

$$\frac{d}{d\xi} \int_{\eta_s}^{\infty} f\bar{u} \, d\eta - f_s \bar{v}_s = \int_{\eta_s}^{\infty} f' \frac{\dot{U}_1}{U_1} (1 - \bar{u}^2) d\eta - f'_s \left. \frac{\partial \bar{u}}{\partial \eta} \right|_{\eta_s} - \int_{\eta_s}^{\infty} f'' \left(\frac{\partial \bar{u}}{\partial \eta} \right)^2 d\eta \quad (30)$$

This is the integro-differential equation of the outer flow.

With regard to inner flow, let us integrate between $\eta = 0$ and $\eta = \eta_s$ to obtain

$$\int_0^{\eta_s} \frac{\partial}{\partial \xi} (f\bar{u}) d\eta + \int_0^{\eta_s} \frac{\partial}{\partial \eta} (f\bar{w}) d\eta = \int_0^{\eta_s} f' \frac{\dot{U}_1}{U_1} (1 - \bar{u}^2) d\eta + \int_0^{\eta_s} f' \frac{\partial^2 \bar{u}}{\partial \eta^2} d\eta \quad (31)$$

It is then easy to see that

$$\frac{d}{d\xi} \int_0^{\eta_s} f\bar{u} \, d\eta + f_s \bar{v}_s = \int_0^{\eta_s} f' \frac{\dot{U}_1}{U_1} (1 - \bar{u}^2) d\eta + f'_s \left. \frac{\partial \bar{u}}{\partial \eta} \right|_{\eta_s} - f'_w \left. \frac{\partial \bar{u}}{\partial \eta} \right|_0 - \int_0^{\eta_s} f'' \left(\frac{\partial \bar{u}}{\partial \eta} \right)^2 d\eta \quad (32)$$

This is the integro-differential equation of the inner flow.

If we let $\partial \bar{u} / \partial \eta$ be a function only of \bar{u} , Equations (30) and (32) become

$$\frac{d}{d\xi} \int_{\bar{u}_s}^1 \frac{f\bar{u} \, d\bar{u}}{\frac{\partial \bar{u}}{\partial \eta}} - f_s \bar{v}_s = \int_{\bar{u}_s}^1 f' \frac{\dot{U}_1}{U_1} \frac{(1 - \bar{u}^2)}{\frac{\partial \bar{u}}{\partial \eta}} d\bar{u} - f'_s \left. \frac{\partial \bar{u}}{\partial \eta} \right|_{\bar{u}_s} - \int_{\bar{u}_s}^1 f'' \frac{\partial \bar{u}}{\partial \eta} d\bar{u} \quad (33)$$

$$\frac{d}{d\xi} \int_0^{\bar{u}_s} \frac{f\bar{u} \, d\bar{u}}{\frac{\partial \bar{u}}{\partial \eta}} + f_s \bar{v}_s = \int_0^{\bar{u}_s} f' \frac{\dot{u}_1}{u_1} \frac{(1 - \bar{u}^2) d\bar{u}}{\frac{\partial \bar{u}}{\partial \eta}} + f_s' \frac{\partial \bar{u}}{\partial \eta} \Big|_{\bar{u}_s} - f_w' \frac{\partial \bar{u}}{\partial \eta} \Big|_0 - \int_0^{\bar{u}_s} f'' \frac{\partial \bar{u}}{\partial \eta} d\bar{u} \quad (34)$$

Note that \bar{u}_s is zero but is retained in its notational form to indicate the integration of Equation (33) is from the $\bar{u} = 0$ line in the flow to $\bar{u} = 1$, while the integration of Equation (34) is between two lines on which $\bar{u} = 0$.

3.2 Velocity Profiles

The choice of velocity profiles is a critical item in the success of the present method. In Reference 4, Dorodnitsyn uses a representation for the velocity gradient $\partial \bar{u} / \partial \eta$ in terms of \bar{u} in such a fashion that if η_s is zero, the integrals in Equation (30) are all converted to integrals of \bar{u} with limits of 0 and 1. Consider only the outer flow and note the following:

$$\begin{aligned} \text{At } \eta = \infty: \quad & \bar{u} = 1 \quad \partial \bar{u} / \partial \eta = 0 \\ \text{At separation, } \eta = 0: \quad & u = 0 \quad \partial u / \partial \eta = 0 \end{aligned} \quad (35)$$

If we assume that the zero at $\bar{u} = 1$ is a simple zero, neither integral with $\partial \bar{u} / \partial \eta$ in the denominator will be divergent because the particular choice of smoothing function has a compensating zero in the numerator. However, if the zero at separation is a simple zero, then the integrals will be divergent. If we choose the zero in $\partial \bar{u} / \partial \eta$ at separation as a square root, the integrals will be convergent. Also, this form is compatible with the fact that $d\bar{u} / d\eta$ is a double-valued function of \bar{u} just downstream of separation. Accordingly, we choose the following form for the velocity profile for the outer flow:

$$\frac{\partial \bar{u}}{\partial \eta} = \frac{(1 - \bar{u}) \sqrt{\bar{u} + c_3}}{c_0 + c_1 \bar{u} + c_2 \bar{u}^2 \dots} \quad (36)$$

In this formulation $c_0, c_1, c_2, c_3, \dots$ are taken as functions of ξ only. Equation (36) is introduced in Equation (33) and as many of the $f_n(\bar{u})$ smoothing functions are used as there are c 's. Since the known singularities are explicitly exhibited and the "smooth part" is represented by a Taylor series, the accuracy of the approximation should increase as the number of terms in the series is increased.

With regard to the inner flow, there is a zero of $\partial\bar{u}/\partial\eta$ at the point of maximum velocity in the reverse flow. This zero causes divergent integrals in Equation (34). Accordingly, Equation (32) will be used for the inner flow since it will not be divergent if \bar{u} is expanded in a power series in η in the usual way. Let us consider the following boundary conditions for the inner flow:

$$\left. \begin{array}{lll} \eta = 0 & \bar{u} = 0 & \frac{\partial\bar{u}}{\partial\eta} = \alpha_w \\ \eta = \eta_s & \bar{u} = 0 & \frac{\partial\bar{u}}{\partial\eta} = \alpha_s \end{array} \right\} \quad (37)$$

The velocity can then be written as a cubic equation

$$\bar{u} = \alpha_w \eta - \frac{(2\alpha_w + \alpha_s)}{\eta_s} \eta^2 + \frac{(\alpha_w + \alpha_s)}{\eta_s^2} \eta^3 \quad (38)$$

3.3 Integral Relations for Outer Flow

In the following work we will use a fourth approximation for the outer flow so that four ordinary differential equations for $c_0, c_1, c_2,$ and c_3 will be required. Through the use of Equations (24), (33), and (36), we obtain

$$\begin{aligned}
\frac{d}{d\xi} \int_0^1 \frac{(1-\bar{u})^{n-1} \bar{u}}{\sqrt{\bar{u} + c_3}} (c_0 + c_1 \bar{u} + c_2 \bar{u}^2) d\bar{u} - \bar{v}_s \\
= \frac{\dot{u}_1}{u_1} \int_0^1 \frac{n(1-\bar{u})^{n-1} (1+\bar{u})}{\sqrt{\bar{u} + c_3}} (c_0 + c_1 \bar{u} + c_2 \bar{u}^2) d\bar{u} - \frac{n\sqrt{c_3}}{c_0} \\
- \int_0^1 \frac{n(n-1)(1-\bar{u})^{n-1} \sqrt{\bar{u} + c_3}}{c_0 + c_1 \bar{u} + c_2 \bar{u}^2} d\bar{u} \quad (39)
\end{aligned}$$

It is to be noted that all the integrals are tractable. If a fifth approximation were used, the last integral would contain a cubic in the denominator, and the definite integrals would involve elliptic integrals. If higher approximations than the fourth are desired, it is probably a practical necessity to evaluate the integral by numerical means rather than analytical means.

To obtain \bar{v}_s we make use of the inner flow velocity profile. From continuity we can write

$$\bar{v}_s = \bar{w}_s = - \frac{d}{d\xi} \int_0^{\eta_s} \bar{u} d\eta \quad (40)$$

Substituting \bar{u} from Equation (38) yields for \bar{v}_s

$$\bar{v}_s = \frac{1}{12} \frac{d}{d\xi} \left[\eta_s^2 (\alpha_s - \alpha_w) \right] \quad (41)$$

wherein from Equations (36) and (37)

$$\alpha_s = \frac{\sqrt{c_3}}{c_0} \quad (42)$$

since $\partial \bar{u} / \partial \eta$ is to be continuous across the $\bar{u} = 0$ line.

Let us define two families of definite integrals encountered in Equation (39) by the following notation:

$$g_n(c_3) = \int_0^1 \frac{\bar{u}^n}{\sqrt{\bar{u} + c_3}} d\bar{u} \quad (43)$$

$$P_n(c_0, c_1, c_2, c_3) = \int_0^1 \frac{\bar{u}^n \sqrt{\bar{u} + c_3} d\bar{u}}{c_0 + c_1 \bar{u} + c_2 \bar{u}^2} \quad (44)$$

Formulas for evaluating $g_n(c_3)$ are derived in Appendix I. The P_n integrals are evaluated numerically because of the numerous subcases in the analytical integration. A set of four equations for c_0 , c_1 , c_2 , and c_3 is obtained from Equation (39) for the four smoothing functions with $n = 1, 2, 3$, and 4 . This set can be somewhat simplified by addition or subtraction of the four equations to yield the following set:

$$g_1 \dot{c}_0 + g_2 \dot{c}_1 + g_3 \dot{c}_2 + (c_0 \dot{g}_1 + c_1 \dot{g}_2 + c_2 \dot{g}_3) \dot{c}_3 + [c_0 g_0 + (c_0 + c_1) g_1 + (c_1 + c_2) g_2 + c_2 g_3] \frac{\dot{U}_1}{U_1} - \bar{v}_s = \frac{\sqrt{c_3}}{c_0} \quad (45)$$

$$g_2 \dot{c}_0 + g_3 \dot{c}_1 + g_4 \dot{c}_2 + (c_0 \dot{g}_2 + c_1 \dot{g}_3 + c_2 \dot{g}_4) \dot{c}_3 - [c_0 g_0 + (c_1 - c_0) g_1 + (c_2 - c_1 - 2c_0) g_2 - (2c_1 + c_2) g_3 - 2c_2 g_4] \frac{\dot{U}_1}{U_1} = -\frac{\sqrt{c_3}}{c_0} + 2(P_0 - P_1) \quad (46)$$

$$g_3 \dot{c}_0 + g_4 \dot{c}_1 + g_5 \dot{c}_2 + (c_0 \dot{g}_3 + c_1 \dot{g}_4 + c_2 \dot{g}_5) \dot{c}_3 + [-2c_0 g_1 - (2c_1 - c_0) g_2 + (3c_0 + c_1 - 2c_2) g_3 + (3c_1 + c_2) g_4 + 3c_2 g_5] \frac{\dot{U}_1}{U_1} = -2P_0 + 8P_1 - 6P_2 \quad (47)$$

$$\begin{aligned}
& g_4 \dot{c}_0 + g_5 \dot{c}_1 + g_6 \dot{c}_2 + (c_0 \dot{g}_4 + c_1 \dot{g}_5 + c_2 \dot{g}_6) \dot{c}_3 - \left[+3c_0 g_2 \right. \\
& \left. + (-c_0 + 3c_1) g_3 + (3c_2 - c_1 - 4c_0) g_4 - (c_2 + 4c_1) g_5 - 4c_2 g_6 \right] \frac{\dot{U}_1}{U_1} \\
& \qquad \qquad \qquad = -6P_1 + 18P_2 - 12P_3
\end{aligned} \tag{48}$$

In Equation (45) the value of \bar{v}_s evaluated using Equation (41) is

$$\bar{v}_s = \left(\frac{\sqrt{c_3}}{6c_0} - \frac{\alpha_w}{6} \right) \eta_s \dot{\eta}_s + \frac{\eta_s^2 \dot{c}_3}{24c_0 \sqrt{c_3}} - \frac{\eta_s^2 \sqrt{c_3}}{12c_0^2} \dot{c}_0 - \frac{\eta_s^2}{12} \dot{\alpha}_w \tag{49}$$

It is noted that Equations (45) to (49) are a simultaneous set of linear ordinary differential equations for c_0 , c_1 , c_2 , c_3 , and U_1 . For a prescribed pressure distribution U_1 is known, and Equations (45) to (48) are adequate for evaluating the boundary-layer flow up to separation. When free interaction is assumed, an additional equation is required.

3.4 Integral Relation for the Inner Flow

Equation (32) for the inner layer involves a finite range of integration and contains no singularities. No particular advantage occurs, therefore, in transforming to \bar{u} from η . In fact divergent integrals are so introduced. Furthermore, there is no necessity to use the same smoothing functions used for the outer flow. However, it is convenient to use $1 - \bar{u}$ as the smoothing function in Equation (32), which now becomes

$$\frac{d}{d\xi} \int_0^{\eta_s} (1 - \bar{u}) \bar{u} \, d\eta + \bar{v}_s = - \int_0^{\eta_s} \frac{\dot{U}_1}{U_1} (1 - \bar{u}^2) \, d\eta - (\alpha_s - \alpha_w) \tag{50}$$

Through Equation (40) we further simplify to

$$-\frac{d}{d\xi} \int_0^{\eta_s} \bar{u}^2 d\eta = -\frac{\dot{U}_1}{U_1} \int_0^{\eta_s} (1 - \bar{u}^2) d\eta - (\alpha_s - \alpha_w) \quad (51)$$

Carrying out the integrations yields the inner flow equation

$$\begin{aligned} & \frac{\sqrt{c_3} \eta_s^3}{c_o^2} \left(\frac{2}{105} \frac{\sqrt{c_3}}{c_o} - \frac{\alpha_w}{70} \right) \dot{c}_o - \frac{\eta_s^3}{c_o \sqrt{c_3}} \left(\frac{\sqrt{c_3}}{105 c_o} - \frac{\alpha_w}{140} \right) \dot{c}_3 \\ & - \eta_s^2 \left(\frac{\alpha_w^2}{35} - \frac{3\alpha_w \sqrt{c_3}}{70 c_o} + \frac{c_3}{37 c_o^2} \right) \dot{\eta}_s - \eta_s^3 \left(\frac{2\alpha_w}{105} - \frac{\sqrt{c_3}}{70 c_o} \right) \dot{\alpha}_w \\ & + \eta_s \left[1 - \eta_s^2 \left(\frac{\alpha_w^2}{105} - \frac{\alpha_w \sqrt{c_3}}{70 c_o} + \frac{c_3}{105 c_o^2} \right) \right] \frac{\dot{U}_1}{U_1} = \alpha_w - \frac{\sqrt{c_3}}{c_o} \end{aligned} \quad (52)$$

3.5 Free-Interaction Equation

The free-interaction equation is one relating the axial pressure gradient to the rate of increase of the boundary-layer displacement thickness. The increase in $d\delta^*/dx$ turns the external flow causing a pressure rise. The pressure rise tends to cause further increases in δ^* . We will assume that the pressure distribution is related to the turning angle ϕ of the external flow by the Prandtl-Meyer relationship for inviscid compressible two-dimensional flow.

$$\frac{dp_1}{p_1} = \frac{\gamma M_1^2 d\phi}{\cos \phi \sqrt{M_1^2 - \cos^2 \phi}} \quad (53)$$

The turning angle ϕ is determined by the slope dw/dx of the boundary and the slopes $d\delta_o^*/dx$ and $d\delta_i^*/dx$ due to the displacement thickness of the outer and inner flows. The relationship is

$$\frac{d\delta_o^*}{dx} + \frac{d\delta_i^*}{dx} + \frac{dw}{dx} = \tan \phi \quad (54)$$

It is Equations (53) and (54) together which govern free interaction between the outer flow and the boundary layer. The values of the boundary-layer terms in Equation (54) are derived in Appendix II for the assumed profiles.

4. PRE-SEPARATION ANALYSIS, PRESCRIBED PRESSURE DISTRIBUTION

In order to see how accurately the present method will predict nonsimilar velocity profiles in the face of an adverse pressure gradient, it would be desirable to compare it with some solution of known accuracy. A suitable example for comparative purposes is given in the work of Hartree and of Leigh, References 5 and 6. These particular numerical solutions apply to an incompressible laminar boundary layer in which the main stream produces a pressure gradient with a free-stream velocity given by

$$\frac{U_1(X)}{U_0(X)} = 1 - \frac{X}{8\ell} \quad (55)$$

We will now apply Equations (45) to (48) to the solution of this problem, and then make a comparison with the previous numerical solutions. The proper initial conditions for this solution are the values of c_0 , c_1 , c_2 , and c_3 which best represent the Blasius profile.

4.1 Initial Conditions for Velocity Profile

It is necessary to specify an initial velocity profile in the ξ, η plane. The initial conditions are specified at some point ξ_0 in front of the separation point, and for $\xi < \xi_0$, it is assumed that the static pressure is constant. In a real flow, interaction starts at the leading edge. However, we will not start the solution at $\xi = 0$ in order to avoid the leading-edge problem associated with infinite shear. The initial velocity profile in the ξ, η plane under the assumed condition will be the Blasius profile. In cases where induced pressure gradients do occur at the leading edge of a plate, the effects of the pressure gradients on the velocity profile will diminish as the downstream distance increases, and the profile will approach the Blasius profile.

Let us consider the analog of the Blasius solution in the Dorodnitsyn plane. The equations in the X, Y plane are those

for incompressible laminar flow. For such flow with no pressure gradient, we have

$$\begin{aligned} U_0 &= U_1 = \text{constant} \\ \rho_0 &= \rho_1 = \text{constant} \\ x &= X, \quad u_1 = U_1, \quad \xi = \frac{X}{\ell} \end{aligned} \quad (56)$$

$$Y = \int_0^Y \frac{\rho}{\rho_1} dy$$

$$\eta = \frac{1}{\ell} \sqrt{\frac{U_0 \ell}{\nu_0}} Y$$

With these relationships the Blasius profile can now be developed using Equations (45) to (48) provided a suitable set of initial conditions are found for these equations. However, the suitable initial profile is the Blasius profile itself. We overcome this dilemma by noting that a laminar boundary layer on a flat plate with no pressure gradient will develop the Blasius profile asymptotically even if the initial conditions vary substantially from the Blasius profile. Accordingly, a rough approximation to the values of c_0 , c_1 , c_2 , and c_3 for the Blasius profile was used for the initial conditions, and the true Blasius profile was sought asymptotically.

The question arises how the asymptotic profile will be recognized in the computed results. We note that the similarity of the Blasius profile states that, for constant Reynolds number in the free stream, the value of Y for a given value of \bar{u} increases as $X^{1/2}$. For the slope $\partial \bar{u} / \partial \eta$, we can thus write asymptotically

$$\frac{\partial \bar{u}}{\partial \eta} = \frac{\ell}{\sqrt{\frac{U_0 \ell}{\nu_0}}} \frac{\partial \bar{u}}{\partial Y} \sim \frac{1}{\sqrt{\xi}}$$

The only way that the desired result can be approached is if

$$\frac{c_0}{\sqrt{\xi}} \rightarrow k_0, \quad \frac{c_1}{\sqrt{\xi}} \rightarrow k_1, \quad \frac{c_2}{\sqrt{\xi}} \rightarrow k_2, \quad c_3 \rightarrow k_3 \quad (57)$$

as $\xi \rightarrow \infty$.

In Table I the initial values of c_0 , c_1 , c_2 , and c_3 are shown and the above ratios are tabulated as a function of ξ to see if a similar solution is developing. It is seen that a similar solution does develop with the following approximate values

$$k_0 = 3.157, \quad k_1 = -1.923, \quad k_2 = -0.3133, \quad c_3 = 1.1000$$

It now remains to compare the profile obtained this way with the Blasius profile. For this purpose we solve Equation (36),

$$\frac{\eta}{\sqrt{\xi}} = Y \sqrt{\frac{U_0}{X v_0}} = \int_0^{\bar{u}} \frac{k_0 + k_1 \bar{u} + k_2 \bar{u}^2}{(1 - \bar{u}) \sqrt{\bar{u} + c_3}} d\bar{u} \quad (58)$$

In this way the value of η for a given \bar{u} can be readily calculated. The velocity gradients vary as $\xi^{1/2}$ so that we have

$$\frac{\partial \left(\frac{U}{U_0} \right)}{\partial \left(Y \sqrt{\frac{U_0}{v_0 X}} \right)} = \sqrt{\xi} \frac{\partial \bar{u}}{\partial \eta} = \frac{(1 - \bar{u}) \sqrt{\bar{u} + c_3}}{k_0 + k_1 \bar{u} + k_2 \bar{u}^2} \quad (59)$$

The values of the velocity profile and its derivative as calculated by the preceding equations are tabulated together with those of Blasius in Table II. The Blasius values are from Reference 7, page 107. From the table it can be seen that for a given value of Y , the values of \bar{u} do not differ by more than 0.002. This accuracy is considered adequate for specifying the initial velocity profile.

The skin friction calculated from the present results is a close approximation to that obtained by the Blasius formula. We thus have

$$\begin{aligned}
 \tau &= \mu_o \left. \frac{\partial U}{\partial Y} \right|_w = \mu_o U_o \sqrt{\frac{U_o}{\nu_o X}} \frac{\partial \bar{u}}{\partial \left(Y \sqrt{\frac{U_o}{X \nu_o}} \right)} \\
 &= \nu_o \rho_o U_o^2 \frac{1}{\sqrt{\nu_o X U_o}} \frac{\sqrt{c_3}}{k_o} \\
 &= 0.332 \rho_o U_o^2 \sqrt{\frac{\nu_o}{U_o X}} \quad (60)
 \end{aligned}$$

4.2 Calculative Example

Utilizing the initial values shown in Table III, a numerical calculation has been made for a pressure gradient prescribed by

$$\frac{U_1}{U_o} = 1 - \frac{1}{8} \frac{X}{l} \quad (61)$$

Under this pressure gradient, we find

$$\xi = \left(\frac{X}{l} \right) - \frac{1}{16} \left(\frac{X}{l} \right)^2 \quad (62)$$

The initial conditions are

$$\xi_o = 0.010000$$

$$\frac{X_o}{l} = 0.010006$$

$$c_o = 3.157 \sqrt{\xi_o} = 0.3157$$

$$c_1 = -1.923 \sqrt{\xi_o} = -0.1923$$

$$c_2 = -0.3133 \sqrt{\xi_o} = -0.3133$$

$$c_3 = 1.1000$$

Starting the solution at $\xi = 0.01$ rather than $\xi = 0$ could influence slightly the value of ξ for separation, but its effect on the actual velocity profile near separation will be unimportant.

The values of c_0 , c_1 , c_2 , and c_3 for this case are tabulated in Table III and plotted in Figure 3 versus axial distance. The separation point occurs where c_3 goes to zero. This value of X_s/l obtained by running the solution on a fine interval near separation is found to be

$$\frac{X_s}{l} = 0.9627$$

This compares very well with the value given by Leigh of

$$\frac{X_s}{l} = 0.958542 \pm 0.000002$$

4.3 Comparison with Results of Leigh

Leigh has presented tabulated velocity profiles for small distances upstream of separation but not at separation itself since his numerical methods did not go through to separation. His positions are as follows:

$$\frac{X_s}{l} - \frac{X}{l} = 0.000142, 0.000542, 0.001542, 0.002542$$

The calculated values of c_0 , c_1 , c_2 , and c_3 are tabulated versus X/l in Table III, and velocity profiles for comparison with those of Leigh are presented in Table IV. It is seen that the results for \bar{u} agree with those of Leigh to about 0.002. We can therefore conclude that the method of integral relationships is yielding excellent approximations to the true velocity profiles for this test case. We can also approach other cases of separation with some degree of assurance that our four-parameter family of velocity profiles will yield a close fit. We can, of course, increase the accuracy by going to a fifth-order approximation.

In comparing our results with those of Leigh we note that the coordinate Y_L of Leigh normal to the wall is related to our coordinates as follows:

$$\eta = Y_L \left(1 - \frac{1}{8} \frac{X_s}{\ell} \right) \quad (63)$$

4.4 Velocity Profiles at Separation

The point was made in the Introduction that a one-parameter family of profiles cannot be expected to represent accurately all possible profiles occurring in separated and attached flows. For instance, one cannot expect all profiles with zero wall shear to reduce to a universal function when considered in the nondimensional form of U/U_1 versus Y/δ^* . Yet, quartic profiles and similarity profiles each yield such universal functions for zero shear, and such universal profiles would be expected to be an accurate representation of the separation profile in all cases including the present calculative example. Since we have shown that the present calculated profile at separation is very accurate, we can use it as a standard of comparison in this particular case. Accordingly, a comparison has been made between the Dorodnitsyn separation profile and the corresponding quartic and similarity profiles in Table V. The Dorodnitsyn profile is accurate to 0.002 in U/U_1 for a given value of Y/δ^* . The quartic profile differs from the accurate result by as much as 0.030. The corresponding figure for the similarity profile is 0.016. These errors apply, of course, only to the Hartree-Leigh case.

The slopes of the velocity profiles are compared for the present calculative case and the quartic case in Table V(b). Substantial errors in slope occur within the boundary layer for the quartic case.

5. CALCULATIVE EXAMPLE FOR FREE INTERACTION

It is now of interest to investigate separated flows under the assumption of free interaction. This will be done first for the pre-separation region, then the post-separation region, and finally the reattachment region. Some particularly interesting results around the separation point will be examined. For the purposes of illustration we have selected a case for which data are available. The configuration for the calculative example is shown in Figure 4.

5.1 Initial Conditions

In addition to the initially prescribed velocity profile, it is necessary to prescribe some initial condition on pressure for the free-interaction equation. The initial condition should be such that a small disturbance will initiate the free interaction which results in the development of a separated flow. Attempts were made to initiate such an interaction by perturbing the velocity profile, by specifying a value of \dot{U}_1 , and by perturbing p_1 . It was found that a small perturbation in the value of p_1 was a satisfactory way to induce separation, and that, as the perturbation became small, the pressure distribution tended to approach a limit.

To determine the change in U_1 accompanying a prescribed increment in p_1 let us first write for the main stream in the compressible plane

$$dp_1 = -\rho_1 u_1 du_1$$

or

$$\frac{dp_1}{p_1} = -\gamma M_1^2 \frac{du_1}{u_1} \quad (64)$$

We now utilize the constancy of the stagnation temperature together with the relationship

$$U_1 = \frac{u_1 a_0}{a_1} \quad (65)$$

to establish the equation

$$\frac{dU_1}{U_1} = \left(1 + \frac{\gamma - 1}{2} M_1^2\right) \frac{du_1}{u_1} \quad (66)$$

Accordingly we obtain the desired relationship

$$\frac{dU_1}{U_1} = - \frac{1 + \frac{\gamma - 1}{2} M_1^2}{\gamma M_1^2} \frac{dp_1}{p_1} \quad (67)$$

giving the change in the initial value of U_1 to induce a prescribed change dp_1/p_1 .

In addition we must specify a value of ϕ_0 for the free-interaction equation. The free-interaction equation can be written

$$\tan \phi_0 = \left. \frac{d\delta^*}{dx} \right|_{x_0} \quad (68)$$

It is convenient to determine this quantity in the Stewartson plane where the displacement thickness δ_S^* and the momentum thickness δ_S^{**} are given for no pressure gradient by

$$\left. \begin{aligned} \delta_S^* &= \lambda_1 \sqrt{\frac{v_0 X}{U_0}}, & \lambda_1 &= 1.73 \\ \delta_S^{**} &= \lambda_2 \sqrt{\frac{v_0 X}{U_0}}, & \lambda_2 &= 0.664 \end{aligned} \right\} \quad (69)$$

where λ_1 and λ_2 are taken from Reference 7. From Appendix II, we can show that, in general,

$$\delta^* = \frac{\rho_0 a_0}{\rho_1 a_1} \left[(1 - m_1) \int_0^\infty \left(1 - \frac{U}{U_1}\right) dY + m_1 \int_0^\infty \frac{U}{U_1} \left(1 - \frac{U}{U_1}\right) dY \right] \quad (70)$$

and in this case

$$\delta^* = (1 + m_0)\lambda_1 \sqrt{\frac{v_0 X}{U_0}} + m_0 \lambda_2 \sqrt{\frac{v_0 X}{U_0}} \quad (71)$$

and $x = X$.

We thus have for the initial value of ϕ_0

$$\tan \phi_0 = \sqrt{\frac{\ell}{x_0}} \frac{1}{\sqrt{\frac{U_0 \ell}{v_0}}} \left[\frac{\lambda_1}{2} + m_0 \left(\frac{\lambda_1 + \lambda_2}{2} \right) \right] \quad (72)$$

A series of runs were made to see how the interaction pressure distribution behaved as the magnitude of Δp_1 applied to the boundary layer at x_0/ℓ was reduced. The following set of initial values was used:

p_1/p_0	1.001039	1.01	1.02012	1.039251
R_0	48000	48000	48000	48000
M_0	2.7	2.7	2.7	2.7
γ	1.4	1.4	1.4	1.4
x_0/ℓ	1	1	1	1
ξ_0	1	1	1	1
c_0	3.157	3.157	3.157	3.157
c_1	-1.923	-1.923	-1.923	-1.923
c_2	-0.3133	-0.3133	-0.3133	-0.3133
c_3	1.1000	1.1000	1.1000	1.1000
U_1/U_0	0.9997500	0.9976041	0.9952046	0.9907388
ϕ_0	0.011872	0.011872	0.011872	0.011872
M_1	2.69932	2.69353	2.68705	2.67499

The free-interaction pressure distributions accompanying the various pressure impulses are shown in Figure 5. The results are readily plotted against $(x - x_0)/x_0$ where x_0 is the point

of the beginning of interaction. The separation pressure ratio is indicated by the points. It is clear that the pressure distributions are approximately parallel to each other by the amount of the initial impulse with little change in the position of separation. Also, the distributions appear to tend toward a limit as the impulse approaches zero. Apart from the question of the existence of a limit, a pressure impulse of one-tenth of a percent is considered small for the present purposes and is used henceforth to initiate interaction.

5.2 Other Parameters of Calculative Example

A calculative example has been made for the CS.25⁰-1 model of Reference 8 for which laminar data are available in Figure 17 of that report. The following initial conditions were used in the calculation:

$$R_o = 39000, \quad M_o = 2.70, \quad \frac{x_o}{l} = 1.000, \quad \xi_o = 1.000, \quad \frac{p_1}{p_o} = 1.001$$

The value of l is taken as the distance from the start of the boundary layer to the onset of free-interaction in the calculative example. For this case we have taken the reference length to be

$$\frac{l}{L_c} = 0.238$$

where L_c is given in Figure 4. The free-interaction was started at the known experimental location since the objective in this case is not to predict the separation point from some reattachment criterion but to test the adequacy of the free-interaction theory to explain the observed pressure distribution.

The initial conditions are

$$\frac{x_o}{l} = 1.000, \quad \xi_o = 1.000$$

$$c_o = 3.157, \quad c_1 = -1.923, \quad c_2 = -0.3133, \quad c_3 = 1.1000$$

$$\frac{U_1}{U_0} = 0.99975, \quad \phi_0 = 0.01317$$

The calculation proceeded without any difficulty and generated the variation of c_0 , c_1 , c_2 , and c_3 with x shown in Figure 6. The variations downstream of separation will subsequently be discussed. The comparison of the calculated pressures with the experimental ones up to the separation point shown in Figure 10 is considered good. It appears that the assumption of free interaction is a valid one up to separation.

5.3 Behavior of the Solution in the Neighborhood of Separation

One point of particular interest is the nature of the singularity at the separation point, and the manner in which the free-interaction theory copes with this singularity. The solution which goes smoothly through the separation point is one based on Equations (45) to (48) and the free-interaction relationship. Equations (45) to (48) have no discontinuities at separation but the free-interaction equation does.

Consider the free-interaction equation

$$\frac{R_0^{1/2}}{1 + m_0} \left(\frac{d\delta_0^*}{dx} + \frac{d\delta_1^*}{dx} \right) = \frac{R_0^{1/2} \tan \phi}{1 + m_0} \quad (73)$$

where the two terms on the left-hand side are given by Equations (II-10) and (II-15) of Appendix II. In crossing the separation point the right-hand term is continuous. Equation (II-15) contributes a discontinuous term $\dot{\eta}_s$ on the left-hand side. However, an equal and opposite discontinuity is contributed in the $\dot{c}_3 c_0 \dot{g}_0$ term of Equation (II-10) so that equality is maintained. The singularity in the $\dot{c}_3 c_0 \dot{g}_0$ term arises from \dot{g}_0 since

$$g_0 = 2 \left(\sqrt{1 + c_3} - \sqrt{c_3} \right) \quad (74)$$

and, therefore,

$$\dot{g}_o = -\frac{1}{\sqrt{c_3}} + \frac{1}{\sqrt{1+c_3}}$$

Since c_3 is zero at separation, \dot{g}_o is infinite. If in the neighborhood of the separation point, we write

$$\begin{aligned}\eta_s &= k_5 (\xi - \xi_s) \\ c_3 &= k_4 (\xi - \xi_s)^2\end{aligned}\tag{75}$$

we readily obtain across the separation point

$$\dot{\eta}_s = k_5 = \lim_{\epsilon \rightarrow 0} \left[(\dot{c}_3 c_o \dot{g}_o)_{\xi_s - \epsilon} - (\dot{c}_3 c_o \dot{g}_o)_{\xi_s + \epsilon} \right]\tag{76}$$

$$\dot{\eta}_s = k_5 = 4c_o \sqrt{k_4}\tag{77}$$

We have thus determined the slope of the $\bar{u} = 0$ line at separation.

Another relationship is needed in addition to those utilized upstream to carry out the integrations downstream of the separation point. It will now be shown that this relationship, compatible with Equation (77), is the continuity of the second derivatives of the velocity profiles at the $\bar{u} = 0$ line. If we use a quadratic for the inner velocity profile we can expand the velocity profile about the $\bar{u} = 0$ line as follows:

$$\bar{u} = \left. \frac{\partial \bar{u}}{\partial \eta} \right|_{\eta_s} (\eta - \eta_s) + \frac{1}{2} \left. \frac{\partial^2 \bar{u}}{\partial \eta^2} \right|_{\eta_s} (\eta - \eta_s)^2\tag{78}$$

where the derivatives evaluated from the outer profile are

$$\left. \frac{\partial \bar{u}}{\partial \eta} \right|_{\eta_s} = \frac{\sqrt{c_3}}{c_o}, \quad \left. \frac{\partial^2 \bar{u}}{\partial \eta^2} \right|_{\eta_s} = \frac{c_3}{c_o^2} \left(-1 + \frac{1}{2c_3} - \frac{c_1}{c_o} \right)\tag{79}$$

Since $\bar{u} = 0$ when $\eta = 0$, we write

$$\eta_s = \frac{2 \frac{\partial \bar{u}}{\partial \eta}}{\frac{\partial^2 \bar{u}}{\partial \eta^2}} \bigg|_{\eta_s} \quad (80)$$

$$\eta_s = \frac{2}{\frac{\sqrt{c_3}}{c_0} \left(-1 + \frac{1}{2c_3} - \frac{c_1}{c_0} \right)}$$

The dominant term as $\xi \rightarrow \xi_s$ in this expression is

$$\eta_s = 4c_0 \sqrt{c_3} \quad \text{as } \xi \rightarrow \xi_s \quad (81)$$

$$\dot{\eta}_s = 4c_0 \sqrt{k_4}$$

The inner velocity profile is thus a quadratic just downstream of separation, and the proper condition required to continue the pre-separation solution smoothly through separation is thus the continuity of the second derivatives of the inner and outer velocity profiles at the $\bar{u} = 0$ line. Only by taking the inner velocity profile as a quadratic immediately downstream of separation has it been possible to make the numerical integration proceed.

It is of interest to note that the conditions of a quadratic inner velocity profile just downstream of separation can be inferred from an analytical continuation argument. Consider several profiles as shown in Figure 7. Downstream of separation the inner profile corresponds to a quadratic which will have two points for a given \bar{u} and the values of $\partial \bar{u} / \partial \eta$ at these two points will be equal and opposite. Thus, that part of the post-separation profile marked "inner profile" will have the u -axis as an axis of symmetry. What this, in effect, means is that the inner profile could be represented as follows:

$$\frac{\partial \bar{u}}{\partial \eta} = \pm \frac{(1 - \bar{u}) \sqrt{\bar{u} + c_3}}{c_0 + c_1 \bar{u} + c_2 \bar{u}^2} \quad (82)$$

where the plus sign refers to the first and second quadrant and the negative sign to the third quadrant. The observed behavior of the inner profile can thus be explained by an analytical continuation of the outer profile into the inner region.

In Figure 8 a plot is shown of the computed values of c_0 , c_1 , c_2 , and c_3 in the neighborhood of the separation point for the case where the solution is continued on the basis of a quadratic profile and a second derivative match. It is noted that $\sqrt{c_3}$ is linear in x so that c_3 is quadratic as previously assumed.

5.4 Adequacy of Boundary-Layer Theory in Neighborhood of Separation Point

While it has been shown that the present boundary-layer calculative method goes smoothly through the separation singularity, it has not been established that boundary-layer theory is a satisfactory representation of the viscous flow in such a neighborhood. In this connection we will show that the slope of the $\bar{u} = 0$ line at separation calculated on the basis of the Navier-Stokes equations is in good agreement with the present calculative results. We will also show that the use of free interaction together with the boundary-layer equations yields reasonable physical behavior at the separation point, whereas the imposition of a prescribed pressure distribution as in the case of Leigh and Hartree can lead to physically implausible behavior there.

With regard to the slope of the dividing streamline and the $\bar{u} = 0$ line at separation, Oswatitsch gives the following results based on the Navier-Stokes equations:

$$\begin{aligned} \tan \beta_D &= -3 \frac{\partial \tau / \partial x}{\partial p / \partial x} \\ \tan \beta_u &= -2 \frac{\partial \tau / \partial x}{\partial p / \partial x} \end{aligned} \tag{83}$$

The angles β_D and β_u are shown in Figure 9. Based on the present analysis it can be shown that

$$\tan \beta_u = \frac{ds}{dx} = \left(1 + \frac{\gamma - 1}{2} M_o^2 \right) \frac{\dot{\eta}_s}{R_o^{1/2}} \quad (84)$$

$$-2 \frac{\partial \tau / \partial x}{\partial p / \partial x} = \left(1 + \frac{\gamma - 1}{2} M_o^2 \right) \frac{U_1}{\dot{U}_1} \left(\frac{1}{R_o} \right)^{1/2} \frac{\dot{c}_3}{\sqrt{c_3 c_o}} \quad (85)$$

The following values at the first calculated point beyond separation were found from the calculations:

$$M_1 = 2.58, \quad M_o = 2.70, \quad c_3 = 5.567 \times 10^{-6}, \quad \dot{c}_3 = 3.43 \times 10^{-3}$$

$$R_o = 39000, \quad \frac{U_1}{U_o} = 0.95675, \quad \frac{\dot{U}_1}{U_o} = -0.09277, \quad c_o = 2.190, \quad \dot{\eta}_s = 6.39$$

The calculated values from Equations (84) and (85) are

$$\tan \beta_u = \frac{ds}{dx} = 0.0795$$

$$-2 \frac{\partial \tau / \partial x}{\partial p / \partial x} = 0.0854$$

It thus appears that the precise result of Equation (83) based on the Navier-Stokes equations are duplicated within 10 percent by the boundary-layer equations at the separation point.

The second point has to do with the rate of change of shear with axial distance at the separation point.

$$\tau \sim \left. \frac{\partial \bar{u}}{\partial \eta} \right|_{\xi_s, \eta=0}$$

$$\tau \sim \frac{\sqrt{c_3}}{c_o} \quad (86)$$

$$\frac{\partial \tau}{\partial \xi} \rightarrow \frac{\dot{c}_3}{\sqrt{c_3 c_o}} \quad \text{as } \xi \rightarrow \xi_s$$

In the present free-interaction solution where

$$c_3 = k_4 (\xi - \xi_s)^2$$

we find a finite limit as $\xi \rightarrow \xi_s$, as follows:

$$\lim_{\xi \rightarrow \xi_s} \frac{\partial \tau}{\partial \xi} \sim \sqrt{k_4} \quad (87)$$

The wall skin friction is thus a linear function of ξ passing through the separation point as shown in Figure 9. In the case treated by Leigh, \dot{c}_3 has a value of about 0.2 at separation so that $\partial \tau / \partial \xi$ is infinite. The difficulties encountered by Goldstein, Reference 9, in finding a physically satisfactory mathematical description of the flow in the neighborhood of the separation point for Leigh's case thus appears to be associated with the inadequacy of the boundary-layer equations in that case to yield a physically realistic flow. The introduction of free interaction into the problem, however, does cause the boundary-layer equation solution to be physically realistic.

5.5 Continuation of Solution Downstream of Separation

We now consider continuing the solution downstream to the point where the ramp starts the recompression. There is some question regarding the best method for accomplishing this. Various cases have been investigated based on different equations and boundary conditions.

In the first place, several different momentum relationships can be applied to the inner layer. We can try the inner momentum relationship represented by Equation (52). However, a simpler wall relationship can be used instead based on applying Equation (1) to the wall.

$$\frac{\partial p}{\partial x} = \frac{\partial}{\partial y} \left(\mu \frac{\partial u}{\partial y} \right) \Big|_{y=0} \quad (88)$$

With regard to the pressure at the outer edge of the boundary layer, two possibilities exist. Firstly, we can continue to use the free-interaction concept in an attempt to produce a unified theory for the entire separation region. Secondly, it is possible to invoke the boundary condition of constant pressure as exemplified by the concept of a plateau pressure region. Another boundary condition which can be invoked is continuity of the velocity derivatives at the $u = 0$ line.

In order to investigate the consequences of various combinations of the foregoing conditions, five different cases were studied as follows:

Case A:

- (1) Quadratic inner profile.
- (2) Wall relationship, Equation (88).

Case B:

- (1) Cubic inner profile.
- (2) Wall relationship.
- (3) Inner momentum equation, Equation (52).

Case C:

- (1) Cubic inner profile.
- (2) Wall relationship.
- (3) Continuity of $\partial^2 \bar{u} / \partial \eta^2$ on $\bar{u} = 0$ line.

Case D:

- (1) Quadratic inner profile.
- (2) Continuity of $\partial^2 \bar{u} / \partial \eta^2$ on $\bar{u} = 0$ line.

Case E:

- (1) Quadratic inner profile.
- (2) Continuity of $\partial^2 \bar{u} / \partial \eta^2$ on $\bar{u} = 0$ line.
- (3) Constancy of static pressure from point where $\dot{U}_1 = 0$ in Case D.

Some calculated results for these cases are shown in Figures 10 and 11. In Figure 10, the calculated pressure distributions are

shown and, in Figure 11, the calculated velocity profiles and velocity gradient profiles. On the basis of these calculated results, certain conclusions are drawn.

Cases A and B, while demonstrating reasonable pressure distribution, show a singularity in $\partial^2 \bar{u} / \partial \eta^2$ in Figure 11(b) at the $\bar{u} = 0$ line. Furthermore, this singularity tended to cause disturbances in the velocity profiles which emanate from the $\bar{u} = 0$ line and propagate both upward and downward as the downstream distance increases. Such disturbances are a result of either flow instabilities or calculative instabilities; it is not known which. As a result, these cases were discarded and it was concluded that continuity of $\partial^2 \bar{u} / \partial \eta^2$ on the $\bar{u} = 0$ line is a required boundary condition.

It was decided to adopt Case C as the one for the automatic computation program rather than Case D or Case E because it uses a cubic rather than a quadratic inner profile and because it permits a unified free-interaction theory for the entire separated region. Also, Cases D and E do not satisfy a momentum relationship for the inner flow.

It is noted that Cases A, B, and C involve a momentum relationship for the inner layer and that Cases D and E do not. It is also noted that the inner profiles for A, B, and C are much flatter than those of D and E. An explanation of this behavior is to be sought in the momentum equation which states that for constant pressure

$$\frac{d\delta^{**}}{dx} = \frac{C_f}{2} \quad (89)$$

If the wall shear is forward; that is, if C_f is negative, δ^{**} should decrease as x increases. Therefore, if the part of the boundary-layer profile above the $\bar{u} = 0$ line tends to fill out, that below it must flatten.

5.6 Asymptotic Behavior of Case C

No downstream boundary conditions or reattachment criterion has yet been used in the analysis. The point of view is taken that a starting point of interaction is assumed, and the downstream conditions are calculated by the computer program. If the calculated downstream conditions are not in accordance with some reattachment criterion (to be specified), the starting point of interaction is changed and a new set of downstream conditions calculated. If a suitable set of downstream conditions is found, then the solution is a possible one. However, a question of flow stability can be raised at this point. No stability analyses are included in the present work.

It is interesting to see what type of downstream boundary conditions are developed by Case C. To investigate this point, the solution was continued far downstream on the computing machine. The resulting pressure distribution is shown in Figure 12, together with calculated positions of dividing streamlines and $\bar{u} = 0$ lines. It is noted that as the pressure falls the reverse flow behind separation point S is flowing against an adverse pressure gradient which reverses the inner flow. As a result, a second dividing streamline and second $\bar{u} = 0$ line develop. It is clear that the solutions can be associated with two bluff downstream bodies, one corresponding to the inner $\bar{u} = 0$ line with a prescribed normal velocity distribution and the other corresponding to the inner dividing streamline with a prescribed slip condition. In the concept of free interaction, the pressure distribution up to the plateau region is independent of the downstream means of causing separation. (The pressure distribution starting at the compression surface, of course, does depend on the shape of the compression surface.) Because separation usually occurs close to the compression surface, no appreciable falling pressure occurs in the plateau region. It thus appears unnecessary to invoke a constant plateau pressure as a boundary condition.

The foregoing flow field actually corresponds to two standing vortices in the separated region with reversed signs. To

obtain this pattern requires going to a cubic inner profile. It is not clear if going to a quartic profile will produce three standing vortices. We have certainly not developed a convergent solution for the inner flow, although the outer flow should be quite accurate for the solid boundary condition previously mentioned. Higher approximations can be made by the present method. However, if a second separation point develops, we can argue logically that the inner profile should be represented by a velocity profile with a square root singularity comparable to that for the outer flow based on the same arguments advanced for the square root singularity in Equation (36).

Let us examine the velocity profile of the outer flow to see if an asymptotic outer profile is developed. It turns out that the profile outside the outer $\bar{u} = 0$ line approaches that given by Chapman in Reference 10. Also, the velocity profile can be non-dimensionalized with respect to x in the same manner as the Chapman solution. In this form the velocity profile U/U_1 is a function only of the parameter ζ defined by Chapman as follows:

$$\zeta = \frac{\psi^*}{\sqrt{x^*}} = \frac{\frac{1}{\rho_\infty} \int_0^y \rho u \, dy}{\sqrt{u_\infty v_\infty (x - x_s) C}} \quad (90)$$

The correspondence between the foregoing notation of Chapman and the notation of the present report is

$$u_\infty = u_1 \quad v_\infty = v_1 \quad T_\infty = T_1 \quad (91)$$

In the present analysis a parameter $\bar{\psi}$ is evaluated as follows:

$$\bar{\psi} = \frac{\int_0^y \rho u \, dy}{\mu_o \sqrt{\frac{U_o \ell}{v_o}}} \quad (92)$$

It is then easy to show that

$$\zeta = \frac{\psi^*}{\sqrt{x^*}} = \sqrt{\frac{U_0}{U_1} \frac{P_0}{P_1}} \frac{\bar{\psi}}{\sqrt{\frac{x - x_s}{l}}} \quad (93)$$

so that a direct comparison with the results of Chapman can now be made.

A comparison is made between the velocity profiles of Case C and that of Chapman (Ref. 10) in Figure 13. The two points where $\bar{\psi} = 0$ and the two points where $\bar{u} = 0$ are seen in the velocity profile for Case C. The velocity profile above the $\bar{u} = 0$ line originating at S' shows a close approximation to that of Chapman in an asymptotic sense.

5.7 Continuation of Solution to Reattachment Point

The present analysis allows for introduction of a compression ramp of fairly arbitrary shape at some point downstream of separation. Case C has been made to go through to the reattachment point by observing that the velocity profile approaching the reattachment point is quadratic just as is the profile coming out of the separation point. As the solution for Case C proceeds downstream of the beginning of the ramp, the cubic velocity profile becomes quadratic. At that point, a quadratic profile is assumed and continued up to reattachment. In this way the solution was made to go smoothly into the reattachment point.

In Figure 14, the calculated flow characteristics are shown. The value of c_3 and \dot{c}_3 are both zero at the reattachment point just as at the separation point. At a point about half way up the compression surface toward the reattachment point, the cubic profile turns into a quadratic profile. At this point the profile is taken as quadratic and is so continued into the reattachment point. The dividing streamline is shown together with the $\bar{u} = 0$ line which is about two-thirds of the distance between the wall and the dividing streamline.

Comparison of the calculated and experimental pressure distributions shows a long delay downstream of the beginning of the ramp before the pressure starts its rise. The significance of this fact can be seen by comparison with the inviscid pressure distribution. The calculative and experimental pressure distributions are in fair agreement. The reversal in curvature of the calculated pressure distribution approaching reattachment is exaggerated by the large scale and is not nearly so pronounced in subsequent calculations to be shown for wedges. It thus appears to be due to the increasing slope of the ramp. As a matter of interest, the calculated total pressure on the dividing streamline is also shown.

In Figure 12 it was seen that without a compression ramp, the reversed flow separated at a point S' located at x/l of 3.9. Since the compression ramp is introduced at x/l of about 2.1, we will still have separation at S' with the ramp. The calculated separation region and velocity profiles for Case C with the ramp are illustrated in Figure 15. It is seen that the ramp causes the inner separated flow to reattach very rapidly. In fact, the small amount of inner separated flow and its very low velocity makes it of no physical importance insofar as the overall flow is concerned.

6. CALCULATIVE PROGRAM

6.1 General Aspects of Calculative Program

It has been the primary objective of this study to develop an automatic computational program for calculating laminar separated flows. The program which has been developed is described completely in an operating manual. While it is not intended to describe in any detail the calculative program herein, nevertheless, certain general features of the program are of interest and should aid in utilizing the program to maximum advantage.

The calculative technique is basically an iterative one. The beginning of interaction between the boundary layer and the outer flow is assumed to start at a certain position, and the resulting separated flow is calculated up to the reattachment point. If the calculated reattachment point does not fulfill the particular reattachment criterion which may be invoked, one then changes the beginning of interaction and computes a new reattachment point. In this sense the method is an iterative one. No particular reattachment criterion has been built into the method. No guarantee of the existence of a solution is given. Even if a solution is found by calculation, no guarantee of its stability is made. A discussion of the reattachment criterion will subsequently be made.

The method can be applied to a compression or expansion ramp of fairly general shape, but the particular program here is written for a flat plate with a flat wedge faired together by a circular arc. The radius of this arc can be varied. Within reasonable limits, the radius size does not influence the calculated results.

The velocity profile external to the $\bar{u} = 0$ line has been taken as a four-parameter profile, and the inner profile has been taken as a cubic except near separation and reattachment. On the basis of comparison of calculated results by the present method with "exact solutions" from other methods and on the basis of comparison between calculated results and experimental results, it is believed that the above profiles will give sufficiently accurate approximations to the flow field for most purposes. Possibilities

for higher approximations are inherent in the method, but none has been carried out. This should be done.

The program is based on the concept of free interaction between the boundary layer and the external flow in that the pressure distribution acting on the body in viscous flow is assumed to be the same as the inviscid pressure distribution for the body thickened locally by the amount of the boundary-layer displacement thickness. The Prandtl-Meyer relationship is used to calculate the pressure. The calculative method will be accurate to the extent that "free interaction" accurately describes the fluid mechanics of the separation and reattachment processes. The calculation is started by assuming that the flow up to some point termed the beginning of interaction is of the Blasius type, and that free interaction starts discontinuously at that point. The precise formulation of the initial conditions will be subsequently discussed. The introduction of free interaction together with a small pressure impulse applied to the boundary layer is sufficient to cause the computing scheme to generate the separated flow solution.

From the mathematical point of view the computational program is simply one that solves a simultaneous set of ordinary differential equations step by step starting at the beginning of interaction and continuing downstream to the reattachment point. The set of equations is obtained from the method of integral relations applied to the laminar-boundary-layer equations and from the free-interaction relationship. The unknowns in the equations are the parameters which specify the velocity profiles and the pressure distribution. For the region in front of the separation point there are four velocity profile parameters which, taken together with the pressure, require five simultaneous differential equations for their determination. Downstream of the separation point a cubic profile is utilized for the inner flow with three parameters determining the inner velocity profile, Equation (38). However, the use of the boundary condition of the continuity of two velocity derivatives at the boundary between the inner and the outer flows results in the addition of only one more differential equation downstream of the separation point.

The program can be utilized for arbitrary values at the beginning of interaction of the Reynolds number, Mach number, and ratio of specific heats. By eliminating the equation of free interaction and specifying an external pressure distribution, the method can be used to calculate with excellent accuracy the change in shape of the laminar velocity profile in the face of an arbitrary pressure gradient. It is possible to increase the accuracy of the program by increasing the order of approximation used to represent the velocity profiles. (Until the stability of the calculative process has been demonstrated, no positive claims can be made.) It is also capable of extension to much broader application as discussed in "Recommendations for Future Work."

6.2 Assumptions of Calculative Program

A number of assumptions have been made in the analysis as listed in Section 2.2. In addition, several additional assumptions or conditions have been specified for the calculative program.

(1) A four-parameter velocity profile has been used for the outer flow.

(2) A cubic profile has been used for the inner flow.

(3) The configuration is a flat plate with a wedge compression surface joined by an arc of constant radius.

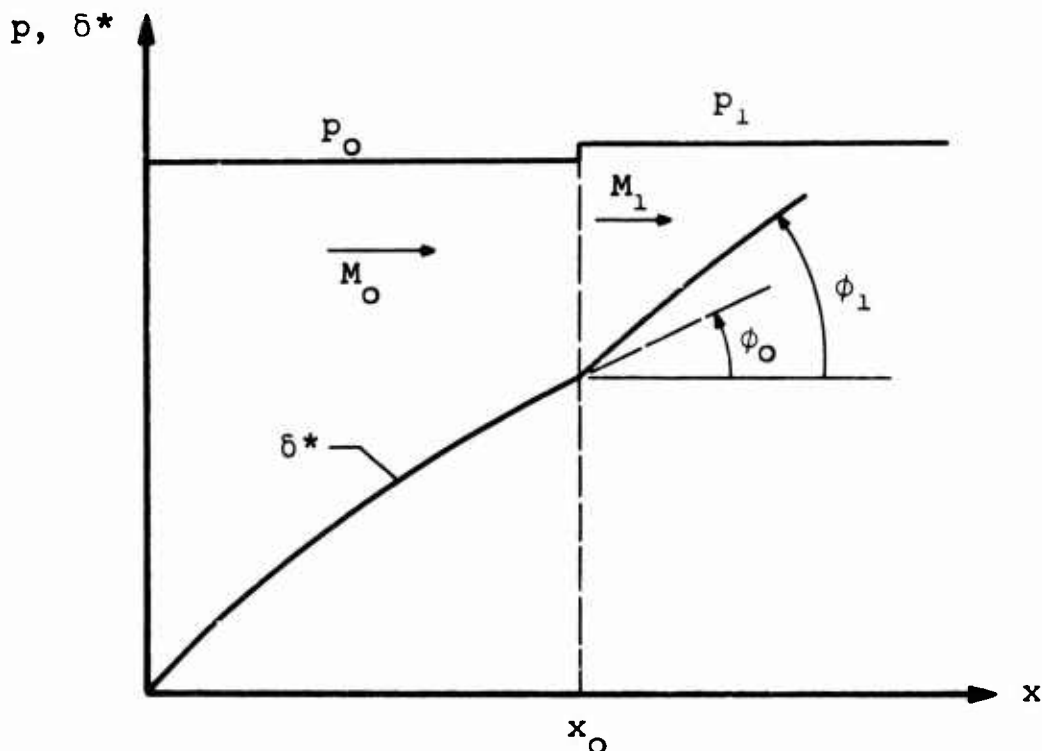
(4) The initial conditions of the boundary layer correspond to those for the Blasius case.

6.3 Initial Conditions

Some discussion of initial conditions is required for cases of very low Reynolds numbers or very large Mach numbers. For these cases it is found that the streamwise slope of the displacement thickness at the beginning of interaction is not small, being of the order of 10^0 in some cases. In the work contained through the first five sections, the assumption was made in calculating the initial conditions that the velocity u_1 at the edge of the boundary layer is parallel to the plate. However, it was found

necessary to take account of the difference in direction between the velocity at the edge of the boundary layer and the direction parallel to the plate for the above cases if the calculative solution is to start smoothly.

Consider the following sketch which illustrates the initial condition problem:



At some point x_0 we assume that the static pressure jumps discontinuously from p_0 to p_1 . This increment is small, being only one-tenth of 1 percent of p_0 . Up to x_0 one assumes the pressure was constant and that the boundary-layer profile just before x_0 corresponds to that for uniform pressure. In some cases, interaction between the boundary layer and the outer flow will produce large induced pressure gradients before x_0 . We have neglected such pressure gradients or alternately consider that the plate was cambered to counteract them and to produce a uniform pressure. At x_0 the slope of the δ^* curve changes by a very small amount from ϕ_0 to ϕ_1 in accordance with the Prandtl-Meyer relationship. The Mach numbers M_0 and M_1 are defined on the basis of the velocity parallel to the wall.

Applying the Prandtl-Meyer relationship to the slope of the streamline at δ^* with the outer flow Mach number defined parallel to the plate, we find

$$\left(\frac{p_1}{p_0}\right)^{(\gamma-1)/\gamma} = \frac{1 + \frac{\gamma-1}{2} \left(\frac{M_0}{\cos \phi_0}\right)^2}{1 + \frac{\gamma-1}{2} \left(\frac{M_1}{\cos \phi_1}\right)^2}$$

$$\frac{M_1}{M_0} = \cos \phi_1 \left(\frac{1}{\frac{\gamma-1}{2} M_0^2}\right)^{1/2} \left[\frac{1 + \left(\frac{\gamma-1}{2}\right) \left(\frac{M_0}{\cos \phi_0}\right)^2}{\left(\frac{p_1}{p_0}\right)^{(\gamma-1)/\gamma}} - 1 \right]^{1/2} = \frac{U_1}{U_0} \quad (94)$$

We wish to determine the values of M_1 and ϕ_1 as initial conditions for the calculation program. In the preceding equation we have used the following initial values to calculate M_1 :

$$\frac{p_1}{p_0} = 1.001 \quad (95)$$

$$\phi_1 \approx \phi_0 = \tan^{-1} \left\{ \frac{1}{R_0^{1/2}} \left[0.860823 + 1.193715 \left(\frac{\gamma-1}{2}\right) M_0^2 \right] \right\} \quad (96)$$

The second relationship is based on Equation (72) and neglects the small difference between ϕ_0 and ϕ_1 in the calculation of M_1 . However, in determining the initial value of ϕ_1 itself, we utilize the relationship between Mach number and turning angle.

$$\phi = -\sqrt{\frac{\gamma+1}{\gamma-1}} \tan^{-1} \sqrt{\frac{\gamma-1}{\gamma+1} \left[\left(\frac{M}{\cos \phi}\right)^2 - 1 \right]} + \tan^{-1} \sqrt{\left(\frac{M}{\cos \phi}\right)^2 - 1} + c \quad (97)$$

The constant C is evaluated from the conditions

$$M = M_0 \quad \phi = \phi_0$$

so that

$$C = \phi_0 + \sqrt{\frac{\gamma + 1}{\gamma - 1}} \tan^{-1} \sqrt{\frac{\gamma - 1}{\gamma + 1} \left[\left(\frac{M_0}{\cos \phi_0} \right)^2 - 1 \right]} - \tan^{-1} \sqrt{\left(\frac{M_0}{\cos \phi_0} \right)^2 - 1} \quad (98)$$

We then compute ϕ_1 from Equation (97) using C evaluated from Equation (98) with $M/\cos \phi$ equal to $M_1/\cos \phi_0$. Iteration of Equations (94) to (97) to establish more precise values of M_1 and ϕ_1 is usually not required because of the small difference between ϕ_0 and ϕ_1 .

In the calculations discussed through Section 5, the $\cos \phi$ term was included in the pressure distribution calculations but was not included in the initial condition calculations. It has, however, been included in both calculations henceforth.

6.4 Calculative Accuracy

In order to assess to what extent any differences between experiment and theory can be ascribed to theory rather than inaccuracies in numerical methods, it is important to investigate the calculative accuracy of the method. In this connection, we will consider the question of interval size, corner radius, and order of approximation of the velocity profiles.

First, a point concerning stability of the calculative method should be mentioned. If a laminar boundary layer on a flat plate is given a distorted profile as an initial condition and is permitted to proceed along the plate at uniform pressure, it will develop a Blasius profile asymptotically to any desired numerical accuracy. If we were to assume a Blasius profile at some point and were to integrate upstream to find the initial conditions, we would have a numerically intractable problem since any number of initial conditions could result in a final Blasius profile within

prescribed numerical accuracy. Integrating the boundary-layer equations downstream of separation into the reversed inner flow has some of the aspects of the foregoing problem. In this case, however, it is complicated by the existence of inner and outer flows. It was found that if the inner profile was represented as a cubic, the integration immediately downstream of separation became unstable. In the program, the inner profile is started as a quadratic and changed to cubic when numerical differences of the order 10^{-4} between the magnitude of the slopes at the wall and the $\bar{u} = 0$ line is found in a side calculation. This procedure eliminates the instability completely. It is not known what caused the instability for the cubic case. The other instability encountered in the calculations occurred as a result of a singularity in the second derivative of the inner and outer velocity profiles at their juncture.

The interval size is not constant in the integration scheme but is variable to maintain certain prescribed accuracies. At the start of the numerical solution a Runge-Kutta integration scheme is used for the first four steps. Thereafter a fourth-order Adams predictor-corrector method is used. With the value of the variables known for steps $j - 3$, $j - 2$, $j - 1$, and j , the value for step $j + 1$ is predicted by the following formula:

$$B_{j+1}^{(p)} = B_j + \frac{h}{24} (55\dot{B}_j - 59\dot{B}_{j-1} + 37\dot{B}_{j-2} - 9\dot{B}_{j-3}) \quad (99)$$

Using the predicted value of $\dot{B}_{j+1}^{(p)}$, a corrected value of $B_{j+1}^{(c)}$ is calculated as follows:

$$B_{j+1}^{(c)} = B_j + \frac{h}{24} (9\dot{B}_{j+1}^{(p)} + 19\dot{B}_j - 5\dot{B}_{j-1} + \dot{B}_{j-2}) \quad (100)$$

The truncation error Δx is estimated by the formula

$$\Delta x = -\frac{19}{270} (B_{j+1}^{(c)} - B_{j+1}^{(p)}) \quad (101)$$

The absolute error estimate is

$$\left| \frac{B_{j+1}^{(c)} - B_{j+1}^{(p)}}{14.2} \right| = |\Delta x| \quad (102)$$

and the relative error estimate is

$$\frac{|\Delta x|}{B_{j+1}^{(c)}} \quad (103)$$

For the calculations of this report, the relative error has been taken as 10^{-5} and the absolute error as 10^{-7} . If the relative error exceeds 10^{-5} but the absolute error is less than 10^{-7} , the integration proceeds. If both tests fail, the increment is halved, and the calculation started again using the Runge-Kutta. If the relative error is less than 1/200 of the relative error bound, the interval is doubled. Also, if the absolute error is less than 1/200 of the absolute error bound, the increment is doubled even though the relative error test fails. These criteria are established to avoid oscillating between two interval sizes. These tests are built into the IBM Fortran II subroutine used to solve the system of differential equations. A discussion of the method and the Runge-Kutta starting technique is presented in F. D. Hildebrand's "Introduction to Numerical Analysis," McGraw-Hill, New York, 1956, Chapter 6.

During the calculations run for comparison with the results of Hartree and Leigh, the allowable relative error was decreased from 10^{-5} to 10^{-4} . The calculated values of x for a given value of c_3 did not change by more than one in 10^{-4} . This was also the accuracy of prediction of the position of the separation point. Accordingly, a value of relative error of 10^{-5} was considered sufficiently accurate for the calculations.

In order not to introduce any discontinuities which might generate calculative instabilities, it was decided to fair the plate into the ramp with a circular arc. For this reason, calculations were made for the configuration of Figure 16 with fairings of several radii. The calculated results for the pressure distribution are shown in Figure 17. It is seen that fairing the corner

causes modification of the pressure distribution only over its length and that the final pressure distribution on the ramp does not depend on the size of the radius. Also, as the size of the radius tends to zero, the calculated pressure distributions tend to a limit. It thus appears that fairing the corner causes no inaccuracies in the calculated pressure distributions. Some local modifications of the velocity profiles may be anticipated in the region of the fairing. In the program, the actual radius of the fairing is left arbitrary.

It has been mentioned that the present method contains within its framework the possibility of obtaining higher-order approximations to the calculated flow. Such approximations are obtained by increasing the number of parameters in the velocity profiles. With regard to the outer profile, a four-parameter formulation has been used throughout the paper and a higher-order approximation has not been investigated. Based on the excellent agreement of the four-parameter approximation with the results of Leigh, it was felt that a fourth approximation for the outer flow is enough for most purposes. Furthermore, we must consider the question of increasing the degree of approximation of the outer profile simultaneously with that for the inner profile.

It is felt, insofar as the pressure distribution is concerned, the number of arbitrary parameters in the inner profile can be less than that for the outer profile. In the case of the cubic profile, we have matched the velocity and its first two derivatives at the boundary between the inner and outer flow, leaving only one free parameter to satisfy an inner momentum relationship (Case C). For Case D with a quadratic inner profile, continuity of the velocity and its first two derivatives fully determines the profile, and momentum is not satisfied for the inner layer (although continuity is).

A comparison between Cases C and D and the data for the particular case is shown in Figure 18. It is clear from a comparison of the calculated results for Cases C and D that for accurate

results we must use a cubic inner profile. For the cubic profile, the agreement between experiment and theory is considered fairly good. How much it would be further improved by going to a quartic inner profile is a question recommended for future study.

7. SOME CALCULATIVE EXAMPLES

7.1 Systematic Calculations

In order to check out the calculative program over a wide range of Reynolds numbers, Mach numbers, and ratios of specific heat, a systematic series of computation runs were made by the IBM 7094 Computer at RTD, W-PAFB, under the supervision of Mr. Eugene Fleeman, Project Monitor. The following tabulated sets are presented to show the influence on the above parameters for a flat plate with a 25° compression wedge:

x_o	R_o	M_o	γ	x_S	x_R
1	10^3	4	1.4	2.073	∞
1	10^4	4	1.4	1.827	6.830
1	10^5	4	1.4	1.559	6.018
1	10^4	2	1.4	1.956	6.082
1	10^4	6	1.4	1.779	7.779
1	10^4	8	1.4	1.743	9.768
1	10^4	10	1.4	1.719	∞
1	10^4	4	1.2	1.461	6.903
1	10^4	4	1.67	2.283	6.573
1					

A value of ∞ for x_R indicates that reattachment did not take place.

The systematic effect of Reynolds number, Mach number, and ratio of specific heats is shown in Figure 19. In this and subsequent figures, the reference length l is taken equal to x_o . In fact, this equality is built into the program so that interaction begins when x/l is unity.

The results for the effect of Reynolds number show a decrease in the distance from the onset of interaction to separation as the Reynolds number increases, as well as a decrease in the value of the plateau pressure. The results cannot be compared directly with the earlier results of this study in Figure 2(a) of

Reference 1 because the beginning of interaction has been defined differently in each case. However, the plateau pressure levels should be comparable and do show good agreement.

With regard to Mach number, there is an increase in plateau pressure and a decrease in the distance between the beginning of interaction and the location of separation as the Mach number increases. The plateau pressures for Mach numbers of 2, 4, and 6 are in good accord with the earlier calculated values in Figure 2(b) of Reference 1. As the ratio of specific heats increases, Figure 19(c) shows an increase in the distance to the separation point but no significant change in the plateau pressure.

7.2 Comparison Between Theory and Experiment

The calculative method has been applied to several cases for which data on laminar separation and reattachment are available in order to assess its accuracy. The Ames Research Center of NASA has furnished several sets of such data for a flat plate with a 10° wedge placed at various angles in the wind tunnel. These data and the calculated pressure distributions are compared in Figures 20 and 21.

In obtaining the calculated pressure distributions, the beginning of interaction was varied until the position of the calculated separation point coincided as closely as could be estimated with the experimental position of the separation point. There was relatively little change in separation point as a result of changes in plate angle of attack. Comparison is shown for the upper surface for angles of attack of 6° , 15° , and 16.7° . It is felt that the agreement between the experimental and calculated results is good. It is of interest to speculate whether the agreement would be further improved by going to a higher approximation in the calculative method. Also, it is of interest to inquire what part of the difference between experiment and theory can be ascribed to the assumption of free interaction. These questions are a fitting subject for future investigation.

8. FLOW IN NEIGHBORHOOD OF REATTACHMENT POINT

Let us now use the calculative program to study the nature of the flow in the neighborhood of the reattachment point and to study relationships between the locations of separation and reattachment. First, a series of computations were made for the flat plate with a 10° wedge systematically varying the position of the beginning of interaction. The calculated pressure distributions, separation points, and reattachment points are shown in Figure 21 where they are compared with the measured pressure distribution. Two points of interest are immediately evident. For all the cases calculated, there are no substantial variations among the calculated wedge pressure distributions; that is, the position of reattachment does not seem to influence the wedge pressure distribution substantially. Secondly, small changes in the position of the beginning of interaction are sufficient to cause large movements in the reattachment point and, for the most upstream position, reattachment did not occur at all.

It is of interest to examine the slope of the dividing streamline approaching reattachment and to see how this is related to the calculated Oswatitsch reattachment angle, Equation (83). For this purpose, the calculated solution from the previous figure corresponding to $l = 0.0550$ was used with the results shown in Figure 22. It is noted that β_D of the dividing streamline decreases approaching the reattachment point. The Oswatitsch reattachment angle calculated from Equation (83) using the numerical values for the present case increases and then decreases approaching reattachment. The values at the reattachment position are considered to be in good accord considering one theory is based on the boundary-layer equations and the other on the Navier-Stokes equations. For position of reattachment lower on the wedge, the agreement is not as good.

Examination of the calculated Oswatitsch reattachment angle as it varies with the position of the beginning of interaction l shows that the reattachment point has an upper limiting position on the wedge. To show this result, Figure 23 has been constructed.

The variation of Oswatitsch reattachment angle for the previous figure is shown together with those for the other positions of the beginning of interaction. It is seen that if the beginning of interaction starts at $l = 0.0525$, reattachment cannot occur for a greater value of x from 0.325 feet. At this point the dividing streamline is tangent to the wedge.

On the basis of the present calculations, it is seen that the reattachment angle decreases as the reattachment point moves up the wedge. An extrapolation of the calculated results to β_D of zero yields a value of $x = 0.34$. The present calculation thus yields the same result as the Oswatitsch theory in that the flow cannot reattach to the wedge above a certain point. This condition corresponds to the most upstream allowable position of the beginning of interaction and to a dividing streamline tangent to the wedge at reattachment.

It has been stated that the present calculative scheme is an iterative one in that the separation point can be moved until some reattachment criterion can be fulfilled. Insofar as the present calculative method is concerned, reattached flows are possible for a certain range of reattachment on the wedge. Which one of these flows will occur in practice depends on downstream boundary conditions, and in this sense the present calculative scheme is an elliptical one. One speculates that if the length of the wedge is less than the length over which reattachment will occur that reattachment might occur at the end of the wedge. This speculation is based on the physical argument that the end of the wedge is the only distinguished point. If the wedge is longer than the critical value, one speculates that reattachment might occur at the critical length from the corner of the wedge since this position is a distinguished one. These speculations require a stability analysis of the flow to establish their validity. In addition to a stability analysis, careful experimental measurements are required.

As a point of interest, the variations in stagnation pressure and Mach number along the dividing streamline for the several

cases are shown in Figure 24. At reattachment, the stagnation pressure on the dividing streamline is equal to the static pressure at this point and these points are shown as solid points in Figure 24(a). It is noted that for the case that did not reattach, the stagnation pressure continues to rise. The Mach number shows an almost linear decrease with distance as it approaches reattachment.

9. CONCLUSIONS

The present paper presents a method for calculating the laminar compressible separated flow past a flat plate with a ramp of arbitrary shape and small slopes from an assumed position for the beginning of interaction to the reattachment point. The method is based on the assumption of free interaction throughout the separated flow region.

(1) The method has been successfully programed for a flat plate with a flat ramp connected by means of a circular arc.

(2) For the several cases investigated, reasonably good agreement was obtained between the experimental and theoretical pressure distributions up to the reattachment point.

(3) In the neighborhood of the separation point induced by a linear decreasing velocity, the present method yielded numerical results in close agreement with the precise results of Hartree and Leigh based on finite difference equations.

(4) For an arbitrarily imposed pressure distribution, there appears to be a singularity in the rate of change of wall skin friction with distance along the wall. The assumption of free interaction between the outer flow and the boundary layer removes this singularity. On this basis the present solution was made to go smoothly through the separation point.

(5) The calculated slope of the dividing streamline at separation is in good accord with the value due to Oswatitsch as calculated from the Navier-Stokes equations.

(6) The analysis indicates that the velocity profile just downstream of separation and just upstream of reattachment is basically quadratic.

(7) The calculative method yielded reversal of the inner flow in certain cases.

(8) It was found for a specific case that reattached flow was possible only over a region of the wedge within a critical distance from the lower corner. At this critical distance, the dividing streamline comes in tangent to the wedge and the separation point is at its most forward position.

(9) The method contains the possibility of high orders of approximation and of extension to other flow problems as described in the next section.

(10) The calculative program has been applied to a wide range of initial Mach numbers, Reynolds numbers, and ratio of specific heats to show the systematic effects of these parameters on the separated flow.

(11) The present method can be applied to the calculation of the laminar-boundary-layer characteristics in the face of a prescribed pressure distribution for any Mach number.

(12) It is believed that the concept of free interaction will yield results in sufficiently good agreement with experiment up to the reattachment point to warrant its continued development. In any event, it can serve as the zero-order approximation for a more precise theory which takes fuller account of upstream influence and the basic elliptic nature of the problem.

(13) It was found necessary to match the second derivatives of the inner and outer velocity profiles at their point of juncture to obtain stable calculated solutions.

10. RECOMMENDATIONS FOR FUTURE WORK

It is believed that the present work is capable of broad extension and exploitation. A number of specific suggestions for future work follows:

- (1) The calculative program should be extended to axially symmetric flow under the assumption that the boundary layer is thin compared to the radius. This the authors intend to do.
- (2) The analysis is capable of extension to nonadiabatic surfaces. Such an extension is contemplated as continuing work under the present program.
- (3) Higher approximations within the framework of the present theory should be attempted. These approximations should consider additional moments of the momentum relationship for the inner flow as well as continuity of velocity derivatives higher than the second at the boundary between the inner and outer flows.
- (4) Extension of the calculative method downstream of the reattachment point is desirable. For this purpose it appears desirable to rotate the coordinate system perpendicular to the ramp.
- (5) An investigation should be made to extend the analysis to higher ramp angles.
- (6) The computational program should be used as an analog device to study separated flows systematically. Effects of Mach number and Reynolds number should be studied as well as reattachment flow and incipient separation.
- (7) A systematic comparison between the results of the present calculative method should be made with all available experimental data to assess its limitations and the necessity of higher-order approximations.
- (8) The present method should be capable of simple extension to blowing or suction in laminar boundary layers including the separated region.
- (9) It would be of interest to apply the method to turbulent boundary layers through the use of the eddy viscosity approach.

(10) The present results for a Prandtl number of unity should be generalized to other Prandtl numbers and to real gases.

(11) Since the Blasius profiles used as initial conditions may be unrealistic at high Mach numbers or low Reynolds numbers because of induced pressure effects, an attempt should be made to start the calculative program at the leading edge.

(12) Well-designed careful experiments are badly needed to obtain detailed flow information in the separated region at both separation and reattachment for evaluating theory.

(13) As a result of the numerical calculations of flow in the neighborhood of the reattachment point, certain speculations concerning a reattachment criterion have been made. Further work is required to develop a sound reattachment criterion both from the theoretical and experimental points of view. Theoretical work is needed for wedges of finite length and infinite length. Experimental studies of the flow in the region of reattachment are definitely needed to guide the theory. Accurate velocity profiles are needed, as well as measurement of reattachment-point locations.

REFERENCES

1. Abbott, D. E., Holt, M., and Nielsen, J. N.: Investigation of Hypersonic Flow Separation and Its Effects on Aerodynamic Control Characteristics. ASD TDR-62-963, Nov. 1962.
2. Lees, L. and Reeves, B. L.: Supersonic Separated and Reattaching Laminar Flows: General Theory and Application to Adiabatic Boundary Layer - Shock Wave Interactions. Firestone Flight Science Lab., GALCIT Tech. Rep. No. 3, Oct. 4, 1963.
3. Stewartson, K.: Correlated Incompressible and Compressible Boundary Layers, Proc. Roy. Soc., Series A, vol. 200, 1949.
4. Dorodnitsyn, A. A.: General Method of Integral Relations and Its Application to Boundary Layer Theory. Advances in Aero. Sci., vol. 3, Von Kármán Ed., 1962.
5. Hartree, D. R.: A Solution of the Laminar Boundary-Layer Equations for Retarded Flow. Aero. Res. Council, R and M No. 2426, 1939.
6. Leigh, D. C. F.: The Laminar Boundary Layer Equation: A Method of Solution by Means of an Automatic Computer. Cambridge Phil. Soc. Proc., vol. 51, 1955, pp. 320-332.
7. Schlichting, H.: Boundary Layer Theory. Pergamon Press, 1955.
8. Chapman, D. R., Kuehn, D. M., and Larson, H. K.: Investigation of Separated Flows in Supersonic and Subsonic Streams with Emphasis on the Effects of Transition. NACA TN 3869, Mar. 1957.
9. Rosenhead, L.: Laminar Boundary Layers. Oxford at the Clarendon Press, 1963, pp. 217-221.
10. Chapman, D. R.: Laminar Mixing of a Compressible Fluid. NACA TR 958.

TABLE I
 CALCULATIVE VALUES TO ESTABLISH c_0 , c_1 , c_2 , c_3 , FOR BLASIUS PROFILE

ξ	$\sqrt{\xi}$	c_0	c_1	c_2	c_3	$\frac{c_0}{\sqrt{\xi}}$	$\frac{c_1}{\sqrt{\xi}}$	$\frac{c_2}{\sqrt{\xi}}$
0.021996	0.148310	0.5184322	-0.3521911	-0.01830257	1.309532	3.49560	-2.374696	-0.1234075
.050220	.224098	.7138566	-.4370389	-.06833900	1.107546	3.18546	-1.950213	-.304951
.100908	.317660	1.006146	-.6136813	-.0990591	1.101603	3.167367	-1.931881	-.3118400
.200236	.447477	1.414092	-.8617823	-.1401039	1.100297	3.160145	-1.925870	-.3130975
.300588	.548259	1.731336	-1.054954	-.1717370	1.100054	3.157880	-1.924190	-.3132406
.359979	.599983	1.894240	-1.154173	-.1879488	1.099995	3.1571561	-1.923676	-.3132570

TABLE II
COMPARISON OF BLASIUS PROFILE WITH
DORODNITSYN APPROXIMATION

$\frac{\eta}{\sqrt{\xi}}$	Blasius		Dorodnitsyn	
	\bar{u}	$\sqrt{\xi} \partial \bar{u} / \partial \eta$	\bar{u}	$\sqrt{\xi} \partial \bar{u} / \partial \eta$
0.0	0.0000	0.3321	0.0000	0.3322
.2	.0664	.3320	.0665	.3330
.4	.1328	.3315	.1331	.3325
.6	.1989	.3301	.1994	.3305
.8	.2647	.3274	.2652	.3271
1.0	.3298	.3230	.3302	.3220
1.2	.3938	.3166	.3939	.3151
1.4	.4563	.3079	.4561	.3064
1.6	.5168	.2967	.5163	.2956
1.8	.5748	.2829	.5742	.2826
2.0	.6298	.2668	.6292	.2675
2.2	.6813	.2484	.6810	.2501
2.4	.7290	.2281	.7291	.2307
2.6	.7725	.2065	.7731	.2094
2.8	.8115	.1840	.8128	.1867
3.0	.8461	.1614	.8478	.1632
3.2	.8761	.1391	.8781	.1398
3.4	.9018	.1179	.9037	.1172
3.6	.9233	.0981	.9250	.0961
3.8	.9411	.0801	.9423	.0773
4.0	.9555	.0642	.9561	.0610
4.2	.9670	.0505	.9669	.0474
4.4	.9759	.0390	.9752	.0363
4.6	.9827	.0295	.9816	.0275
4.8	.9878	.0219	.9863	.0206
5.0	.9916	.0159	.9899	.0154
5.2	.9943	.0113	.9926	.0114
5.4	.9962	.0079	.9946	.0084
5.6	.9975	.0054	.9960	.0062
5.8	.9984	.0037	.9971	.0046
6.0	.9990	.0024	.9979	.0033
6.2	.9994	.0016	.9984	.0024
6.4	.9996	.0010	.9989	.0018
6.6	.9998	.0006	.9992	.0013
6.8	.9999	.0004	.9994	.0010
7.0	.9999	.0002	.9996	.0007
7.2	1.0000	.0001	.9997	.0005
7.4	1.0000	.0001	.9998	.0004
7.6	1.0000	.0000	.9998	.0003
7.8	1.0000	.0000	.9999	.0002
8.0	1.0000	.0000	.9999	.0001
8.2	1.0000	.0000	.9999	.0001
8.4	1.0000	.0000	1.0000	.0001
8.6	1.0000	.0000	1.0000	.0001
8.8	1.0000	.0000	1.0000	.0000

TABLE III
VALUES OF c_0 , c_1 , c_2 , AND c_3 FOR CALCULATIVE
EXAMPLE CORRESPONDING TO LEIGH CASE

ξ	x/l	c_0	c_1	c_2	c_3
0.0100	0.0100	0.3157	-0.1923	-0.0313	1.1000
.0403	.0404	.6174	- .3806	- .0565	.9991
.1005	.1011	.9350	- .5829	- .0775	.8550
.1485	.1499	1.0980	- .6881	- .0854	.7495
.2022	.2049	1.2325	- .7744	- .0906	.6425
.2509	.2549	1.3255	- .8328	- .0939	.5559
.2969	.3027	1.3959	- .8753	- .0967	.4821
.3507	.3589	1.4616	- .9125	- .0998	.4055
.4019	.4125	1.5117	- .9381	- .1035	.3409
.4480	.4613	1.5488	- .9543	- .1073	.2890
.5094	.5268	1.5889	- .9677	- .1136	.2281
.5555	.5763	1.6134	- .9723	- .1193	.1878
.6016	.6261	1.6341	- .9729	- .1261	.1517
.6528	.6818	1.6535	- .9693	- .1351	.1159
.7040	.7380	1.6699	- .9618	- .1456	.0845
.7501	.7890	1.6828	- .9520	- .1567	.0596
.8013	.8460	1.6960	- .9386	- .1708	.0356
.8525	.9035	1.7095	- .9242	- .1863	.0155
.8986	.9556	1.7265	- .9182	- .1978	.0014
.9011	.9585	1.7279	- .9189	- .1978	.0008
.9024	.9600	1.7288	- .9194	- .1977	.0005
.9037	.9614	1.7297	- .9202	- .1976	.0002

TABLE IV
COMPARISON OF LEIGH PROFILE
WITH PRESENT SOLUTION

(a) $x_s/l - x/l = 0.000142$

y_L	u/u_o	
	Leigh	Dorodnitsyn
0.0	0.0000	0.0000
.2	.0026	.0027
.4	.0096	.0099
.6	.0210	.0216
.8	.0366	.0376
1.0	.0564	.0578
1.2	.0802	.0819
1.4	.1078	.1098
1.6	.1390	.1412
1.8	.1735	.1757
2.0	.2110	.2130
2.2	.2510	.2527
2.4	.2931	.2944
2.6	.3368	.3376
2.8	.3815	.3819
3.0	.4266	.4267
3.2	.4716	.4714
3.4	.5158	.5156
3.6	.5586	.5586
3.8	.5995	.5999
4.0	.6381	.6389
4.4	.7065	.7082
4.8	.7619	.7640
5.2	.8039	.8054
5.6	.8338	.8340
6.0	.8536	.8525
6.4	.8658	.8638
6.8	.8729	.8706
7.2	.8767	.8745
7.6	.8787	.8767
8.0	.8802	.8780

Dorodnitsyn

$$x_s/l = 0.962814$$

$$x/l = 0.962672$$

$$c_o = 1.730535$$

$$c_1 = -0.92109$$

$$c_2 = -0.197233$$

$$c_3 = 2.32 \times 10^{-5}$$

TABLE IV.- CONCLUDED

(b) $x_s/l - x/l = 0.002542$

y_L	U/U_o	
	Leigh	Dorodnitsyn
0.0	0.0000	0.0000
.2	.0041	.0042
.4	.0126	.0129
.6	.0255	.0260
.8	.0426	.0435
1.0	.0638	.0650
1.2	.0890	.0905
1.4	.1180	.1197
1.6	.1504	.1522
1.8	.1861	.1877
2.0	.2246	.2260
2.2	.2655	.2665
2.4	.3083	.3089
2.6	.3524	.3526
2.8	.3974	.3972
3.0	.4427	.4421
3.2	.4875	.4868
3.4	.5314	.5307
3.6	.5737	.5732
3.8	.6138	.6138
4.0	.6515	.6520
4.4	.7178	.7193
4.8	.7708	.7726
5.2	.8106	.8116
5.6	.8384	.8382
6.0	.8566	.8552
6.4	.8678	.8656
6.8	.8741	.8717
7.2	.8775	.8753
7.6	.8792	.8773
8.0	.8805	.8785

Dorodnitsyn

$x_s/l = 0.962814$

$x/l = 0.960272$

$c_o = 1.728945$

$c_1 = -0.919618$

$c_2 = -0.197710$

$c_3 = 4.588 \times 10^{-4}$

TABLE V (a)
 COMPARISON OF DORODNITSYN, QUARTIC, AND
 SIMILARITY VELOCITY PROFILES
 AT SEPARATION

Y/δ^*	Dorodnitsyn U/U_1	Quartic U/U_1	Similarity U/U_1
0	0	0	0
0.0848	0.0046	0.0066	0.0040
.1696	.0183	.0252	.0158
.3391	.0719	.0914	.0636
.5935	.2098	.2406	.1927
.8478	.3961	.4177	.3802
1.0174	.5315	.5368	.5230
1.2717	.7226	.7004	.7278
1.4413	.8252	.7927	.8364
1.7804	.9470	.9252	.9598
1.9500	.9736	.9644	.9839
2.6282	.9987	1.0000	.9999

TABLE V(b)

COMPARISON OF DORODNITSYN AND QUARTIC VELOCITY
 PROFILE DERIVATIVES THROUGH THE
 BOUNDARY LAYER AT SEPARATION

Y/δ^*	Dorodnitsyn $\frac{\partial(U/U_1)}{\partial(Y/\delta^*)}$	Quartic $\frac{\partial(U/U_1)}{\partial(Y/\delta^*)}$
0	0	0
0.0848	0.1081	0.1519
.1696	.2144	.2829
.3391	.4141	.4865
.5935	.6554	.6627
.8478	.7882	.7110
1.0174	.7977	.6870
1.2717	.6786	.5894
1.4413	.5256	.4962
1.7804	.2095	.2832
1.9500	.1116	.1812
2.6282	.0059	.0132

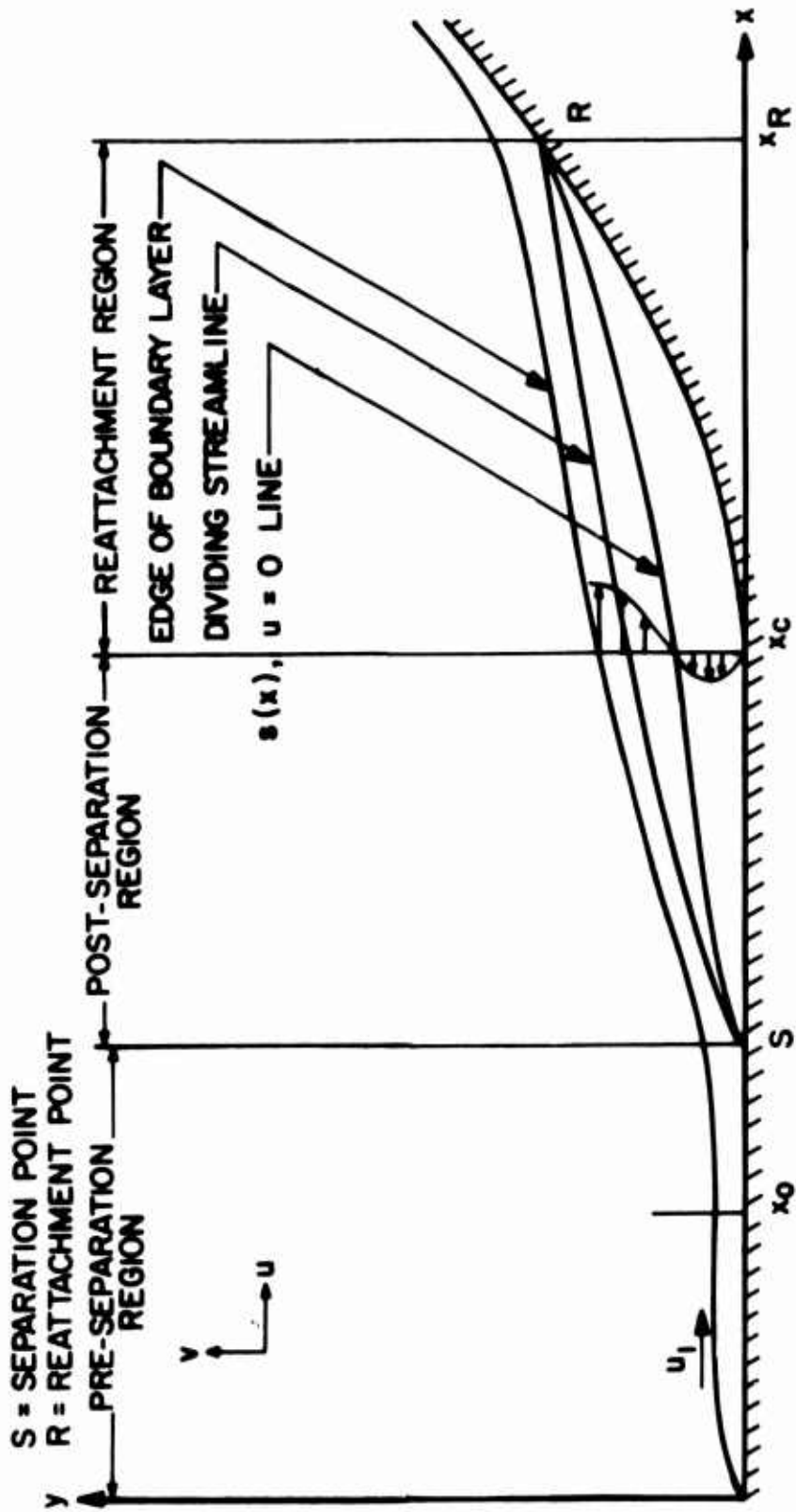


FIGURE I. - SEPARATED LAMINAR SUPERSONIC FLOW OVER A FLAT PLATE WITH A RAMP.

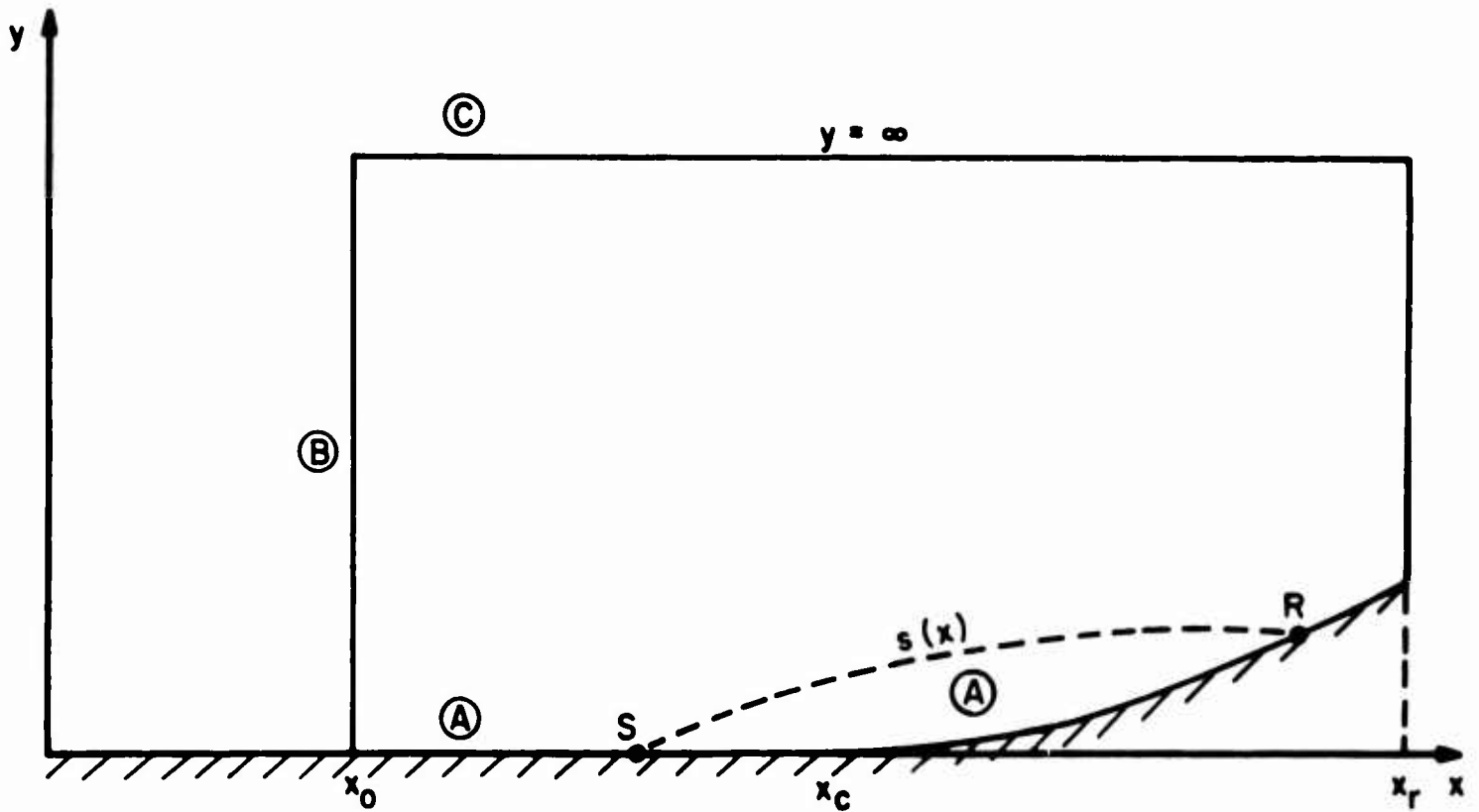


FIGURE 2. - DOMAIN OF BOUNDARY-VALUE PROBLEM.

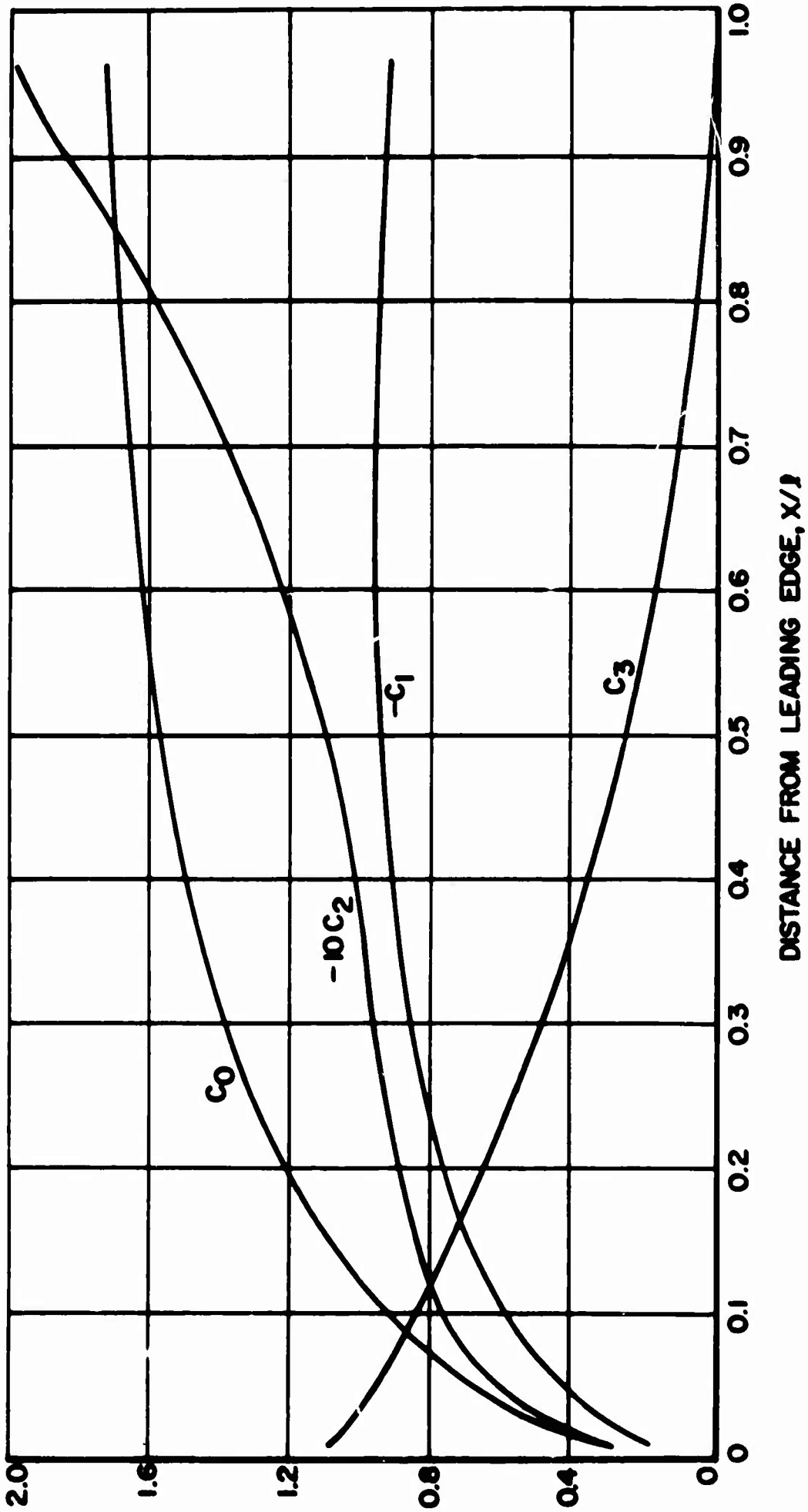
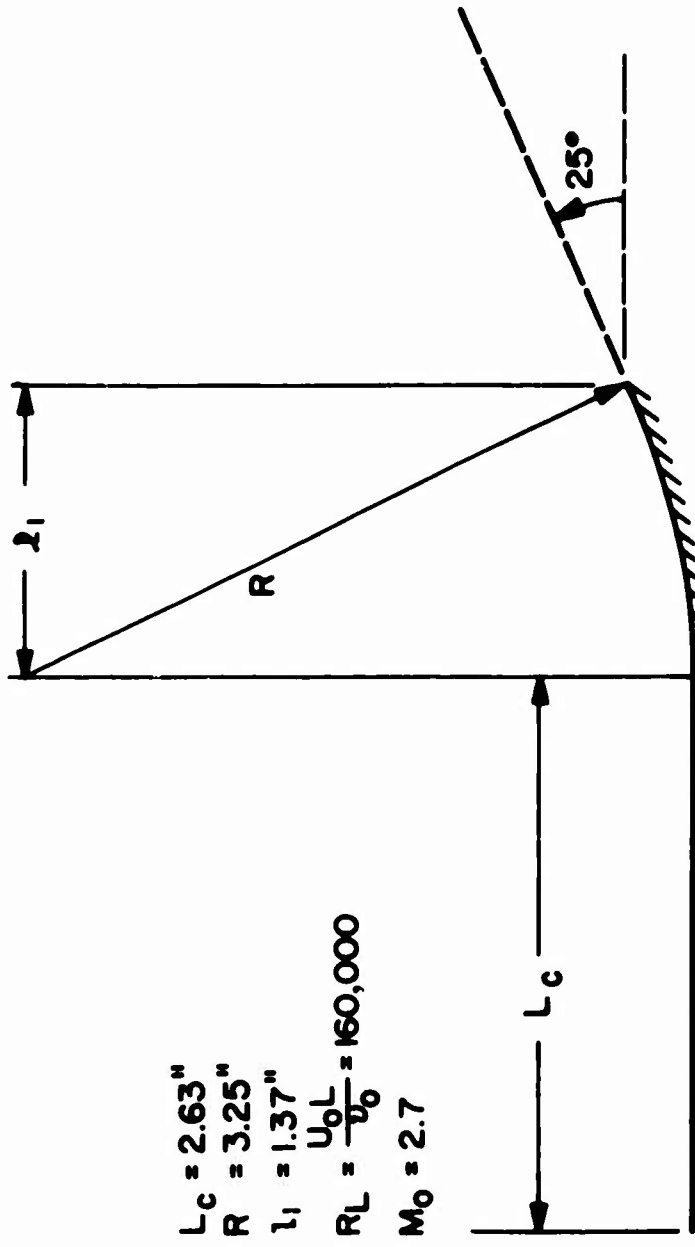


FIGURE 3. - VARIATIONS OF PARAMETERS IN VELOCITY PROFILE FOR PRESCRIBED PRESSURE DISTRIBUTION; PRE-SEPARATION REGION.



$L_c = 2.63''$
 $R = 3.25''$
 $l_1 = 1.37''$
 $RL = \frac{U_0 L}{V_0} = 160,000$
 $M_0 = 2.7$

FIGURE 4. - DIMENSIONS OF EXAMPLE CONFIGURATION.

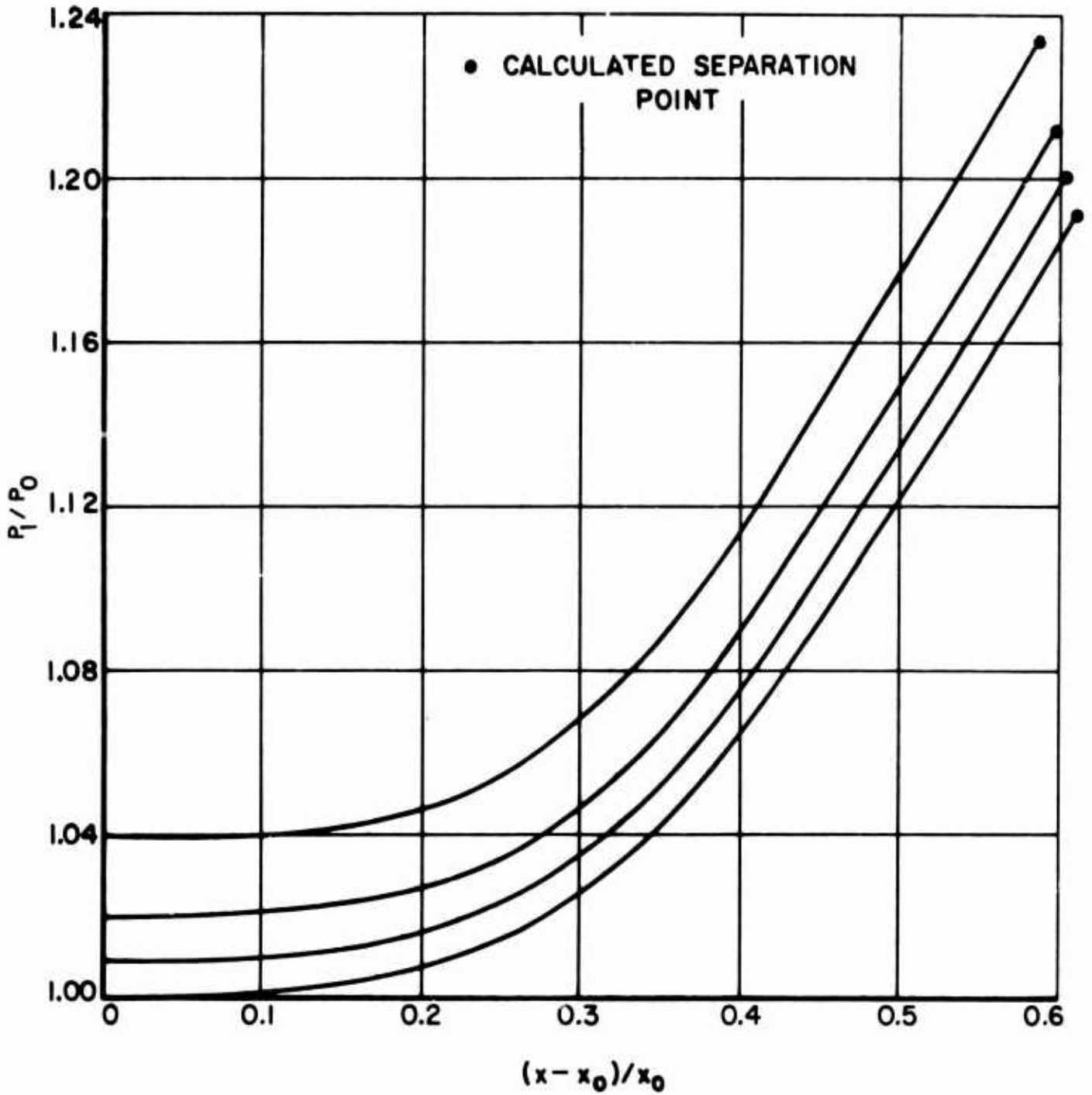


FIGURE 5. - PRE-SEPARATION PRESSURE DISTRIBUTIONS FOR INITIAL PRESSURE DISTURBANCES OF VARIOUS MAGNITUDES.

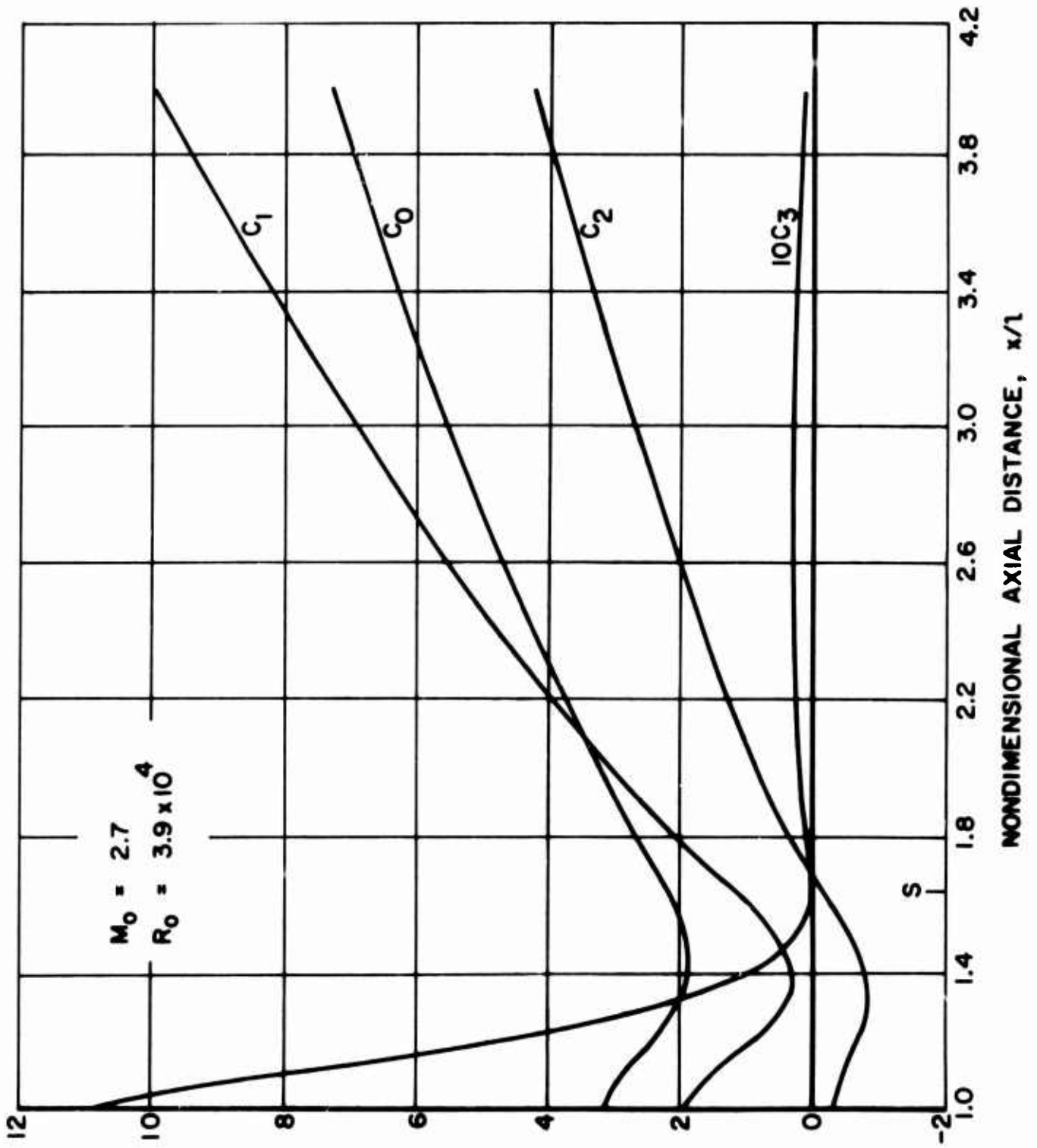


FIGURE 6. - VARIATION OF C_0 , C_1 , C_2 , AND C_3 WITH AXIAL DISTANCE.

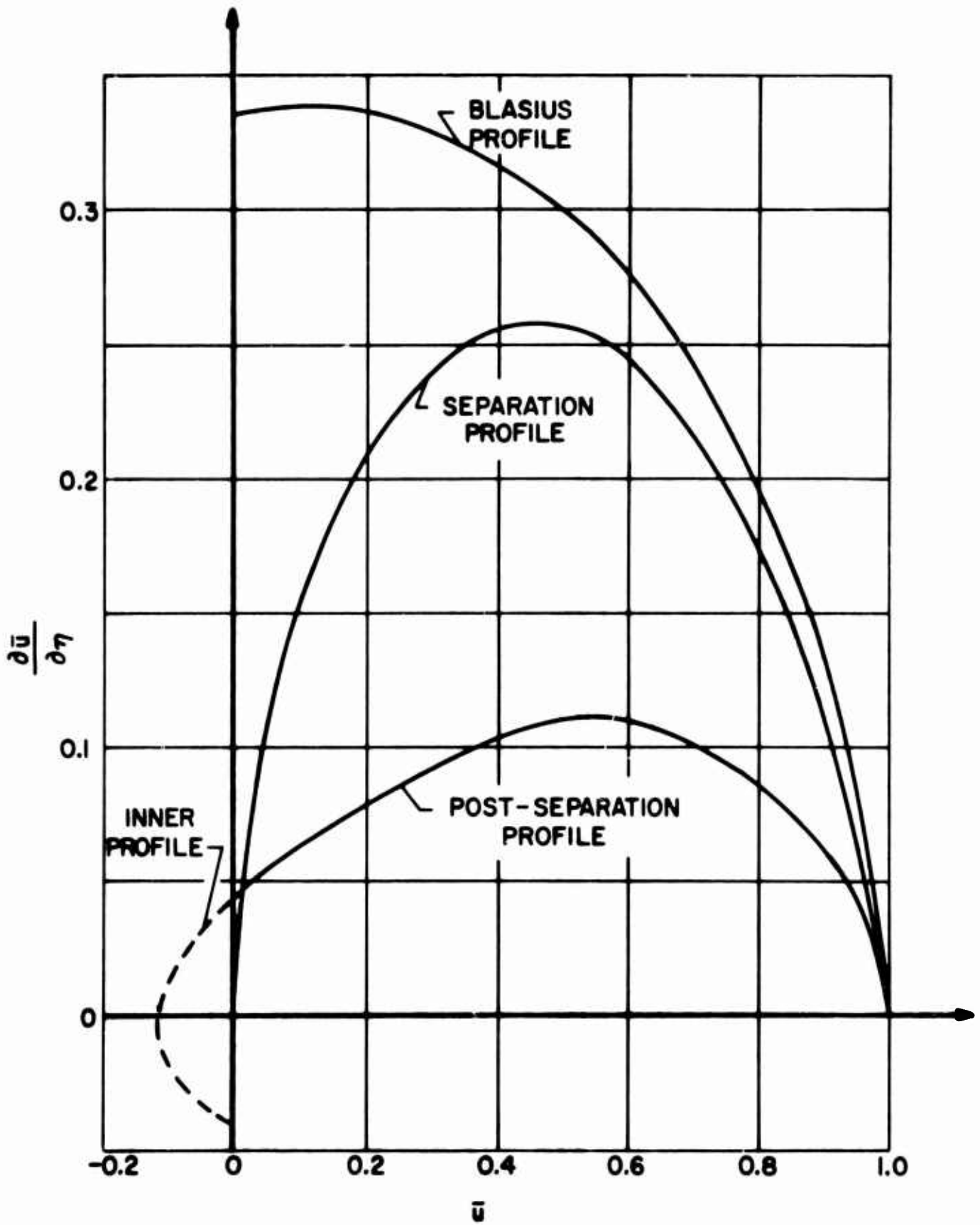


FIGURE 7. - EXAMPLE VELOCITY PROFILES GIVEN BY EQUATION (36).

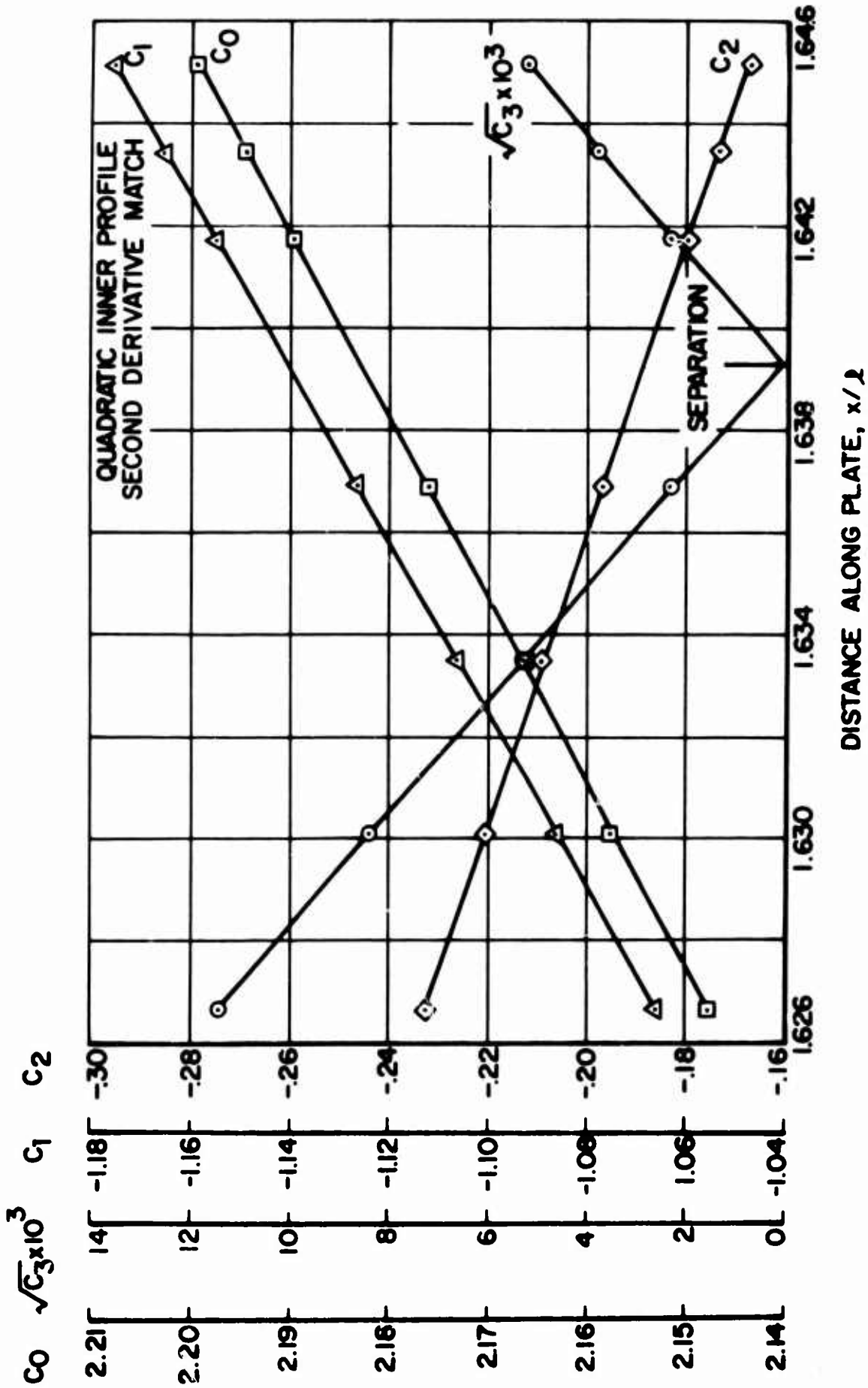


FIGURE 8. - BEHAVIOR OF C_0 , C_1 , C_2 , C_3 , GOING THROUGH SEPARATION POINT.

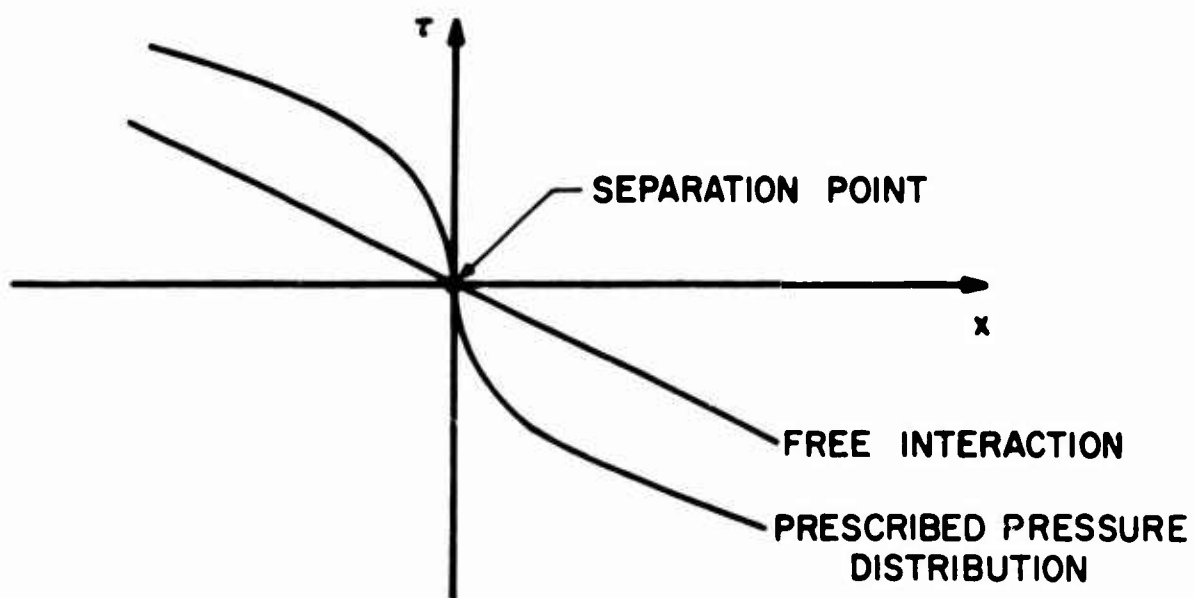
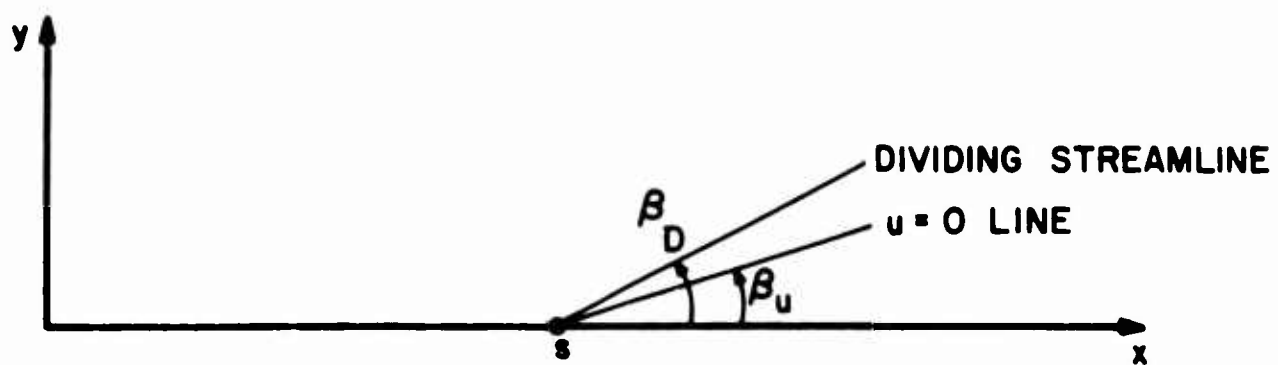


FIGURE 9. - SKETCHES.

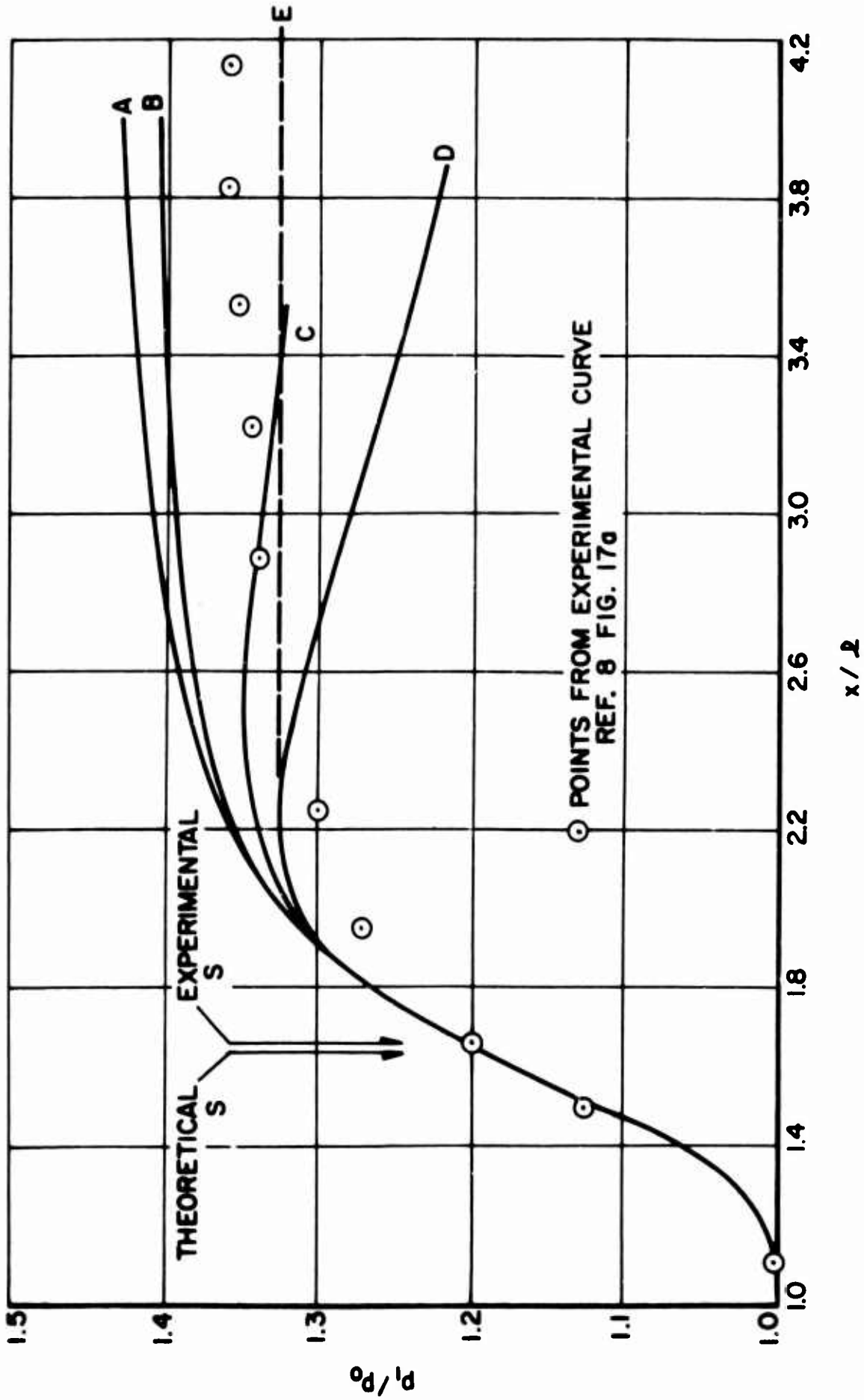
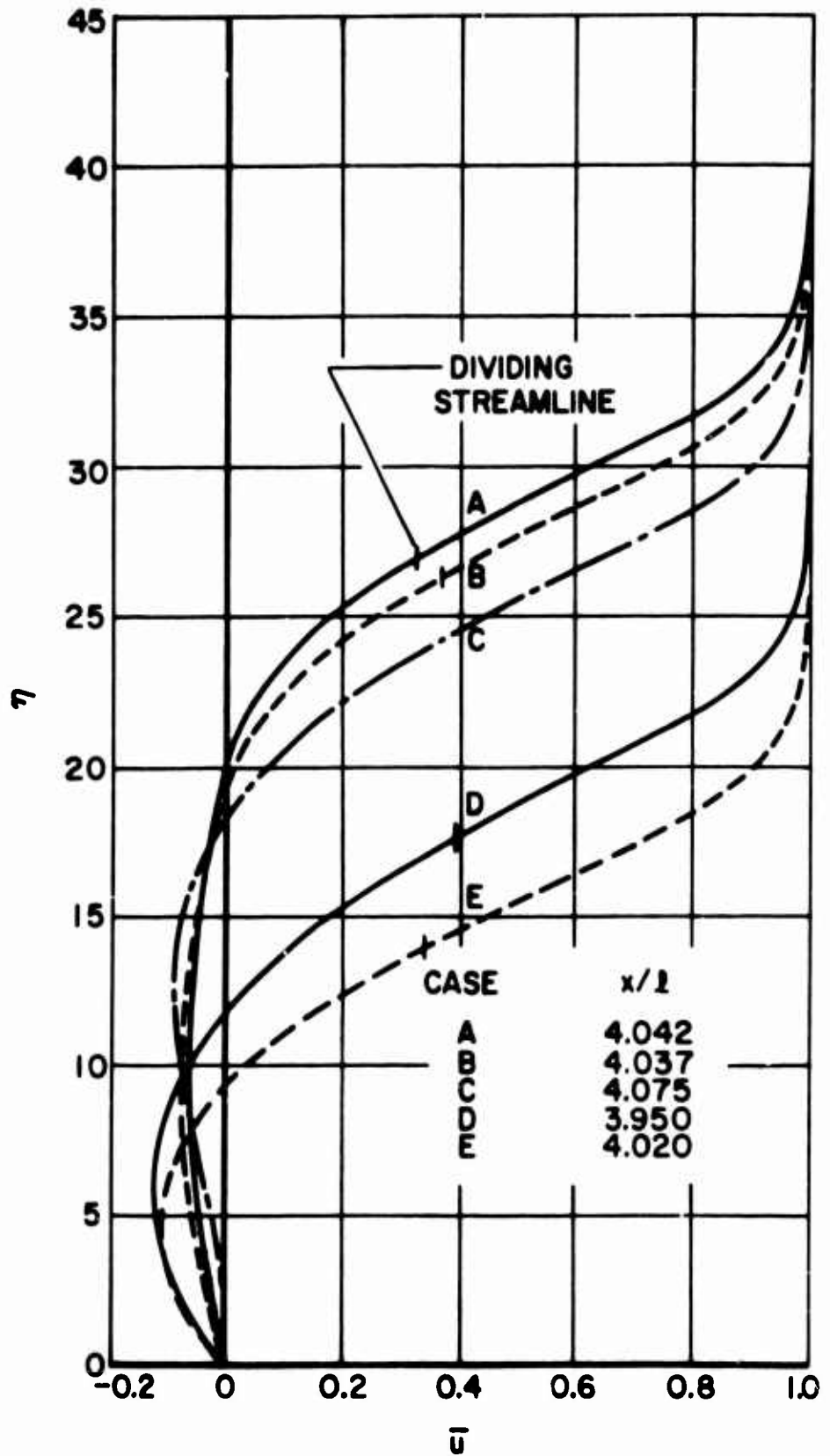
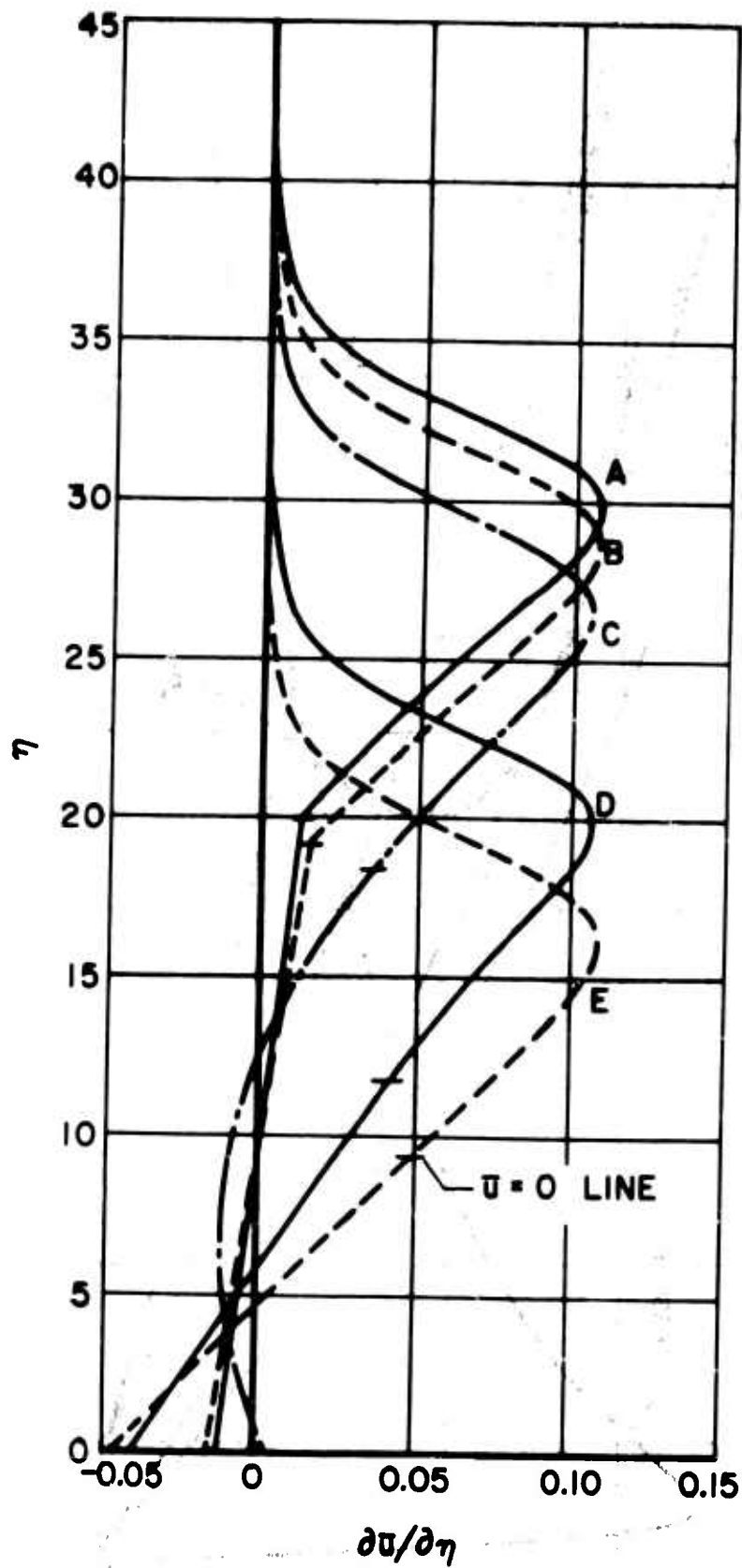


FIGURE 10. - COMPARISON OF VARIOUS SCHEMES FOR CALCULATING POST-SEPARATION PRESSURE DISTRIBUTIONS.



(a) VELOCITY PROFILES.

FIGURE II.- VELOCITY PARAMETERS FAR DOWNSTREAM OF SEPARATION ON BASIS OF VARIOUS ASSUMPTIONS.



(b) VELOCITY GRADIENTS.

FIGURE II. - CONCLUDED.

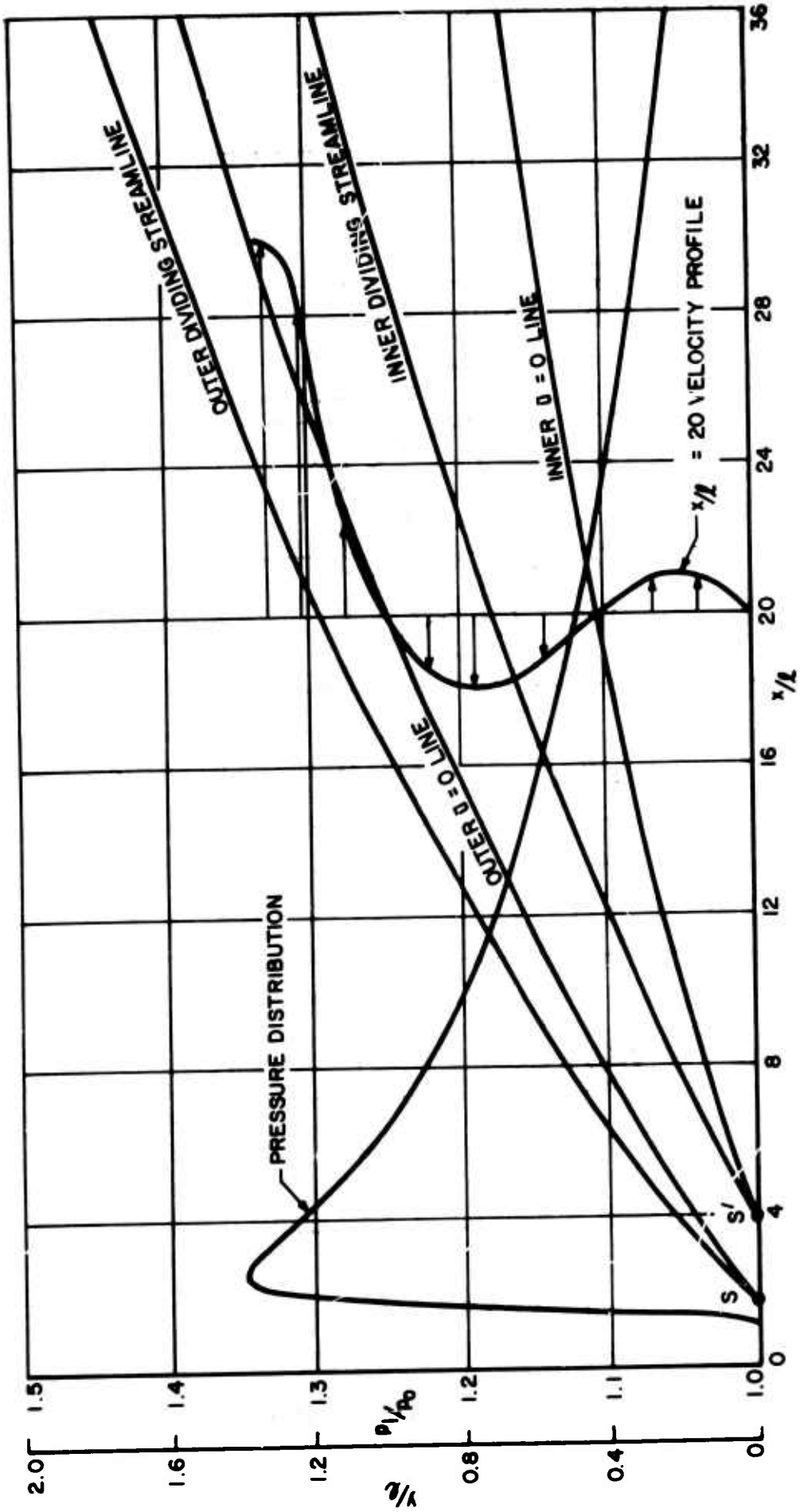


FIGURE 12.- DOWNSTREAM FLOW CONDITIONS DEVELOPED ASYMPTOTICALLY BY SOLUTION FOR CASE C.

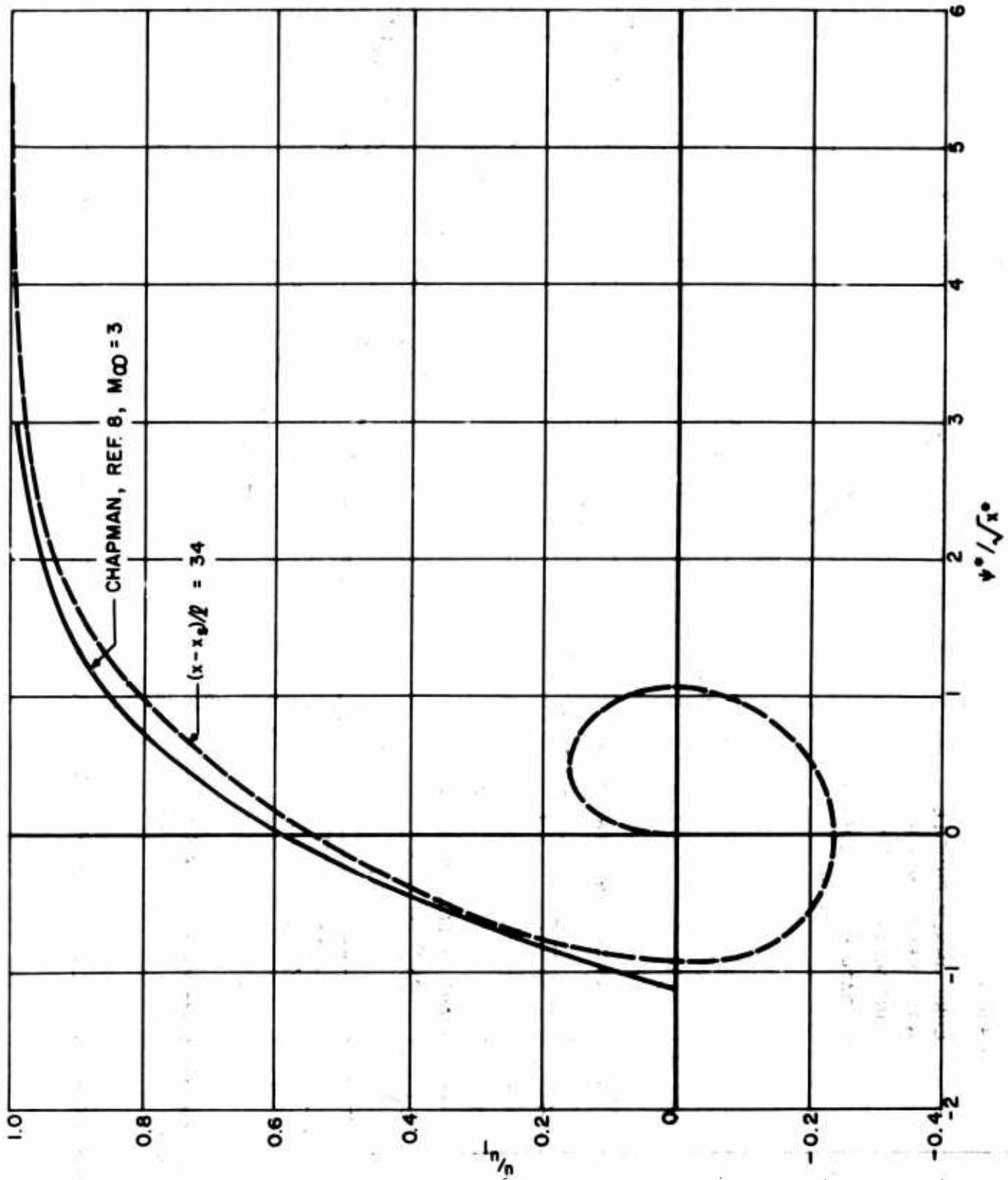


FIGURE 13.- NONDIMENSIONAL VELOCITY PROFILES DEVELOPED ASYMPTOTICALLY BY SOLUTION FOR CASE C.

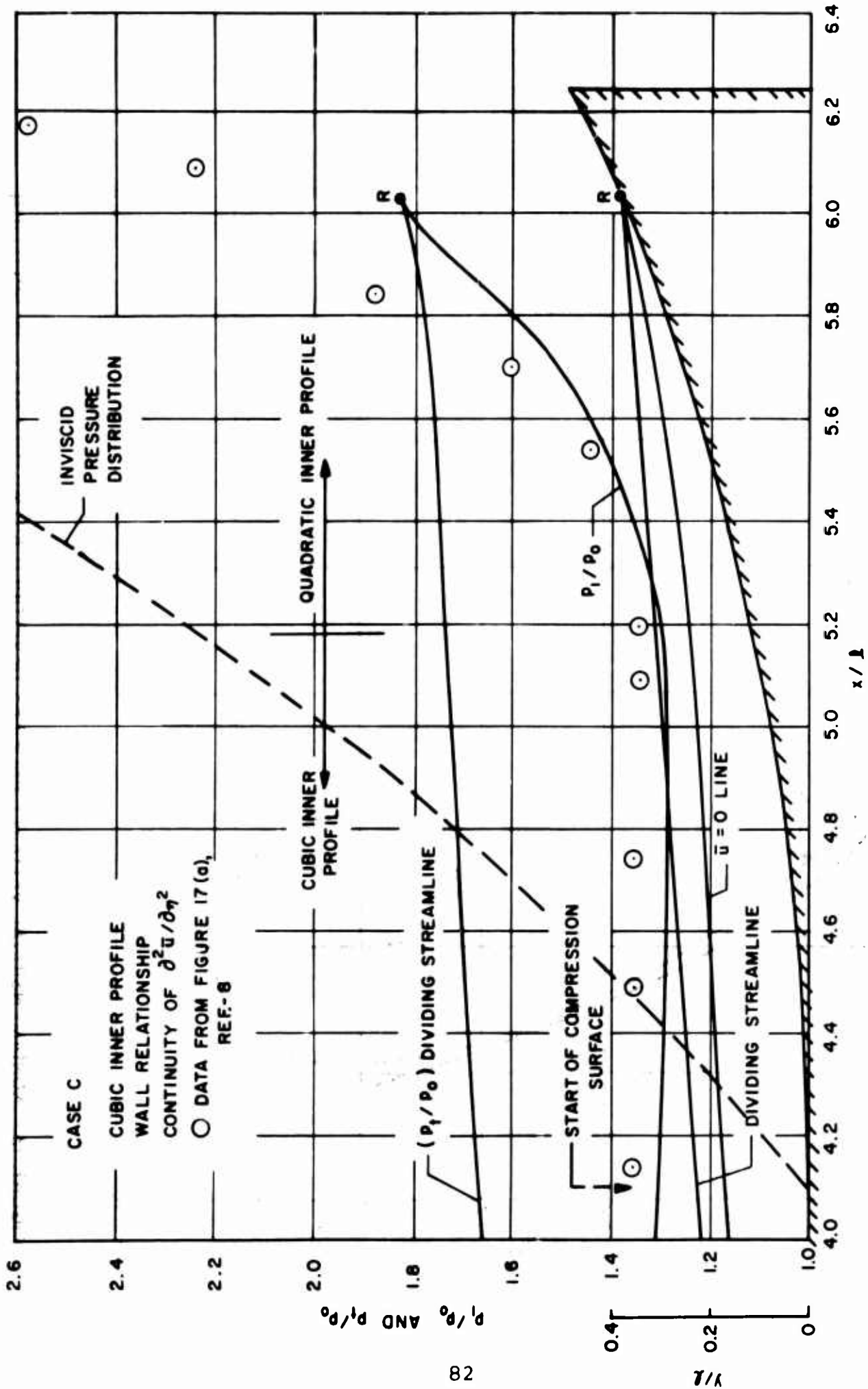


FIGURE 14.- CALCULATED FLOW PATTERN AND PRESSURE DISTRIBUTION IN REATTACHMENT REGION.

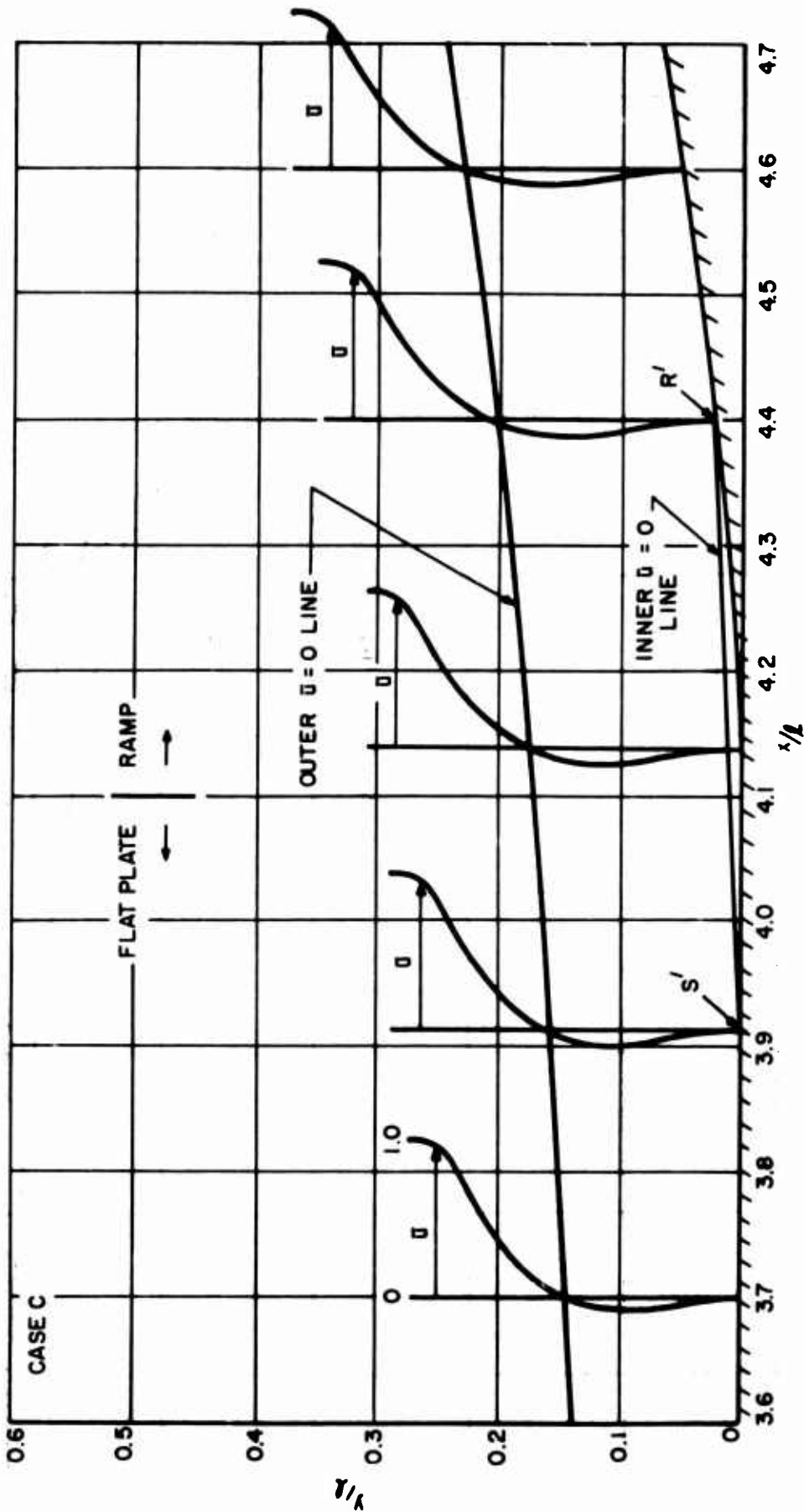


FIGURE 15.-VELOCITY DISTRIBUTION THROUGH THE BOUNDARY LAYER IN THE REGION OF THE COMPRESSION CORNER FOR CASE C.

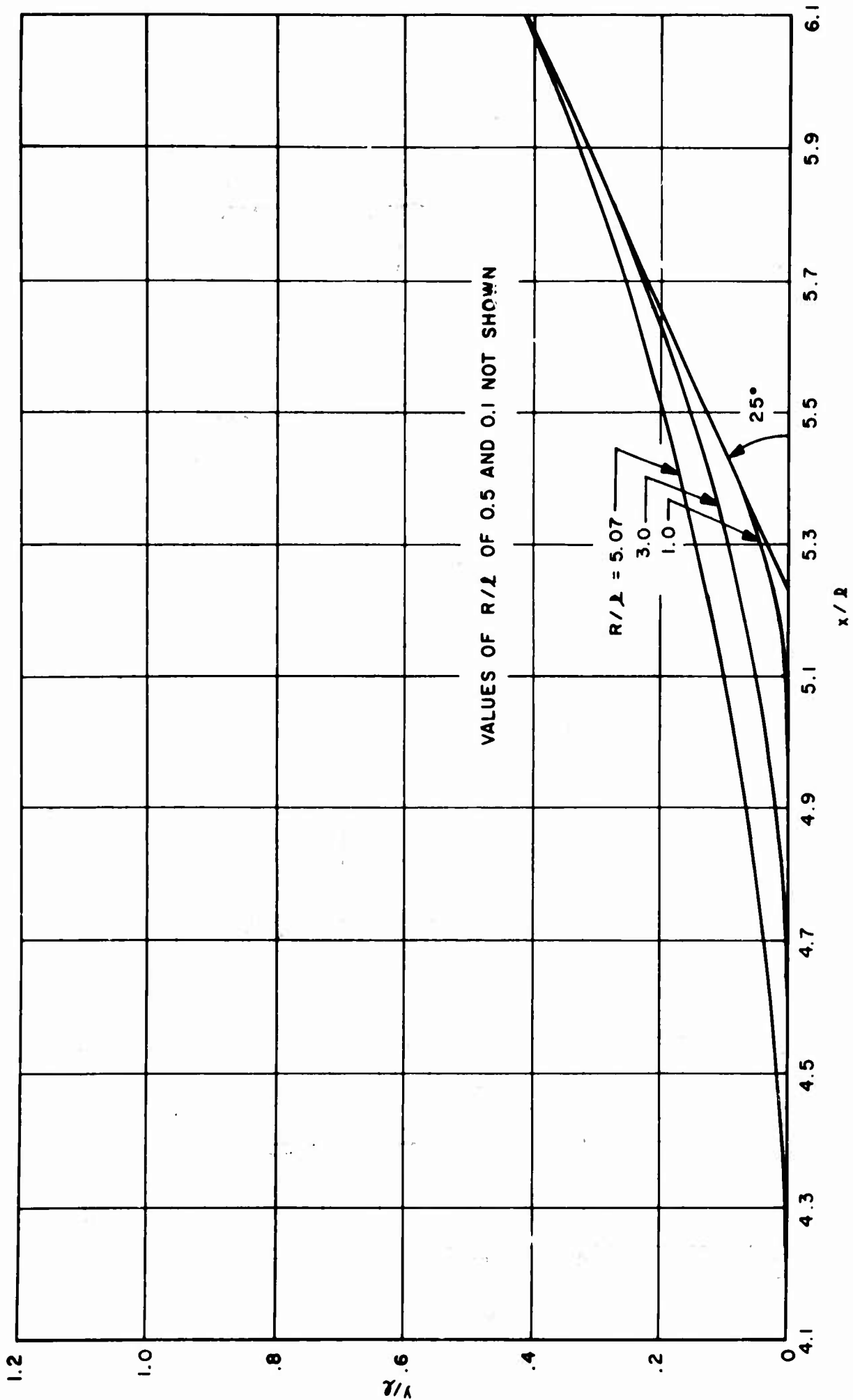


FIGURE 16.- FLAT PLATE WITH WEDGE WITH CIRCULAR ARC FAIRINGS OF VARIOUS RADII.

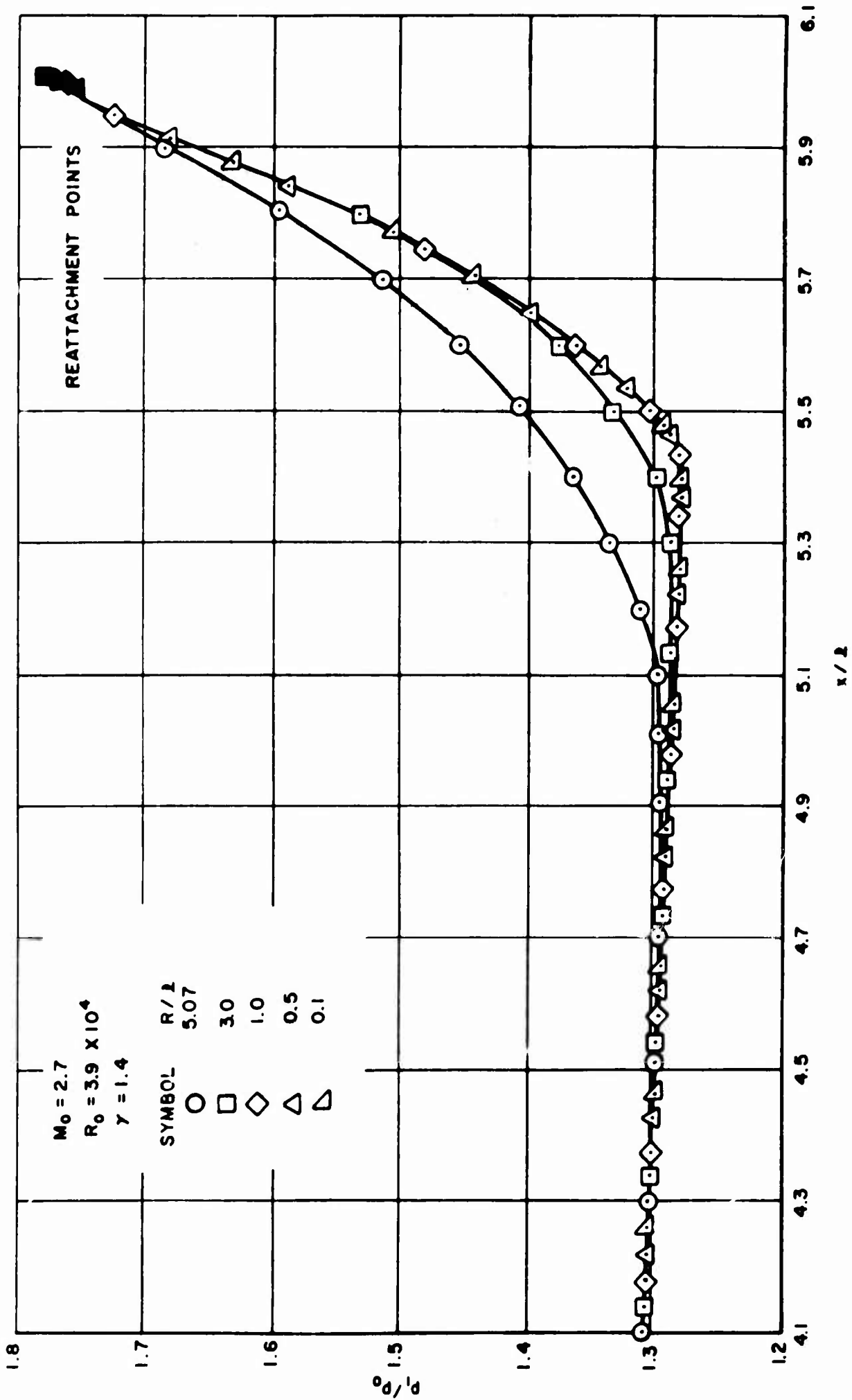


FIGURE 17.- EFFECT OF FAIRING RADIUS ON CALCULATED PRESSURE DISTRIBUTIONS.

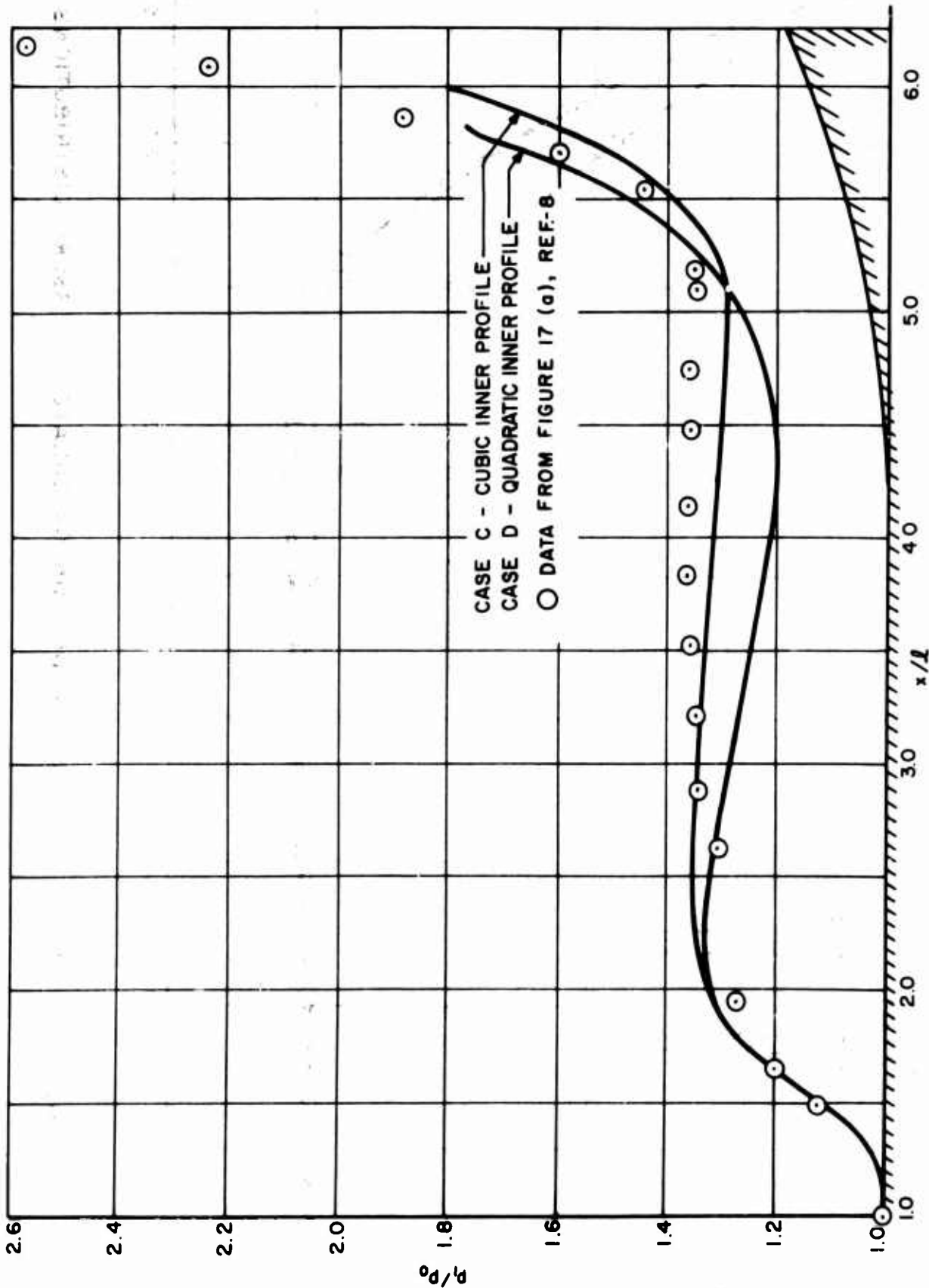


FIGURE 18.- EFFECT OF INNER VELOCITY PROFILE APPROXIMATION ON CALCULATED PRESSURE DISTRIBUTION.

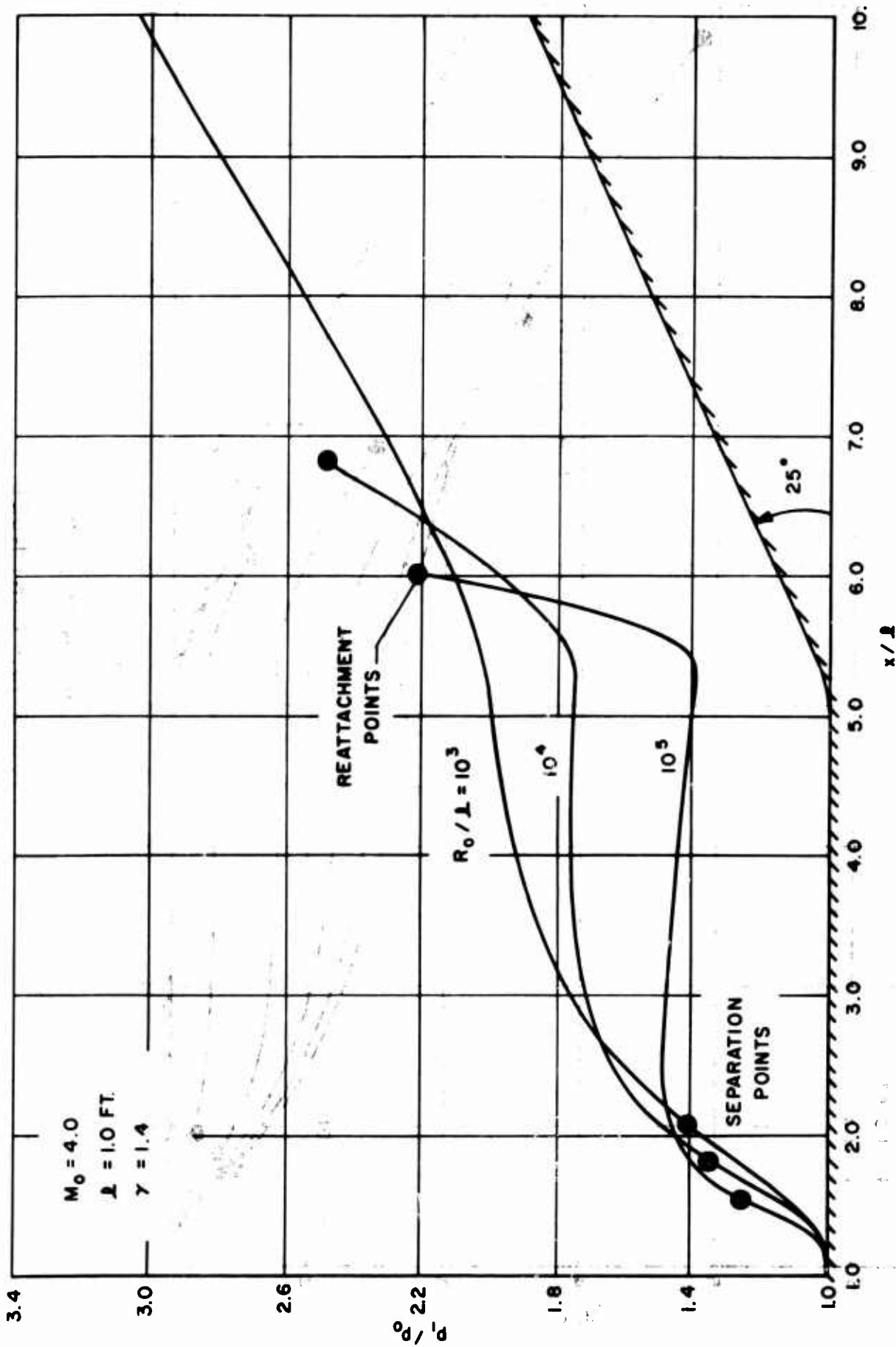
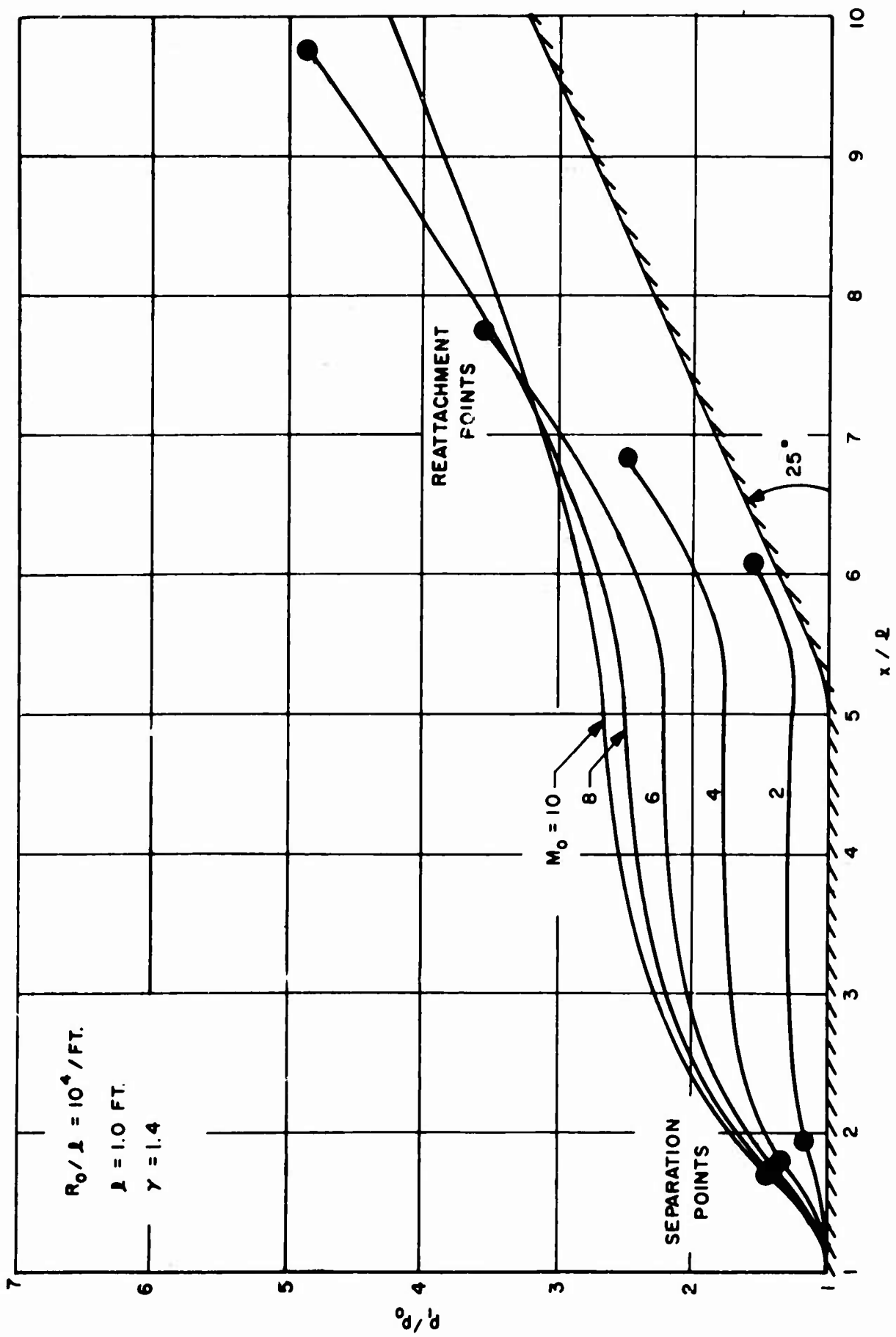
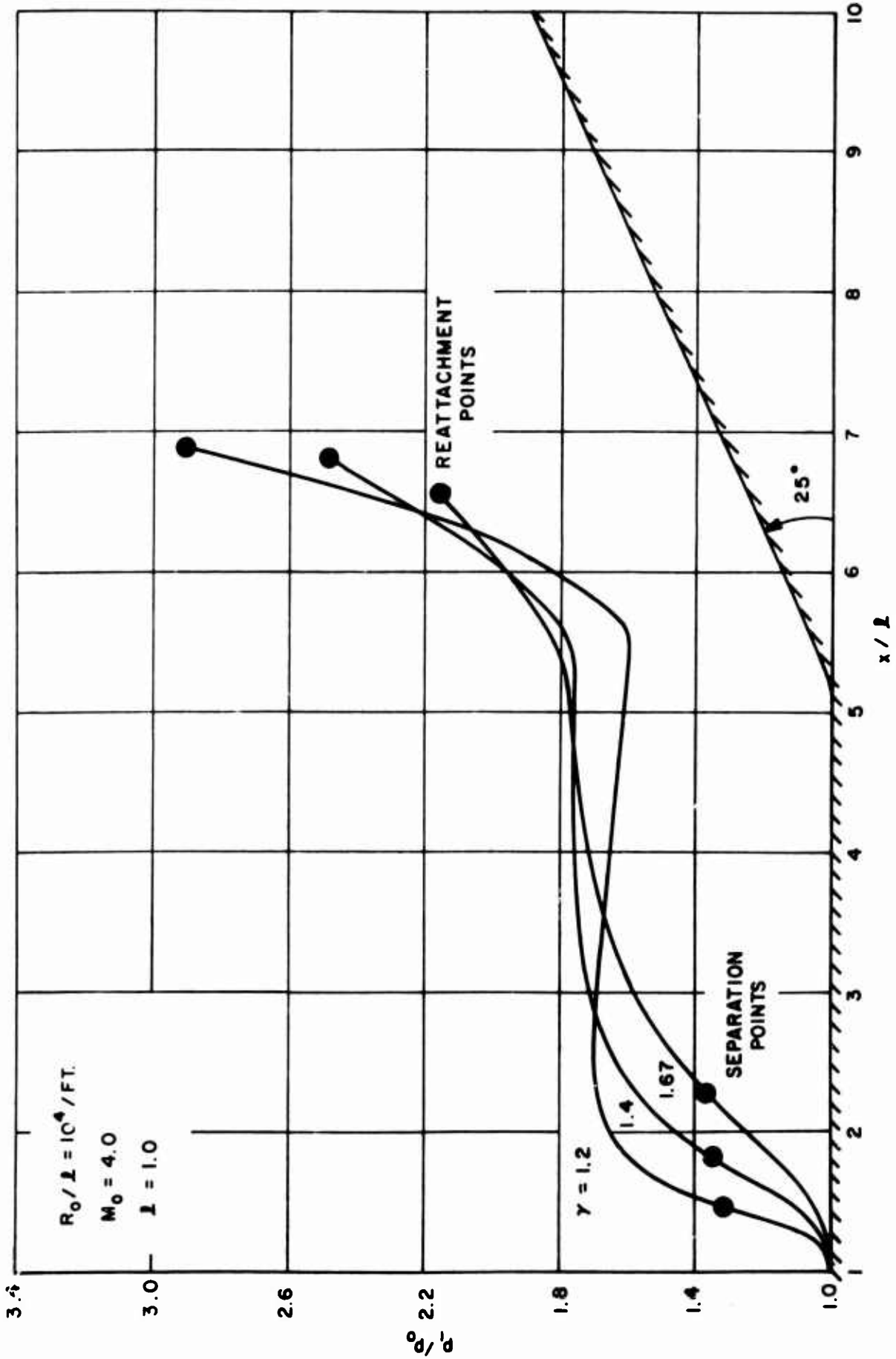


FIGURE 19.- EFFECT OF INITIAL PARAMETERS ON LAMINAR SEPARATION WITH FREE INTERACTION. (o) REYNOLDS NUMBER.



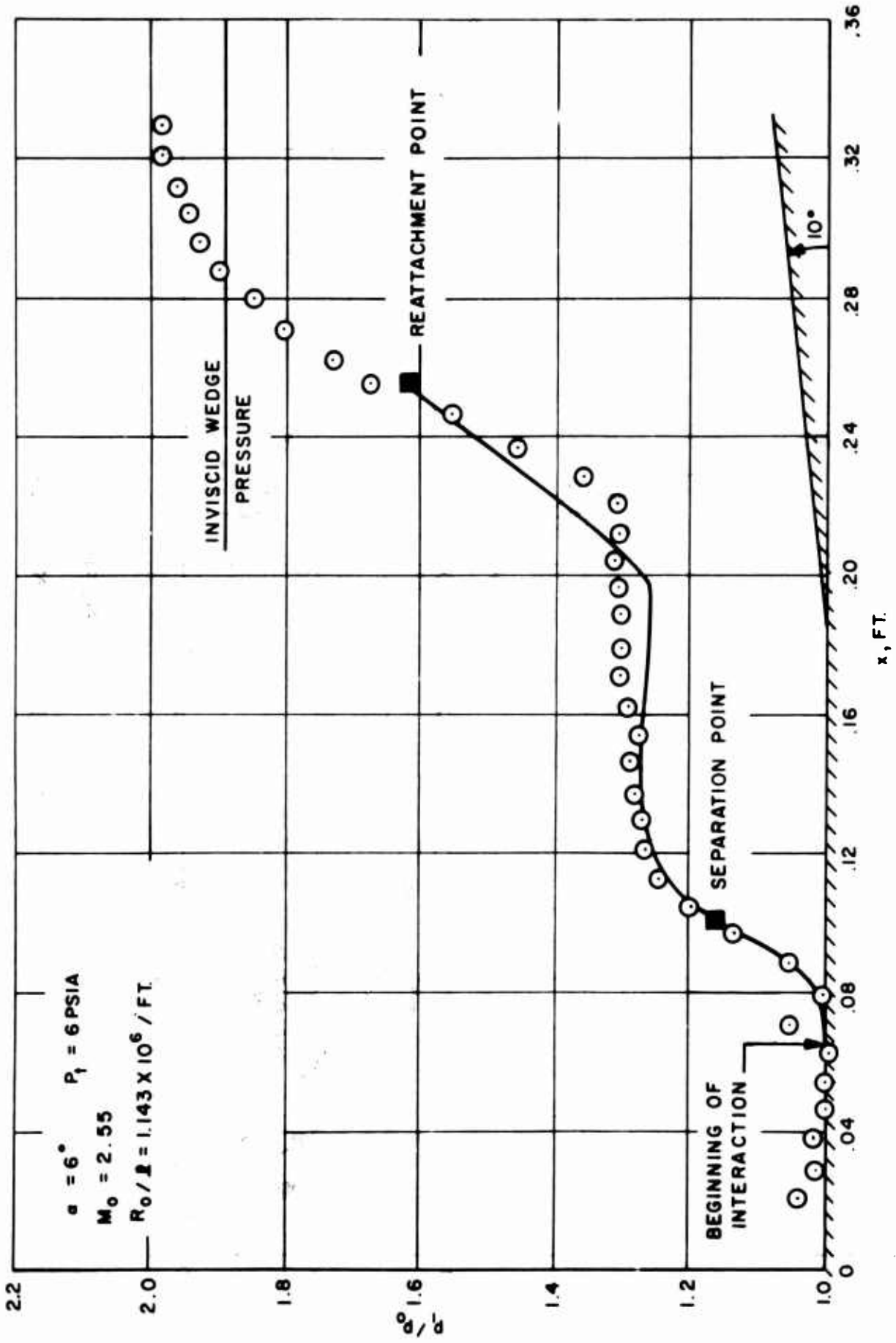
(b) MACH NUMBER.

FIGURE 19. - CONTINUED.



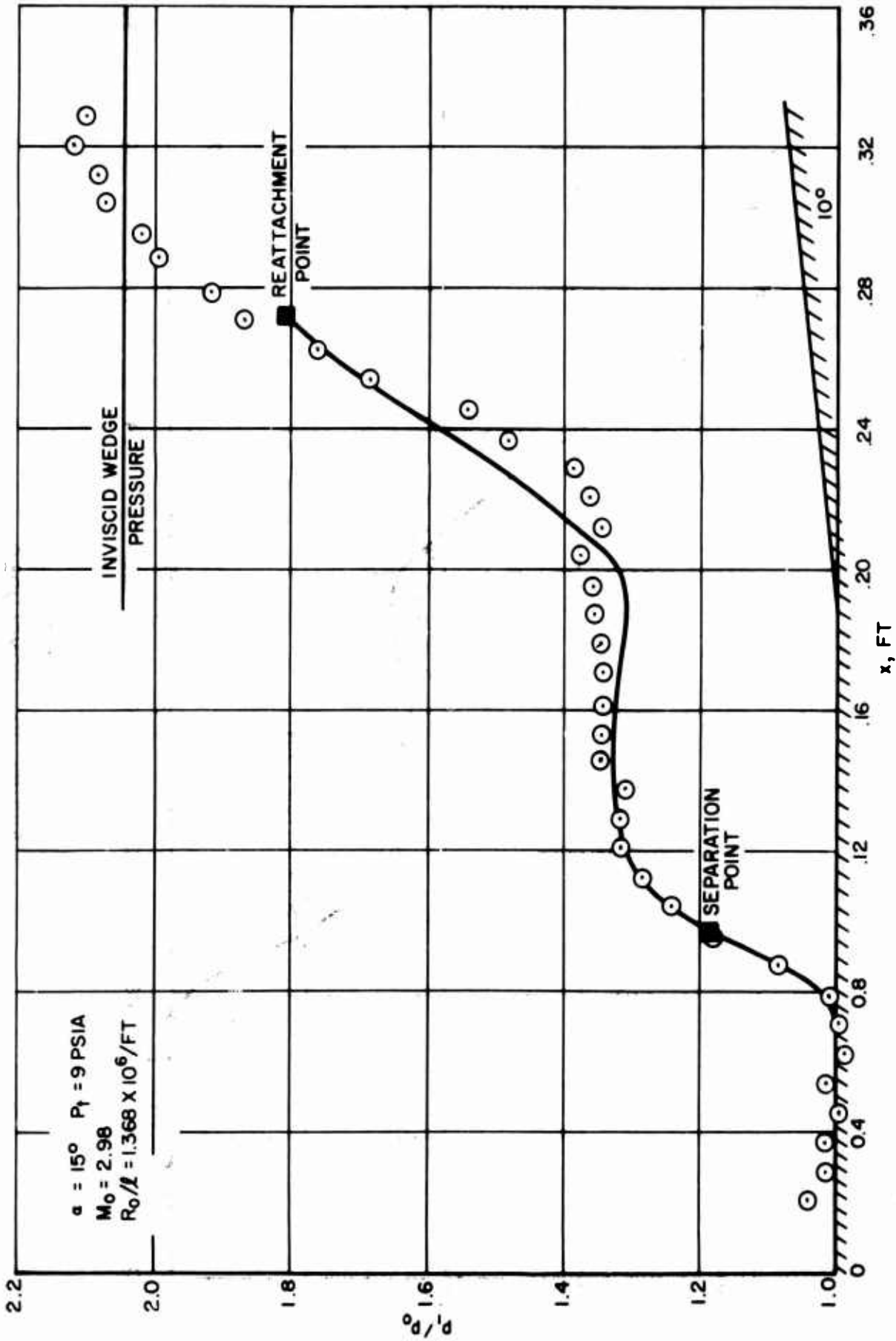
(c) RATIO OF SPECIFIC HEATS.

FIGURE 19. - CONCLUDED.

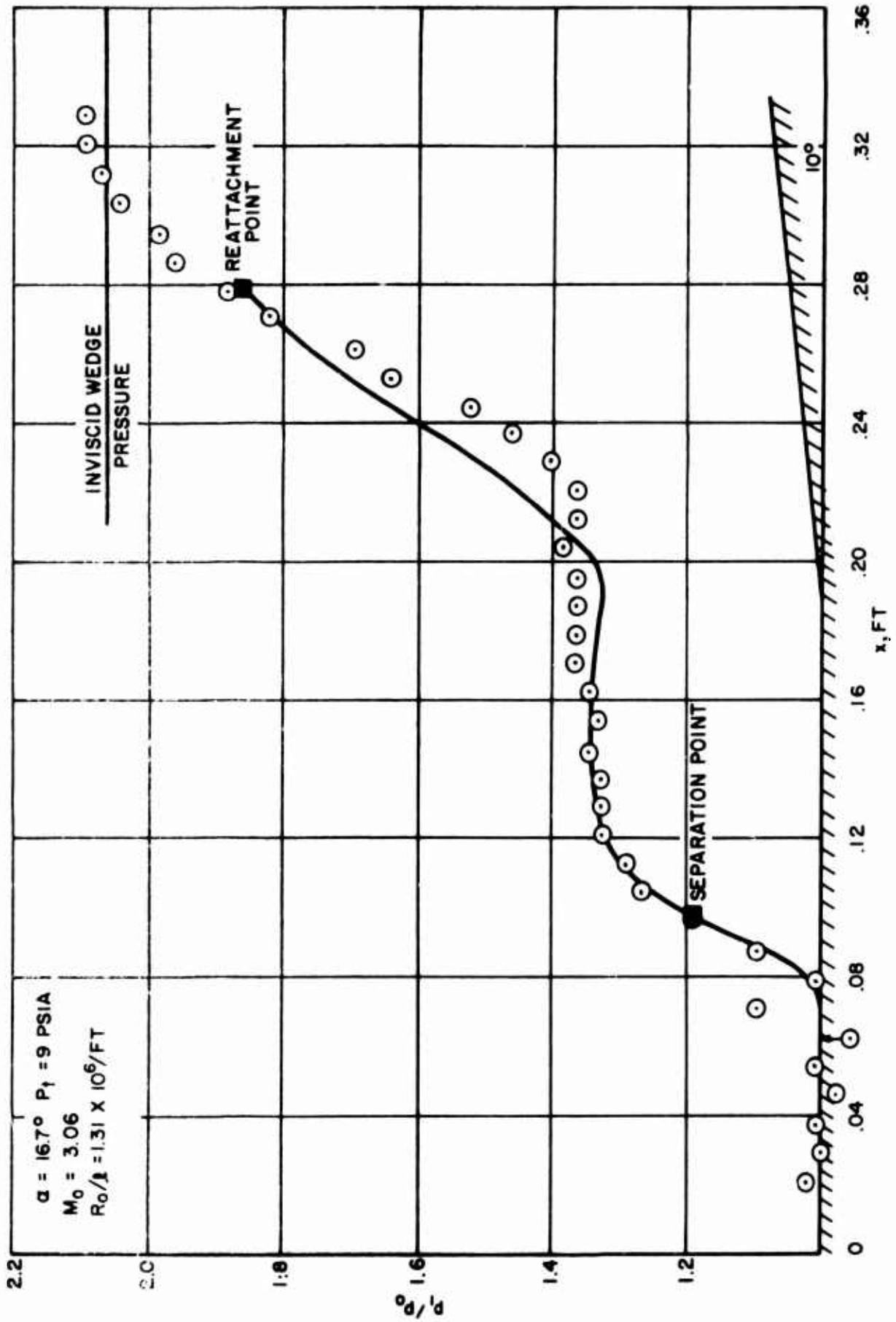


(a) $\alpha = 6^\circ$

FIGURE 20.- COMPARISON BETWEEN MEASURED AND CALCULATED PRESSURE DISTRIBUTIONS FOR FLAT PLATE WITH 10° WEDGE.



(b) $\alpha = 15^\circ$.
 FIGURE 20 . - CONTINUED.



(c) $\alpha = 16.7^\circ$
 FIGURE 20.- CONCLUDED.

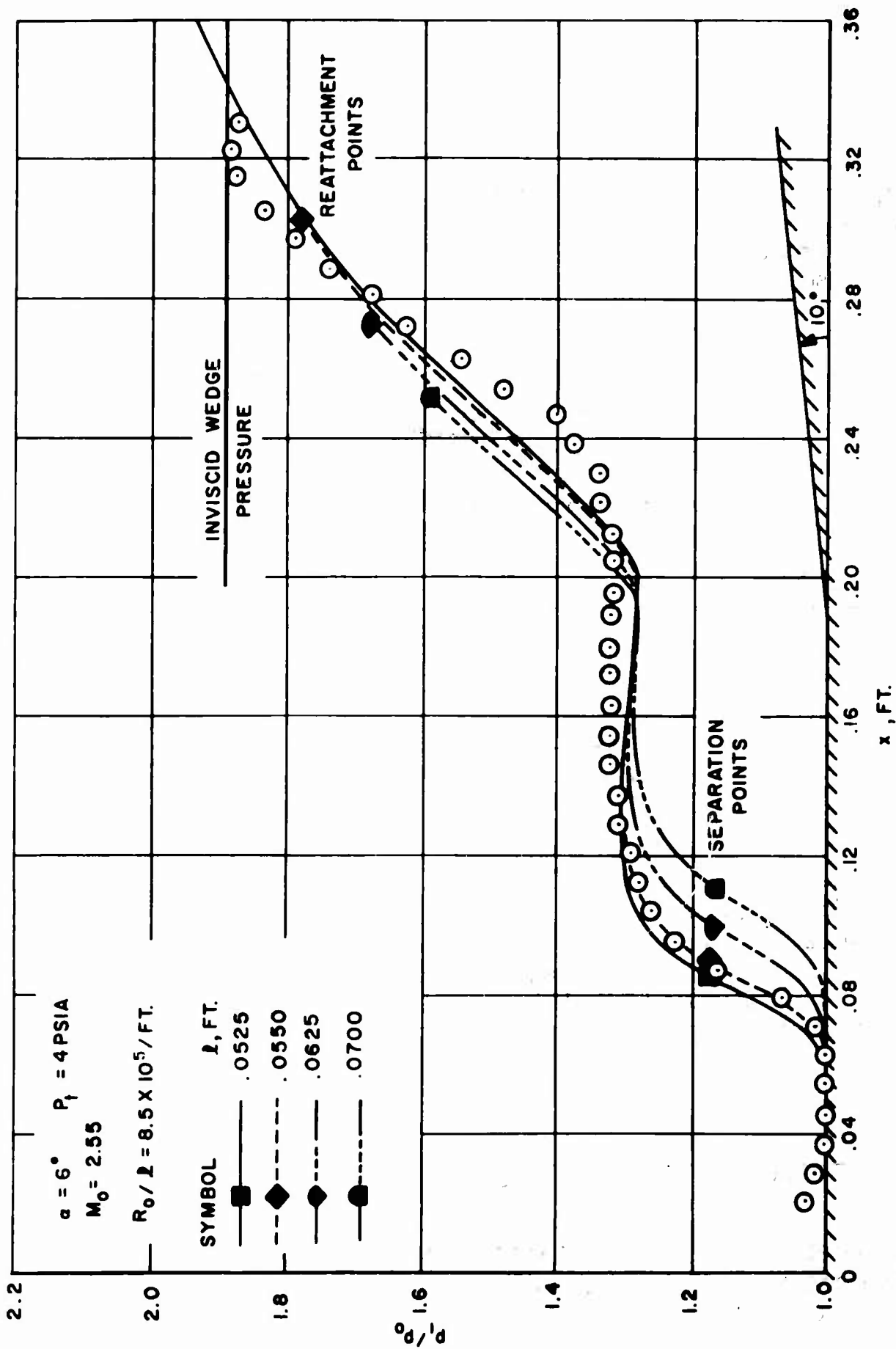


FIGURE 21. - EFFECT ON CALCULATED PRESSURE DISTRIBUTION OF SYSTEMATIC VARIATIONS IN BEGINNING OF INTERACTION.

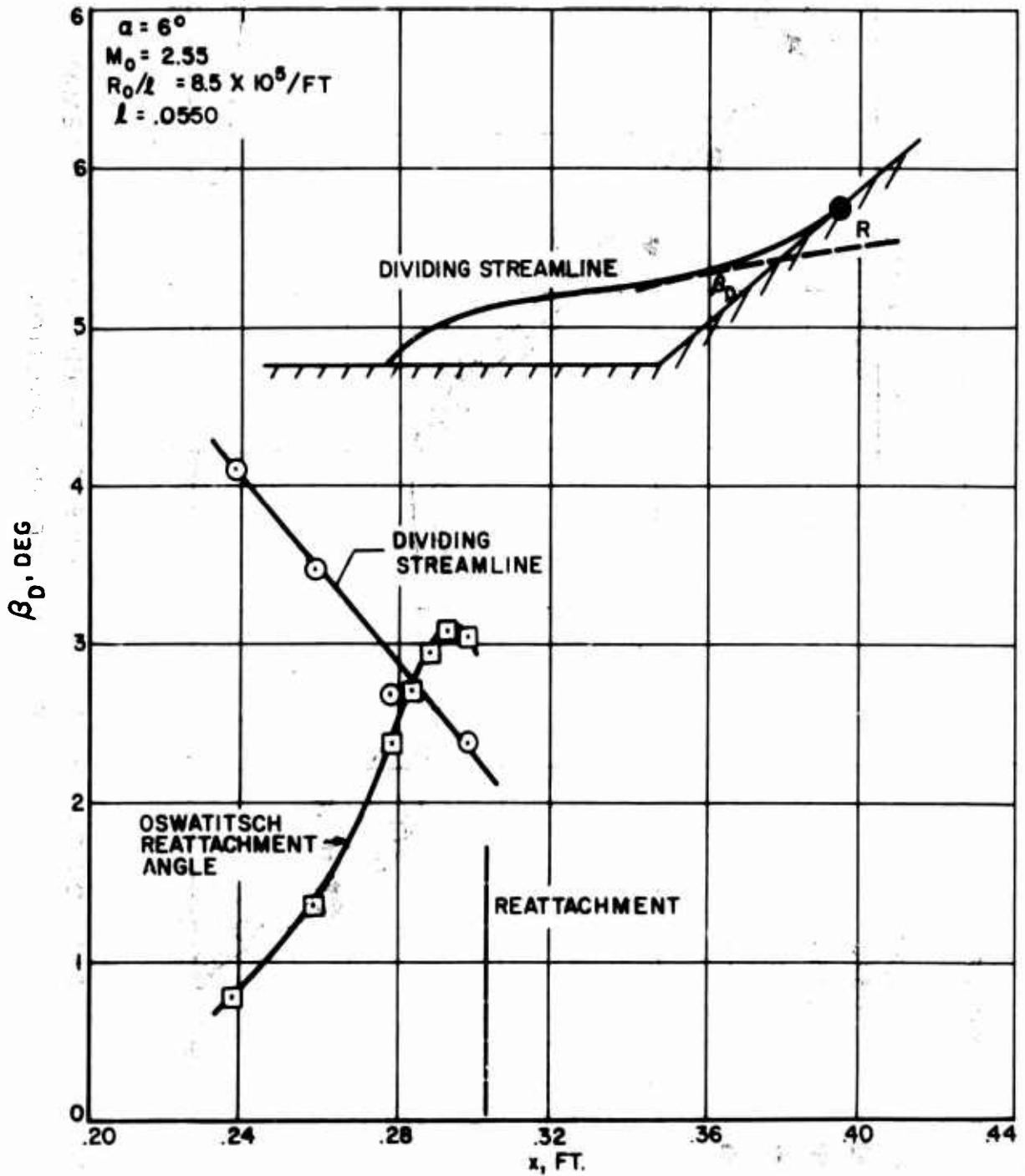


FIGURE 22.- VARIATION WITH DOWNSTREAM DISTANCE OF OSWATITSCH REATTACHMENT ANGLE AND DIVIDING STREAMLINE SLOPE (RELATIVE TO WEDGE).

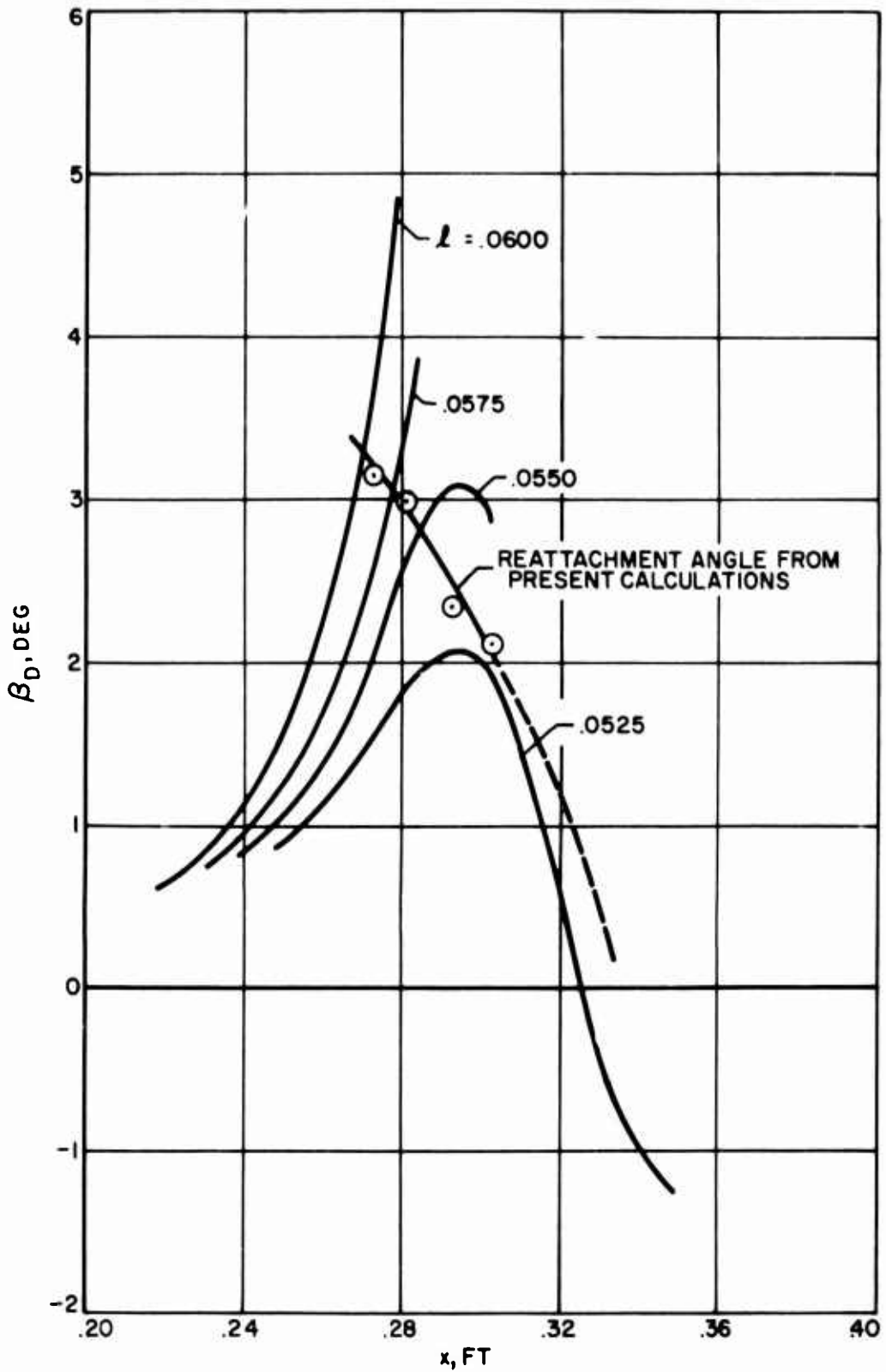
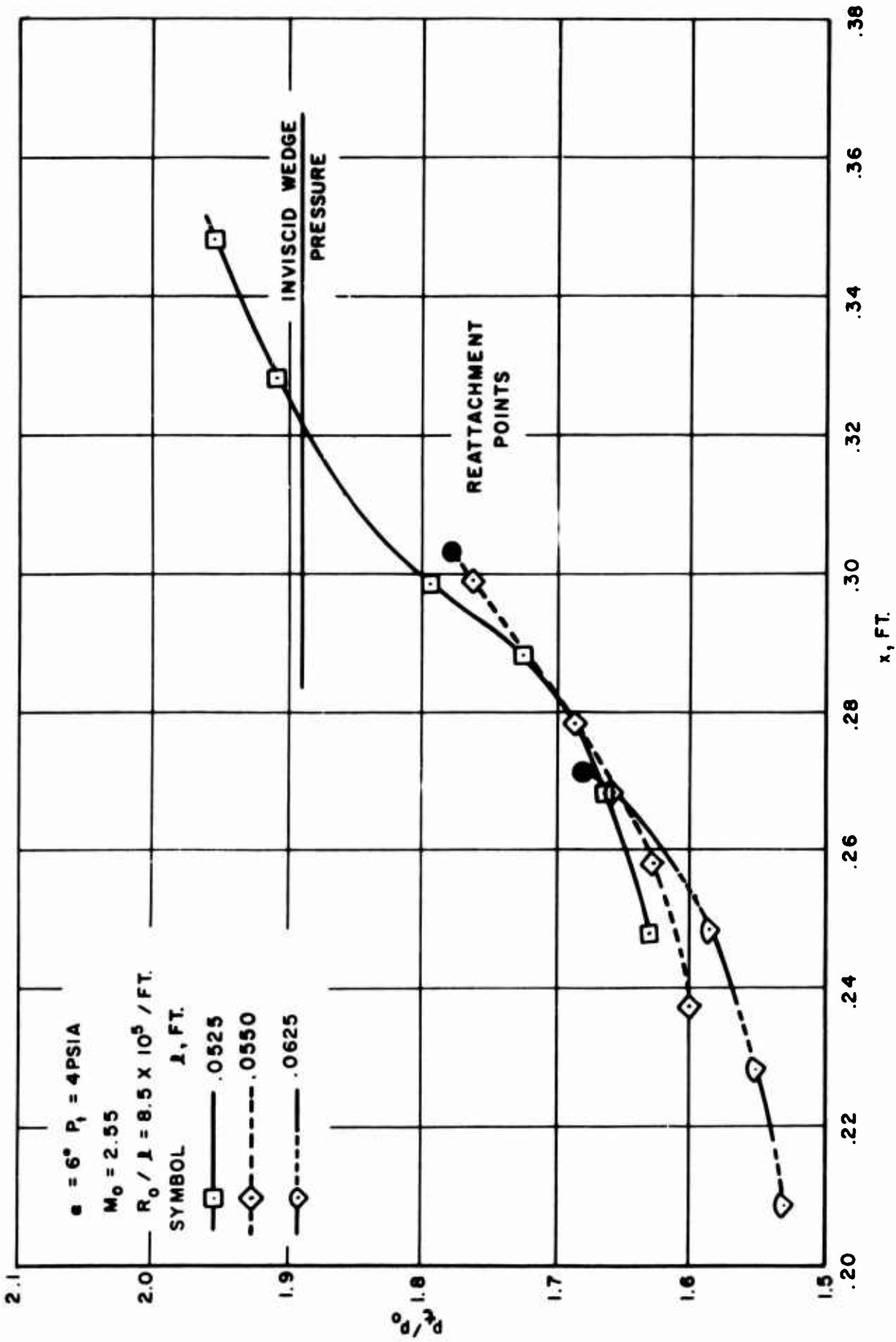
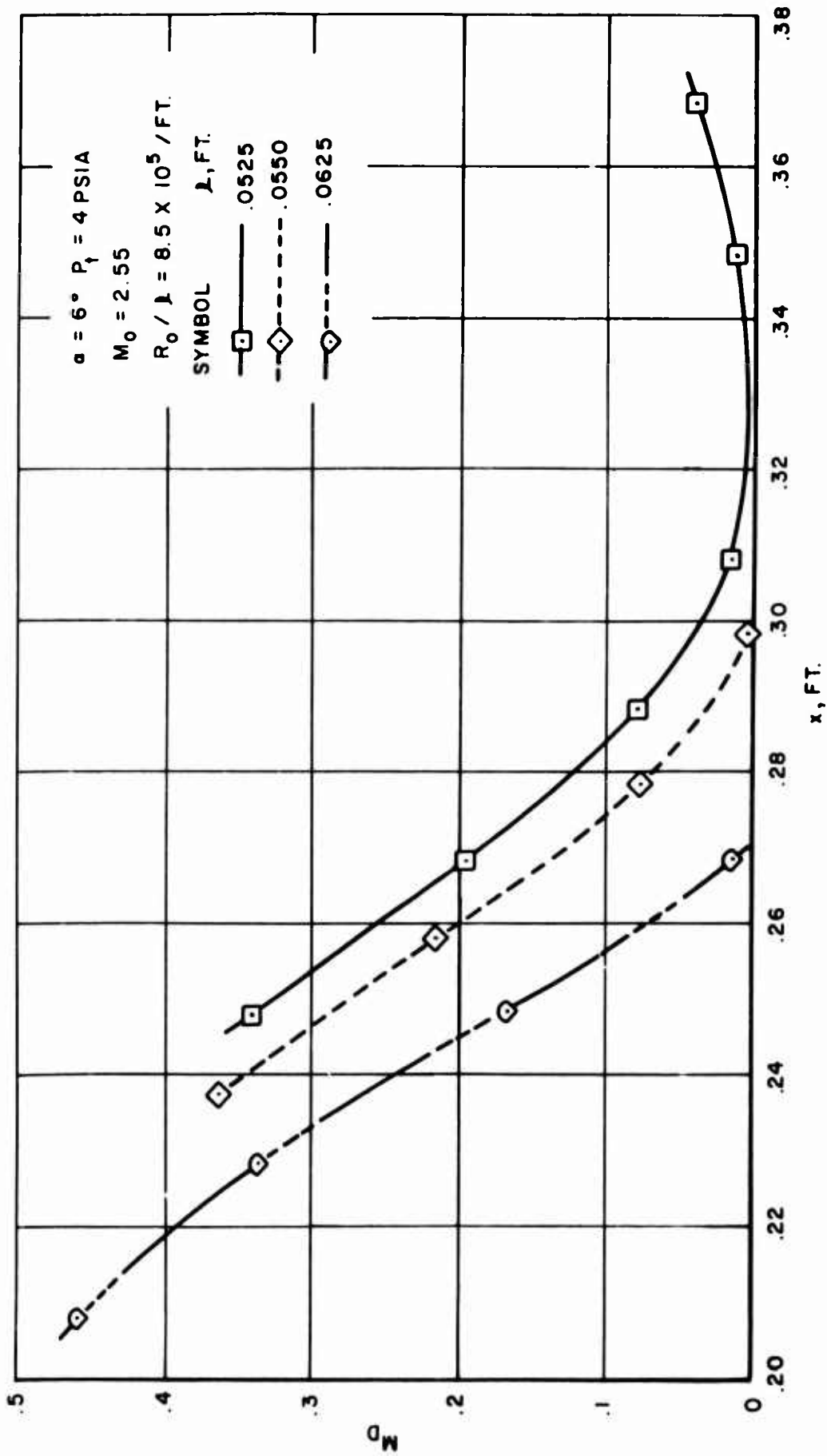


FIGURE 23.- VARIATION OF OSWATITSCH REATTACHMENT ANGLE FOR DIFFERENT POSITIONS OF BEGINNING OF INTERACTION.



(a) TOTAL PRESSURE ON DIVIDING STREAMLINE.
 FIGURE 24.- VARIATION OF QUANTITIES ALONG DIVIDING STREAMLINE APPROACHING REATTACHMENT.



(b) MACH NUMBER ON DIVIDING STREAMLINE.

FIGURE 24.- CONCLUDED.

APPENDIX I
CALCULATION OF g_n FUNCTIONS

The family of functions of a single variable occurring in the analysis are given by Equation (43) as follows:

$$g_n(c_3) = \int_0^1 \frac{u^n du}{\sqrt{u + c_3}}, \quad c_3 \geq 0 \quad (\text{I-1})$$

Simple integration yields,

$$g_0(c_3) = 2(\sqrt{1 + c_3} - \sqrt{c_3}) \quad (\text{I-2})$$

The other g_n functions can then be simply generated by the following recursion relationship

$$g_n = \frac{2}{2n + 1} (\sqrt{1 + c_3} - nc_3 g_{n-1}) \quad (\text{I-3})$$

For large values of c_3 the recursion formula requires many more decimals of calculation than significant figures in the calculated result so that a series solution rapidly convergent for large c_3 is desirable.

The following results are used for large c_3

$$g_n(c_3) = \int_0^1 \frac{u^n du}{\sqrt{c_3} \left(1 + \frac{u}{c_3}\right)^{1/2}} = \frac{1}{\sqrt{c_3}} \int_0^1 \left(u^n + \sum_{k=1}^{\infty} \frac{j_k u^{n+k}}{c_3^k} \right) du \quad (\text{I-4})$$

$$g_n(c_3) = \frac{1}{\sqrt{c_3}} \left[\frac{1}{n+1} + \sum_{k=1}^{\infty} \frac{j_k}{n+k+1} \left(\frac{1}{c_3}\right)^k \right] \quad (\text{I-5})$$

$$j_k = \frac{(-1)^k (2k-1)!}{2^{2k-1} k! (k-1)!} \quad (\text{I-6})$$

APPENDIX II

DERIVATION OF FREE-INTERACTION RELATIONSHIP

The basic assumption for calculating the pressure gradients of the external flow field is that such gradients are the same as those for an inviscid flow with the solid boundaries augmented by an amount δ^* due to the boundary layer. The particular inviscid flow relationship used for the calculation is not germane to the basic assumption, and in this case was taken to be the Prandtl-Meyer shock-expansion relationship

$$\frac{dp_1}{p_1} = \frac{\gamma M_1^2}{\cos \phi \sqrt{M_1^2 - \cos^2 \phi}} d\phi \quad (\text{II-1})$$

It is noted that in free interaction the pressure distribution is thus dependent on the variation of δ^* along the body, and the variation of δ^* in turn depends on the pressure distribution. This interrelationship will be termed the free-interaction equation. Specifically, it will consist of two equations, Equation (II-1) and the following equation relating ϕ to the boundary-layer quantities.

$$\frac{d\delta_o^*}{dx} + \frac{d\delta_i^*}{dx} + \frac{dw}{dx} = \tan \phi \quad (\text{II-2})$$

where

δ_o^* displacement thickness of outer flow

δ_i^* displacement thickness of inner flow

$\frac{dw}{dx}$ slope of streamwise boundary

Pre-Separation Region

The calculation of δ_o^* and its derivative is a fairly laborious algebraic operation which will now be carried out. The definition of δ_o^* is

$$\delta_o^* = \int_s^\infty \left(1 - \frac{\rho u}{\rho_1 u_1} \right) dy \quad (\text{II-3})$$

We will transform the integral to η

$$\delta_o^* = \frac{\rho_o a_o}{\rho_1 a_1} \frac{\sqrt{U_o l v_o}}{U_1} \int_{\eta_s}^\infty \left(\frac{\rho_1}{\rho} - \frac{u}{u_1} \right) d\eta \quad (\text{II-4})$$

Now since

$$T \left(1 + \frac{\gamma - 1}{2} \frac{u^2}{a^2} \right) = T_1 \left(1 + \frac{\gamma - 1}{2} \frac{u_1^2}{a_1^2} \right)$$

$$m_1 = \frac{u_1^2}{a_1^2} \frac{(\gamma - 1)}{2}$$

$$u = U \frac{a_1}{a_o}$$

we have

$$\frac{\rho_1}{\rho} = \frac{T}{T_1} = (1 + m_1) - m_1 \frac{U^2}{U_1^2} = (1 + m_1) - m_1 \bar{u}^2 \quad (\text{II-5})$$

so that

$$\delta_o^* = \frac{\rho_o a_o}{\rho_1 a_1} \frac{\sqrt{U_o l v_o}}{U_1} \int_{\eta_s}^\infty \left[(1 + m_1)(1 - \bar{u}) + m_1 \bar{u}(1 - \bar{u}) \right] d\eta \quad (\text{II-6})$$

In the outer flow the velocity profile is given by

$$\frac{\partial \bar{u}}{\partial \eta} = \frac{(1 - \bar{u}) \sqrt{\bar{u} + c_3}}{c_o + c_1 \bar{u} + c_2 \bar{u}^2}$$

with the result that

$$\delta_o^* = \frac{\rho_o a_o}{\rho_1 a_1} \frac{\sqrt{U_o l v_o}}{U_1} \left[(1 + m_1) (c_o g_o + c_1 g_1 + c_2 g_2) + m_1 (c_o g_1 + c_1 g_2 + c_2 g_3) \right] \quad (\text{II-7})$$

We now form the quantity

$$\frac{R_o^{1/2}}{1 + m_o} \frac{d\delta_o^*}{dx} = U_o l \left(\frac{1}{1 + m_o} \right)^{(3\gamma-1)/2(\gamma-1)} \frac{d\xi}{dX} \frac{dX}{dx} \frac{d}{d\xi} \left\{ \frac{(1 + m_1)^{(\gamma+1)/2(\gamma-1)}}{U_1} \left[(1 + m_1) (c_o g_o + c_1 g_1 + c_2 g_2) + m_1 (c_o g_1 + c_1 g_2 + c_2 g_3) \right] \right\} \quad (\text{II-8})$$

Carrying out a tedious differentiation and noting that

$$\frac{dm_1}{d\xi} = \dot{m}_1 = 2m_1 \frac{\dot{U}_1}{U_1} \quad (\text{II-9})$$

yields

$$\begin{aligned} \frac{R_o^{1/2}}{1 + m_o} \frac{d\delta_o^*}{dx} &= \left(g_o + g_1 \frac{m_1}{1 + m_1} \right) \dot{c}_o + \left(g_1 + g_2 \frac{m_1}{1 + m_1} \right) \dot{c}_1 + \left(g_2 + g_3 \frac{m_1}{1 + m_1} \right) \dot{c}_2 \\ &+ \left[c_o \dot{g}_o + c_1 \dot{g}_1 + c_2 \dot{g}_2 \right] + \frac{m_1}{1 + m_1} (c_o \dot{g}_1 + c_1 \dot{g}_2 + c_2 \dot{g}_3) \dot{c}_3 \\ &+ \frac{m_1}{1 + m_1} \left[(c_o g_o + c_1 g_1 + c_2 g_2) \left(\frac{3\gamma - 1}{\gamma - 1} - \frac{1 + m_1}{m_1} \right) \right. \\ &\left. + (c_o g_1 + c_1 g_2 + c_2 g_3) \left(1 + \frac{\gamma + 1}{\gamma - 1} \frac{m_1}{1 + m_1} \right) \right] \frac{\dot{U}_1}{U_1} \\ &= R_o^{1/2} \frac{(\tan \phi - \frac{dw}{dx})}{1 + m_o} \quad (\text{II-10}) \end{aligned}$$

Equation (II-10) taken together with Equation (II-1) constitutes the free-interaction relationship.

Post-Separation Region

After the separation point the inner flow causes the turning of the inviscid flow by an amount depending on δ_i^* . By analyzing Equation (II-6) we can write an equation for δ_i^* as follows:

$$\delta_i^* = \frac{\rho_0 a_0}{\rho_1 a_1} \frac{\sqrt{U_0 l v_0}}{U_1} \int_0^{\eta_s} \left[(1 + m_1)(1 - \bar{u}) + m_1 \bar{u}(1 - \bar{u}) \right] d\eta \quad (\text{II-11})$$

In this case the velocity profile is given by

$$\bar{u} = \alpha_w \eta - \left(\frac{\alpha_s + 2\alpha_w}{\eta_s} \right) \eta^2 + \left(\frac{\alpha_s + \alpha_w}{\eta_s^2} \right) \eta^3 \quad (\text{II-12})$$

The resulting equation for δ_i^* is

$$\begin{aligned} \frac{\delta_i^*}{l} = & \frac{U_0}{U_1} \frac{1}{R_0^{1/2}} \left(\frac{1 + m_1}{1 + m_0} \right)^{(\gamma+1)/2(\gamma-1)} \left\{ (1 + m_1) \left[\eta_s - \frac{\eta_s^2}{12} (\alpha_w - \alpha_s) \right] \right. \\ & \left. + m_1 \left[\frac{\eta_s^2}{12} (\alpha_w - \alpha_s) - \eta_s^3 \left(\frac{\alpha_w^2}{105} - \frac{\alpha_w \alpha_s}{70} + \frac{\alpha_s^2}{105} \right) \right] \right\} \quad (\text{II-13}) \end{aligned}$$

where

$$\alpha_s = \left. \frac{\partial \bar{u}}{\partial \eta} \right|_{\eta_s} = \frac{\sqrt{c_3}}{c_0} \quad (\text{II-14})$$

Carrying out a differentiation as before yields

$$\begin{aligned}
\frac{R_o^{1/2}}{1+m_o} \frac{d\delta_i^*}{dx} = & \left[-\frac{\eta_s^2 \sqrt{c_3}}{12c_o^2} + \frac{m_1}{1+m_1} \left(\frac{\eta_s^2 \sqrt{c_3}}{12c_o^2} - \frac{\eta_s^3 \alpha_w \sqrt{c_3}}{70c_o^2} + \frac{2\eta_s^3 c_3}{105c_o^3} \right) \right] \dot{c}_o \\
& + \left[\frac{\eta_s^2}{24\sqrt{c_3}c_o} + \frac{m_1}{1+m_1} \left(-\frac{\eta_s^2}{24c_o\sqrt{c_3}} + \frac{\eta_s^3 \alpha_w}{140c_o\sqrt{c_3}} - \frac{\eta_s^3}{105c_o^2} \right) \right] \dot{c}_3 \\
& + \left[1 - \frac{\eta_s \alpha_w}{6} + \frac{\eta_s}{6} \frac{\sqrt{c_3}}{c_o} + \frac{m_1}{1+m_1} \left(\frac{\eta_s}{6} \alpha_w - \frac{\eta_s}{6} \frac{\sqrt{c_3}}{c_o} \right. \right. \\
& \left. \left. - \frac{\eta_s^2}{35} \alpha_w^2 + \frac{3\eta_s^2 \alpha_w \sqrt{c_3}}{70c_o} - \frac{\eta_s^2 c_3}{35c_o^2} \right) \right] \dot{\eta}_s \\
& + \left[-\frac{\eta_s^2}{12} + \frac{m_1}{1+m_1} \left(\frac{\eta_s^2}{12} - \frac{2\alpha_w \eta_s^3}{105} + \frac{\eta_s^3 \sqrt{c_3}}{70c_o} \right) \right] \dot{\alpha}_w \\
& + \frac{m_1}{1+m_1} \left\{ \left[1 + \frac{m_1}{1+m_1} \left(\frac{\gamma+1}{\gamma-1} \right) \right] \left(\frac{\eta_s^2}{12} \alpha_w - \frac{\eta_s^2 \sqrt{c_3}}{12c_o} \right. \right. \\
& \left. \left. - \frac{\eta_s^3 \alpha_w^2}{104} + \frac{\eta_s^3 \alpha_w \sqrt{c_3}}{70c_o} - \frac{\eta_s^3 c_3}{105c_o^2} \right) \right. \\
& \left. + \left(\frac{3\gamma-1}{\gamma-1} - \frac{1+m_1}{m_1} \right) \left(\eta_s + \frac{\eta_s^2}{12} \frac{\sqrt{c_3}}{c_o} - \frac{\eta_s^2 \alpha_w}{12} \right) \right\} \frac{\dot{U}_1}{U_1}
\end{aligned} \tag{II-15}$$

Introduction of $d\delta_i^*/dx$ in Equation (II-2) along with $d\delta_o^*/dx$ yields the free-interaction equation when taken together with Equation (II-1). Note that the wall may have any arbitrary shape given by $w(x)$. If case a quadratic rather than a cubic is used for the inner velocity profile, we set

$$\alpha_w = -\alpha_s = -\frac{\sqrt{c_3}}{c_o} \tag{II-16}$$

DOCUMENT CONTROL DATA - R&D		
<small>(Security classification of title, body of abstract and indexing annotation must be entered when the overall report is classified)</small>		
1 ORIGINATING ACTIVITY (Corporate author) Vidya Division, Itek Corporation 1450 Page Mill Road Palo Alto, Calif.		2a. REPORT SECURITY CLASSIFICATION Unclassified
		2b. GROUP N/A
3 REPORT TITLE CALCULATION OF LAMINAR SEPARATION WITH FREE INTERACTION BY THE METHOD OF INTEGRAL RELATIONS		
4 DESCRIPTIVE NOTES (Type of report and inclusive dates) Technical Documentary Report, Part I - March 1964 to May 1965		
5 AUTHOR(S) (Last name, first name, initial) Nielsen, Jack N. Lynes, Larry L. Goodwin, Frederick K.		
6 REPORT DATE October 1965	7a. TOTAL NO. OF PAGES 118	7b. NO. OF REFS 10
8a. CONTRACT OR GRANT NO. AF33(615)-1591	9a. ORIGINATOR'S REPORT NUMBER(S) AFFDL-TR-65-107	
b. PROJECT NO. 8219	9b. OTHER REPORT NO(S) (Any other numbers that may be assigned this report) None	
Task: 821902		
d		
10 AVAILABILITY/LIMITATION NOTICES None		
11 SUPPLEMENTARY NOTES None	12 SPONSORING MILITARY ACTIVITY AFFDL (FDCC) Wright-Patterson AFB, Ohio 45433	
13 ABSTRACT <p>Methods are presented for calculating the laminar boundary-layer flow through separation to reattachment under the influence of a prescribed pressure gradient or, in the case of a supersonic main stream, under the influence of "free interaction" between the boundary layer and the main flow. In contrast to the earlier work of the authors using the Tani method and quartic profiles, the present method is based on the Dorodnitsyn method of integral relations and uses a rational velocity profile which accounts properly for the separation singularity. As a result, the possibility of higher approximations is inherent in the method. The calculated solution for free interaction goes smoothly through the separation point and is in good agreement with certain features of the Navier-Stokes solution in the neighborhood of separation. Good agreement is exhibited between experimental and calculated pressure distributions up to reattachment for the several cases for which the comparisons were made. A computer program based on the work has been prepared for two-dimensional flow. It is planned to continue the work to cover nonadiabatic boundary layers and axisymmetric bodies.</p>		

14 KEY WORDS	LINK A		LINK B		LINK C	
	ROLE	WT	ROLE	WT	ROLE	WT
Laminar boundary layer						
Separated flow						
Supersonic flow						
Aerodynamics						

INSTRUCTIONS

1. **ORIGINATING ACTIVITY:** Enter the name and address of the contractor, subcontractor, grantee, Department of Defense activity or other organization (*corporate author*) issuing the report.

2a. **REPORT SECURITY CLASSIFICATION:** Enter the overall security classification of the report. Indicate whether "Restricted Data" is included. Marking is to be in accordance with appropriate security regulations.

2b. **GROUP:** Automatic downgrading is specified in DoD Directive 5200.10 and Armed Forces Industrial Manual. Enter the group number. Also, when applicable, show that optional markings have been used for Group 3 and Group 4 as authorized.

3. **REPORT TITLE:** Enter the complete report title in all capital letters. Titles in all cases should be unclassified. If a meaningful title cannot be selected without classification, show title classification in all capitals in parenthesis immediately following the title.

4. **DESCRIPTIVE NOTES:** If appropriate, enter the type of report, e.g., interim, progress, summary, annual, or final. Give the inclusive dates when a specific reporting period is covered.

5. **AUTHOR(S):** Enter the name(s) of author(s) as shown on or in the report. Enter last name, first name, middle initial. If military, show rank and branch of service. The name of the principal author is an absolute minimum requirement.

6. **REPORT DATE:** Enter the date of the report as day, month, year; or month, year. If more than one date appears on the report, use date of publication.

7a. **TOTAL NUMBER OF PAGES:** The total page count should follow normal pagination procedures, i.e., enter the number of pages containing information.

7b. **NUMBER OF REFERENCES:** Enter the total number of references cited in the report.

8a. **CONTRACT OR GRANT NUMBER:** If appropriate, enter the applicable number of the contract or grant under which the report was written.

8b, 8c, & 8d. **PROJECT NUMBER:** Enter the appropriate military department identification, such as project number, subproject number, system numbers, task number, etc.

9a. **ORIGINATOR'S REPORT NUMBER(S):** Enter the official report number by which the document will be identified and controlled by the originating activity. This number must be unique to this report.

9b. **OTHER REPORT NUMBER(S):** If the report has been assigned any other report numbers (*either by the originator or by the sponsor*), also enter this number(s).

10. **AVAILABILITY/LIMITATION NOTICES:** Enter any limitations on further dissemination of the report, other than those

imposed by security classification, using standard statements such as:

- (1) "Qualified requesters may obtain copies of this report from DDC."
- (2) "Foreign announcement and dissemination of this report by DDC is not authorized."
- (3) "U. S. Government agencies may obtain copies of this report directly from DDC. Other qualified DDC users shall request through _____."
- (4) "U. S. military agencies may obtain copies of this report directly from DDC. Other qualified users shall request through _____."
- (5) "All distribution of this report is controlled. Qualified DDC users shall request through _____."

If the report has been furnished to the Office of Technical Services, Department of Commerce, for sale to the public, indicate this fact and enter the price, if known.

11. **SUPPLEMENTARY NOTES:** Use for additional explanatory notes.

12. **SPONSORING MILITARY ACTIVITY:** Enter the name of the departmental project office or laboratory sponsoring (*paying for*) the research and development. Include address.

13. **ABSTRACT:** Enter an abstract giving a brief and factual summary of the document indicative of the report, even though it may also appear elsewhere in the body of the technical report. If additional space is required, a continuation sheet shall be attached.

It is highly desirable that the abstract of classified reports be unclassified. Each paragraph of the abstract shall end with an indication of the military security classification of the information in the paragraph, represented as (TS), (S), (C), or (U).

There is no limitation on the length of the abstract. However, the suggested length is from 150 to 225 words.

14. **KEY WORDS:** Key words are technically meaningful terms or short phrases that characterize a report and may be used as index entries for cataloging the report. Key words must be selected so that no security classification is required. Identifiers, such as equipment model designation, trade name, military project code name, geographic location, may be used as key words but will be followed by an indication of technical context. The assignment of links, rules, and weights is optional.